Assessing placement of controllers and nonlinear behavior of electrical power system using normal form information

by

Shu Liu

A dissertation submitted to the graduate faculty

in partial fulfillment of the requirements for the degree of

DOCTOR OF PHILOSOPHY

Major: Electrical Engineering

Program of Study Committee:
Vijay Vittal, Major Professor
Venkataramana Ajjarapu
Degang Chen
David A. Hennessy
Wolfgang Kliemann
James D. McCalley

Iowa State University

Ames, Iowa

2006

Graduate College
Iowa State University

This is to certify that the doctoral dissertation of

Shu Liu

has met the dissertation requirements of Iowa State University

Signature was redacted for privacy.

Major Professor

Signature was redacted for privacy.

For the Major Program

TABLE OF CONTENTS

LIST OF TABLES

LIST OF FIGURES

ACKNOWLEDGEMENTS

First, I would like to thank my advisor, Dr. Vijay Vittal, for his invaluable comments during the whole work with this dissertation. He was always there to listen and give advice, encourage and guide me to a deeper and broader understanding of the work, and show me the need to be persistent to accomplish any goal.

I am very grateful to Dr. Arturo Roman Messina, who gave me great help to complete the writing of several technical papers as well as the challenging research that lies behind it. He was so generous to share his time to meet and talk about my ideas, and taught me different ways to approach a research idea.

I would like to thank the rest of my thesis committee: Dr. James McCalley, Dr. Venkataramana Ajjarapu, Dr. Degang Chen, Dr. Wolfgang Kliemann, and Dr. David Hennessy. I greatly appreciate their valuable comments on this work as well as their other contributions as members of my committee. Thank you for all your good questions to help me think through my work.

Let me also say 'thank you' to my friends in our power group. I am fortunate to have the opportunity to meet them and work with them. I have enjoyed every moment that we have worked together. I want especially to thank Wenzheng Qiu, Xiaoming Wang, Badri Narayanan Ramanathan, Wei Shao for sharing their technical wisdom, research ideas, and many things about life. I appreciate all their friendships and encouragement.

A special thanks goes to my family. My parents' encouragement and unconditional support are always with me and give me endless strength. My husband Ziyu's love help me go through all the though time and become a better person.

To all of you, thank you.

ABSTRACT

In this dissertation, normal form (NF) theory is used to characterize and quantify nonlinear modal interaction near critical equilibria. The research focus is on the analysis of second-order modal interaction and the study of nonlinear aspects of system behavior of interest to the design and location of system controllers.

A systematic approach to derive second-order NF representations in the neighborhood of equilibrium points is presented. Nonlinear interaction measures based on this model are then obtained to assess the extent and distribution of nonlinearity in the system. Finally, analytical criteria are developed to predict the existence of nonlinear modal interactions that significantly affect system dynamic performance.

A nonlinear analysis framework based on normal form (NF) theory and center manifold reduction is proposed to most effectively select generating units which should be equipped with power system stabilizers (PSS). The effect of control action on nonlinear behavior is approximated via suitable modification of initial conditions in the nonlinear coordinate transformations that relate the physical system to the NF coordinates. Using this representation, nonlinear PSS sensitivity indices are then proposed to determine the optimum sites at which to locate PSS. The technique can predict aspects of a system's nonlinear behavior not obtainable from linear approaches and can therefore result in improved placement of system controllers.

Test cases developed on standard test systems are presented to demonstrate the effect of nonlinear interaction and to estimate the controllers' effects on system dynamic performance. The efficacy and accuracy of the method is demonstrated through comparison with conventional analysis techniques.

1 INTRODUCTION

To recognize a foundation of practically every aspect of our economy and society, the United States National Academy of Engineering has acclaimed electrical power as the 20th century's most beneficial engineering innovation. To satisfy the desire for both qualitative and quantitative increases in electrical power production, many efficient and intelligent processes have been introduced into ongoing work. The increasing complexity of electrical networks and interconnections make today's power system probably the most critical dynamic infrastructure system. With the advent a competitive market environment, power systems are being operated in the presence of more uncertainty and with less conservatism than in the past. This presents new challenges for maintaining system stability in a market environment. Accurate identification and proper mitigation of stability problems is therefore more necessary than ever before if reliable and economic operation of power systems is to be obtained.

Power system stability may be broadly defined as that property of a power system that enables it to remain in a state of operating equilibrium under normal operating conditions, and to regain an acceptable state of equilibrium after being subjected to a disturbance [1]. Power system stability can be classified into rotor-angle stability, voltage stability, and mid-term and long-term stability. Many modern power systems encounter the problem of low-frequency electromechanical oscillations. These oscillations are often poorly damped and often have a negative impact on the power transfer capabilities of the system [2]. Enhanced knowledge of rotor angle stability is essential to solving the problem of such inherent electromechanical oscillations.

A disturbance in a power system is a sudden change or a sequence of changes in one or more of the parameters of the system, or in one or more of the system operating quantities [3]. Depending on the impact of a given disturbance, its rotor angle stability phenomena are usually characterized in terms of small-signal stability and transient stability.

1.1 Transient Stability Analysis

Transient stability is the ability of a power system to maintain synchronism when subjected to a severe disturbance such as a fault on transmission facilities, loss of generation, or loss of a large load [1]. Both the initial operating condition and the severity of the disturbance may affect a system's stability.

With growing stress on modern power systems, the threat of transient stability problems becomes more and more serious. Transient stability analysis is becoming an increasingly important issue for reliable system operation. While in the past transient stability analysis has usually been performed at the planning stages, there is an increasingly pressing need for on-line transient studies.

Transient stability analysis involves the determination of nonlinear system dynamic response to large disturbances. Such a analysis can be achieved by various methods: efficient step-by-step time-domain simulation, direct methods, pattern recognition techniques, expert systems, and neural networks. For a given disturbance, step-by-step time-domain simulation can determine the accurate response of all system variables by solution of system differential and algebraic equations. This conventional method produces the most reliable and accurate information in system transient stability analysis. However, it is quit time-consuming, and therefore not well-suited to the efficient computation requirements of real-time applications. Among other methods, so-called direct methods have received considerable attention. This approach is defined in [1] as a method able to determine stability without explicitly solving the system differential equations. In addition to supplying a more direct and effective assessment of power system transient stability, direct methods offer a quantitative measurement of how stable a particular operating condition may be, but the modeling limitations and unreliability of the computational techniques involved may impede their practical application, especially for analysis of stressed systems. A combination of conventional time-domain simulation and direct methods appears to be a promising approach for minimizing the problems of each method and enhancing the capability of transient stability analysis.

1.2 Small-Signal Stability Analysis

Small-signal (or small-disturbance) stability refers to the ability of a power system to maintain synchronism when undergoing small disturbances. The disturbances are considered sufficiently small for linearization of system equations to be permissible for purposes of analysis [1]. Such disturbances may occur frequently on systems undergoing small generation and load variations.

Instability of this type can be of two forms [1]:

1. Steady increase in rotor angle due to lack of sufficient synchronizing torque.
2. Rotor oscillations of increasing amplitude due to lack of sufficient damping torque.

As a conventional analysis tool for studying dynamic system behavior, small-signal stability analysis can provide an understanding of the modal structure of a power system which may not be clearly observable from time-domain simulations. Based on local linearization of the system model at stationary points of vector fields, small-signal stability analysis may allow the appropriate application of powerful linear analysis methods for the study of a power system's dynamic characteristics.

As a first step, the system dynamic differential equations are linearized at some stable operating point. The characteristic of eigenvalues of the system matrix can then be used to determine system stability. The system is considered stable if all its eigenvalues are located in the left half of the complex plane. Real eigenvalues correspond to non-oscillatory modes. Complex eigenvalues represent damping coefficients and frequencies that may be observed in the oscillations of system variables. The system's response with a given initial condition can be expressed approximately by closed-form solutions using eigenvalues and eigenvectors.

Small-signal stability analysis based on local linearization can be a powerful and relatively simple analysis tool for studying system dynamic behavior. However, the analysis is limited to a neighborhood of the operating point in which the linear approximation is valid.

1.3 Modes and Modal Interaction

In today's practical power systems, small-signal stability is largely a problem related to insufficient damping of oscillations. The stability of the following types of oscillations is of concern [1]:

1. Local modes or machine-system modes are associated with the swinging of units at a generating station with respect to the rest of the power system. The term *local* is used because the oscillations are localized at one station or a small part of the power system.
2. Inter-area modes are associated with the swinging of many machines in one part of the system against machines in other parts. They are caused by two or more groups of closely coupled machines being interconnected by weak ties.
3. Control modes are associated with generating units and other controls. Poorly tuned exciters, speed governors, HVDC converters and static var compensators are the usual causes of instability in these modes.
4. Torsional modes are associated with the rotational components of the turbine-generator shaft system. Instability of torsional modes may be caused by interaction with excitation controls, speed governors, HVDC controls, and series-capacitor-compensated lines.

Modern power systems are increasingly becoming more stressed as the demand on systems keeps increasing and fewer transmission enhancements are incorporated. As system stress increases, complex phenomena involving interaction between the fundamental modes of the system may occur [4]. Recent analytical studies have shown that nonlinear modal interaction of the fundamental modes of oscillation of the system may significantly affect the power system response to large perturbations and may thus adversely influence control performance [5, 6, 7, 8, 9]. Furthermore, under certain ranges of operating conditions system modes may interact nonlinearly leading to second (or higher) order resonances and hence may result in the onset of more complex dynamical phenomena. In recent work, the problem of near resonance between modes has been

addressed by Dobson *et al.* [10]. Further, the occurrence of second-order near resonance has been reported in a number of studies [5, 6, 11].

Since nonlinear modal interaction may play an important role in the dynamic behavior of a power system under stressed operating conditions, second and possibly higher order nonlinearities can no longer be neglected. Local linearization of the modal equations at stationary points of vector fields may fail to provide complete characterization of system performance or may result in incomplete system information, especially under heavy system stress or near the onset of unstable behavior. The dynamic characteristics of the system may not be accurately analyzed without making use of more detailed system representations. A clear understanding of nonlinear phenomena is only now emerging, and accurate analytical techniques are required to assess the effects of such phenomena on various aspects of system behavior. Fundamental to this analysis is the detection of quasi-resonance between the modes of oscillation in the system and the development of techniques that allow a more precise analytical characterization of system behavior near singularities.

Because of the complexity involved in such analysis, prediction of the effects of these phenomena is extremely difficult. The identification of both the magnitude and nature of the interaction process constitutes a first step in the characterization of system behavior. Furthermore, understanding the nature of the nonlinearity provides additional insight into the mechanisms responsible for nonlinear behavior and may lead to improved assessment and control of system dynamic performance.

1.4 Placement of Power System Controller

Many modern power systems have some poorly-damped oscillation modes which often result in troublesome oscillations. In order to improve system stability, power system damping controllers such as power system stabilizers and FACTS(Flexible AC Transmission Systems)-based stabilizers are often used to damp such oscillations and increase damping of the oscillatory modes.

The first step in designing such a controller is to find its optimum location. With linear analysis techniques, conventional approaches to system dynamic analysis can often provide reliable methods for controller design. For the commonly used PSS (Power System Stabilizer), the most effective and popular techniques involve the mode shape, participation factor, and residue. However, these methods only include linear information about dynamic systems and may fail to provide a complete characterization of system performance, especially under heavy stress or near the onset of unstable behavior.

As systems become more stressed, in addition to interactions between the fundamental modes of the system, more complex dynamical phenomena leading to second (or higher) order resonances may occur. Accurate analytical techniques are required for in-depth study of such nonlinear dynamic behavior. To extend the linear concepts to include second-order information, an analytical technique based on normal forms of vector fields will be developed. This should allow more precise characterization of system behavior.

1.5 Method of Normal Forms

Nonlinear analysis techniques provide an opportunity to not only quantify the effects of modal interaction on system dynamic behavior, but also to assess its impact on control performance. Among various nonlinear analysis techniques, the method of normal forms (NF) has been applied in the past few years to obtain closed-form analytical approximations to system behavior [12, 13].

The method of normal forms of vector fields is a well-known nonlinear analysis technique [14, 15, 16, 17, 18], based on the process of eliminating higher order terms in a system of differential equations. Based on the series expansion of system nonlinear differential equations, the normal form technique has been applied to power system to investigate various aspects of local system nonlinear behavior in the neighborhood of a stationary or equilibrium point [6, 7, 11, 19, 20, 21, 22, 23].

This method provides simultaneous assessment of both the extent and the

distribution of nonlinearity and can be used to identify nonlinearly interacting modes. By selectively including second-order (or higher) terms in the system model, NF theory allows the prediction of salient phenomena such as nonlinear modal interaction, as well as analysis and distribution of nonlinearity in the system.

In addition to determining structural characteristics, there is growing interest in extending nonlinear analysis to assess the role of nonlinear behavior on control system performance and location. A recent review article synthesizes the main approaches currently used to analyze nonlinear behavior and discusses practical experience with the application of the method [24].

1.6 Objectives and Scope of the Research

In this work, the use of NF theory to characterize and quantify nonlinear modal interaction near critical equilibria is discussed. Normal form analysis will be utilized to analyze system dynamic behavior and evaluate excitation control performance under different operating conditions.

The objectives of this research include the following broad issues:

1. Detection of a system's dynamic characteristic at critical operating conditions in which the system exhibits near first and second-order resonances.
2. Identification of nonlinear aspects of modal interaction phenomenon which are of interest in analysis and design of system controllers.
3. Generalization of analytical procedures for assessing placement of controllers using nonlinear information.
4. Determination of the strength of nonlinear interactions caused by excitation control in power system behavior.

A set of near first and second-order resonance conditions is presented on a two-area four-machine test system [25]. The normal form method is used to provide additional information in the description of nonlinear system behavior near resonance conditions.

Conventional techniques for assessing placement of controllers are reviewed. Previous ideas are extended to measure closed-loop nonlinear mode-state relationships which account for the effect of supplemental control action. Based on a second order NF representation, the effect of control action on nonlinear behavior is approximated via suitable modification of the initial conditions in the nonlinear coordinate transformations which relate the physical system to the NF coordinates. A new approach is developed to determine the most effective selection of generating units to be equipped with power system stabilizers (PSS).

The PSS model is included in the existing normal form program, so that characterization of nonlinear modal interactions within the system with a properly designed PSS can thus be investigated. These results provide more information on the effect of excitation control on nonlinear behavior and modal interaction.

Examples of application of these approaches on the two-area four-machine test system and the IEEE 50-generator test system [26] are provided to analyze system dynamic characteristics and to determine the most effective locations for PSS to improve both small-signal and transient stability. The improvements provided by these proposed approaches are then compared with those of conventional techniques.

1.7 Thesis Outline

The thesis is organized into 8 chapters. The introduction in Chapter 1 provides background as well as the statement of the problem. The motivation and objectives of this research work are also described in this chapter.

Chapter 2 provides a detailed summary of the literature review, including background information, a concise record of the source material for this work, and related topics.

Chapter 3 describes Power System Models used in this work. Chapter 4 introduces the method of normal forms based on these models. The structural properties of normal form transformation are discussed, starting with an introduction describing this

method. Closed-form analytical solutions, numerical estimates of mode-state participations, and the study of nonlinear modal interaction are developed in the following sections, enabling the application of normal forms of vector fields to power systems.

Starting with the illustration of an exact strong resonance, a more typical near-strong resonance condition is introduced in Chapter 5. The generality of strong resonance of critical modes in power system is discussed in this chapter. Since this phenomenon may lead to complex behaviors, the analysis of local results near the onset of resonances with the method of normal form will be needed to reveal a complete interpretation.

Chapter 6 introduces several conventional techniques to assess placement of controllers in power systems. Only including linear information of the dynamic systems may fail to provide complete characterization of system performance. In this chapter, two kinds of indices that also include second order information are developed using normal form theory.

Chapter 7 provides numerical results and observations regarding application data for the proposed approach to the test system (the two-area four-machine test system and the IEEE 50-generator test system).

Chapter 8 presents conclusions of this work and suggestions for future work.

Appendix A and B provide the complete power flow data and dynamic data for 4-machine test system and IEEE 50-machine test system respectively.

2 LITERATURE REVIEW

Much work has been done to analyze and characterize power system behavior. Many concepts for power system modeling, stability analysis, and simulation are given by Kundur [1] and Anderson and Fouad [27].

In modern systems, the great amounts of power interchanged between electric companies and geographical regions causes much more stress in systems than in earlier times. This stress may also impacts system dynamic performance. Recent analytical studies have shown that nonlinear modal interaction of the fundamental system modes may significantly affect power system behavior. Vittal, et. al. [5] presented an analysis of the inter-area mode phenomenon in stressed power systems following large disturbances showing that this phenomenon could occur as a result of nonlinear interaction between the natural modes of oscillation in the system. Starrett and Fouad [19] investigated the significance of higher-order terms on system response and developed a methodology based on normal forms of vector fields to extend linear concepts to include the second-order information. Messina, et. al. [28] presented the application of perturbation methods to analysis of inter-area oscillations in complex power systems. Conventional linear analysis is used to study the nature of the oscillatory modes of the system. A nonlinear approach based on normal form methods focuses on the analysis of non-linear interaction under stressed operating conditions. Both of these approaches are implemented in a production-grade computer program used to assess the nature of inter-area oscillations. The combined use of these methodologies was suggested as an approach to get more physical insight into the nature of inter-area oscillation. In [29], Ni, et. al. developed a scanning tool based on the normal form techniques for the investigation of nonlinear modal behavior of ac/dc power systems with dc power modulation. Thapar, et. al. [30] used the normal forms of vector fields to predict the onset of inter-area separation in power systems following large disturbances. An index to capture the structural characteristics of dynamic system behavior and predict the nature of dynamic system

performance following large disturbances was developed. Saha, et. al. [31] presented an approach for approximating the stability boundary of a power system without integration by including second order information. The stability boundary and its behavior under stressed system conditions was examined using normal forms of vector fields. Based on Normal Form analysis at the instant of removal of the fault, Xie, et. al. [32] developed a variable-structure trajectory-predictive algorithm. Since the proposed prediction method is based on Prony's nonlinear approximation, significant online system trajectory prediction for emergency transient stability control becomes feasible. By using the method of normal forms, Jang, et. al. [33] studied nonlinear oscillations in a real power system. It is suggested that nonlinear information be used to improve stability and reduce the nonlinearity of the stressed power system. Under the stressed conditions normal-forms analysis results shows the existence of nonlinear modal interactions and identifies the participating states of the interacting modes. The nonlinear results must be considered to obtain desired control effects on some critical modes.

Power transactions are increasing in both volume and variety in many restructured electric power systems. As power transfers, redispatch, or other power system parameters change, power system linearization and modes vary. Dobson, et. al. [10] suggested that approaching strong resonance can be expected in general power system models. When such an approach occurs two oscillatory modes may interact to cause one of the modes to subsequently become unstable. In [34], Dobson, et. al. analyzed the behaviors of modes and general perturbations of weak resonance. Since these phenomena lead to complex behavior, detailed analysis of local results are required to produce a complete interpretation. An approach based on normal form theory for identification of unfavorable operating regions by searching for resonance and near resonance has been proposed by Zhu. et. al. in [7]. This work also points out that near resonance among critical inertial modes and control modes may contribute to unsatisfactory behavior of a system. In [35], Betancourt, et. al. present a general technique for computing real normal forms of resonant vector fields. By using a special real-valued nonlinear transformation of coordinates in physical space, this approach

simplifies the computation of initial conditions in normal form space.

Nonlinear interactions among the various modal components can also be interpreted using other techniques. In [36], Shanechi, et. al. devised a general nonlinear modal representation of large scale power systems. By employing Laplace transformation, this method provides a solution to system nonlinear differential equations. By representing the system in terms of its modes and their interactions, the method can be used for analyzing and understanding system dynamic behavior under stressed conditions. Another interesting technique is the Hilbert spectra of nonlinear processes proposed in [37, 38]. This technique is well-suited for analyzing nonstationary phenomena and is capable of quantifying the extent of nonlinearity directly from observed oscillations or simulated data. Normal form theory (NF) and Hilbert spectra analysis (HSA) can be used in a complementary fashion to investigate the occurrence of nonlinear modal interaction in stressed power systems. The NF method is utilized to obtain closed-form analytical approximations to system behavior following large disturbances. On the basis of this model, analytical measures are derived to assess the extent of interaction between fundamental modes of oscillation. HSA is then applied to characterize and quantify the time evolution of the modulation process directly from simulated power system data obtained from transient stability simulations as well as to validate normal form results.

Many modern power systems face the problem of troublesome dynamic oscillations in which small disturbances may induce complicated dynamic oscillations in the range of 0.2 to 2.5 *Hz* associated with some poorly-damped oscillation modes. Power system damping controllers are used to both damp these oscillations and increase the damping of swing modes. Kundur, et. al. [39] present analysis of the effects of the different power system stabilizer parameters on the overall dynamic performance of power systems and show how stabilizer settings may be selected so as to enhance both steady-state and transient stability of local plant modes as well as inter-area modes in large interconnected systems. Using the normal forms of vectors fields, Lin, et. al. [6] evaluated nonlinear modal interaction in a power system and showed that the control

modes have significant interaction with the inertial modes, especially with the inter-area modes. Nonlinear interaction between modes may also impact control performance when control design is based on pure linear analysis. Jang, et. al. [11] analyze the effect of nonlinear modal interaction on control performance using normal forms of vector fields and developed a control design procedure that considers nonlinear information. Barocio and Messina et. al. [40, 41, 42] propose an analytical technique based on normal form theory for analysis of nonlinear inter-area oscillations in stressed power systems that incorporate the operation of static VAR compensators (SVCs). Zou, et. al. studied interactions among multiple SVC controllers in power systems in [43]. An analytical approach based on normal form theory is proposed for analysis of nonlinear interactions among the multiple SVC controllers in power system. A nonlinear interaction index used to investigate interactions among multiple SVC controllers is developed in this work. For other widely used FACTS devices such as unified power flow controllers (UPFC), one of the most important features is the production of multiple control functions implemented by multiple controllers. Since recent studies have demonstrated the existence of dynamic interactions among different controller channels of UPFC, Zou, et. al. investigated the interactions among the multi-control channels of UPFC using normal forms of vector fields in [44]. In [45], Yue and Schlueter use a bifurcation subsystem-based control design methodology to study nonlinear effects of a robust μ-synthesis power system stabilizer (MPSS). In order to include nonlinear information, a normal form representation of a nonlinear power system model is introduced, and second-order interaction indices of a system with MPSS and conventional excitation control are proposed.

The first step in a design applying a PSS to increase the damping of a certain oscillation mode in a multimachine power system is to determine the PSS location. Wang [46] presents electric torque, residue, functional sensitivity, participation and Partial Multi-Modal Decomposition (PMMD), and describes the connections among these technologies. Since a PSS on a machine in a power system represents a closed-loop controller, both its input and its control effect on the system should be considered in

selecting the PSS location. Zhou, et. al. [47, 48] presented the concept of Sensitivity of PSS Effect (SPE), which considers both the activity of state variables and the control effect of control signals. It is also shown that the SPE is equal to the sensitivity of a mode with respect to the change of PSS transfer function. By using SPE, the displacement of a system mode caused by the installation of a PSS can be predicted. Based on this prediction the PSS location decision can be made and the PSS parameters tuned. This method was used to identify the best PSS location by Zhou in a 13-machine system to increase the damping of and inter-area mode. In [49], Hongesombu, et. al. introduced a method for simultaneously tuning PSSs in a multimachine power system. The tuning approach, based on a multiobjective function comprising the damping ratio, damping factor and number of PSSs, is realized by using a hierarchical genetic algorithm (HGA) and a parallel micro-genetic algorithm (parallel micro-GA). The stabilizers are tuned to simultaneously shift the poorly-damped oscillation modes to a specific stable zone. The appropriate choice of PSS locations can be identified by using an eigenvalue-based multiobjective function. In order to guarantee robustness, many scenarios with different operating conditions should be included in the process of simultaneous tuning. Chung, et. al. [50] presented an application of probabilistic theory to the selection of robust PSS locations and parameters to enhance the damping of multiple electromechanical modes in a multimachine system over a large range of operating conditions. By extending conventional eigenvalue analysis to the probabilistic environment, the statistical nature of eigenvalues corresponding to different operating conditions can be represented by their expectations and variances. Probabilistic sensitivity indices to facilitate "robust PSS" site selection and a probabilistic eigenvalue-based objective function for coordinated synthesis of PSS parameters are proposed in this work.

3 POWER SYSTEM MODELS

The general form of the relevant system dynamic equations can be expressed by

$$\dot{x} = f(x) \tag{3.1}$$

where x is the vector of the system states.

In this work, loads are modeled as constant impedances, and the network is reduced to its internal generator nodes. A generator can be expressed as either the classical model or the two-axis model [27]. Let us assume that there are m generators represented by the two-axis model and equipped with exciters in an n-generator system, while the remaining generators are represented by the classical model

$$x^T = [x_1^T, x_2^T] \tag{3.2}$$

where x_1 is the vector of system states with generators represented by the two-axis model and equipped with exciters, and x_2 is the vector of the system states with generators represented by the classical model.

3.1 Generators Represented by Two-axis Model and Equipped with Exciters

With assumption [27]:

1. The transient effects are accounted for, while the subtransient effects are neglected.
2. In the stator voltage equations the variation of $d-q$ flux linkages are negligible compared to the speed voltage terms.
3. $\omega \cong \omega_R = 1$ pu.

the equations for generators represented by the two-axis model can be given by

$$\dot{E}'_{qi} = \frac{1}{\tau'_{d0i}}(E_{FDi} - E'_{qi} + (x_{di} - x'_{di})I_{di}) \tag{3.3}$$

$$\dot{E}'_{di} = \frac{1}{\tau'_{q0i}}(-E'_{di} - (x_{qi} - x'_{qi})I_{qi}) \tag{3.4}$$

$$\dot{\omega}_i = \frac{1}{M_i}(P_{mi} - (I_{di}E'_{di} + I_{qi}E'_{qi}) + (x'_{qi} - x'_{di})I_{di}I_{qi} - D_i(\omega_i - \omega_S)) \tag{3.5}$$

$$\dot{\delta}_i = \omega_i - \omega_S \qquad i = 1,2,...,m \tag{3.6}$$

where,

τ'_{do}, τ'_{qo} : open-circuit d and q axes transient time constants, respectively

E'_d, E'_q : d and q axes stator EMFs corresponding to rotor transient flux components, respectively

E_{FD} : stator EMF corresponding to the field voltage

x_d, x_q : d and q axes synchronous reactances, respectively

x'_d, x'_q : d and q axes transient reactances, repectively

I_d, I_q : d and q axes stator currents, respectively

D : damping coefficient.

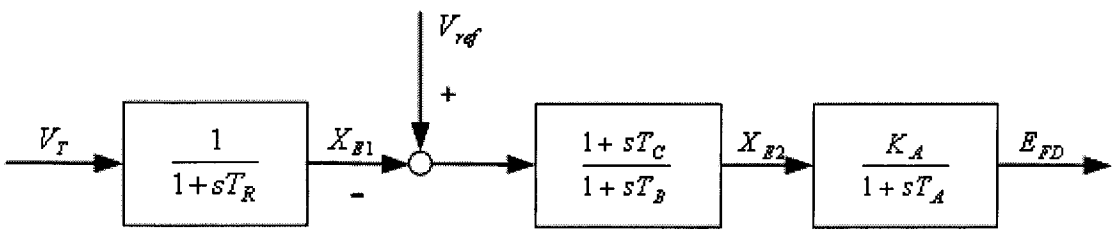

Figure 3.1 Block diagram of the exciter (IEEE Type AC4A)

Figure 3.1 shows the block diagram of the exciter model. The dynamic equations can be expressed by

$$\dot{E}_{FDi} = \frac{K_{Ai}X_{E2i}}{T_{Ai}} - \frac{1}{T_{Ai}}E_{FDi} \tag{3.7}$$

$$\dot{X}_{E1i} = -\frac{1}{T_{Ri}} X_{E1i} + \frac{1}{T_{Ri}} V_{Ti} \tag{3.8}$$

$$\dot{X}_{E2i} = \frac{1}{T_{Bi}}(\frac{T_{Ci}}{T_{Ri}} - 1) X_{E1i} - \frac{1}{T_{Bi}} X_{E2i} - \frac{T_{Ci}}{T_{Bi} T_{Ri}} V_{Ti} + \frac{1}{T_{Bi}} V_{refi} \tag{3.9}$$

Where,

V_T : generator terminal voltage. V_T is given by

$$V_T = (E_q^{'} + x_d^{'} I_d) + j(E_d^{'} - x_q^{'} I_q) \quad i = 1,2,...,m \tag{3.10}$$

V_{ref} : exciter reference voltage

Then x_1 can be expressed by

$$\begin{aligned} x_1^T = [&E_{q1}^{'}, E_{d1}^{'}, \omega_1, \delta_1, E_{FD1}, X_{E11}, X_{E21}, \cdots, \\ &E_{qm}^{'}, E_{dm}^{'}, \omega_m, \delta_m, E_{FDm}, X_{E1m}, X_{E2m}] \end{aligned} \tag{3.11}$$

3.2 Generators Represented by Classical Model

With the following assumptions [27]:

1. Mechanical power input is constant.
2. Damping or asynchronous power is negligible.
3. The constant-voltage-behind-transient-reactance model for the synchronous machines is valid.
4. The mechanical rotor angle of a machine coincides with the angle of the voltage behind the transient reactance.
5. Loads are represented by passive impedances.

the generator equations for the classical model are given by

$$\dot{\omega}_i = \frac{1}{M_i}(P_i - P_{ei}) \tag{3.12}$$

$$\dot{\delta}_i = \omega_i - \omega_S \quad i = m+1, m+2, ..., n \tag{3.13}$$

where,

$$P_i = P_{mi} - E_i^2 G_{ii}$$

$$P_{ei} = \sum_{j=1, j\neq i}^{n} [E_i E_j B_{ij} \sin(\delta_i - \delta_j) + E_i E_j G_{ij} \cos(\delta_i - \delta_j)]$$

and

M_i : inertia constant of generator i,

P_{mi} : mechanical power input of generator i,

E_i : internal bus voltage of generator i,

G_{ii} : driving point conductance of node i

G_{ij}, B_{ij} : conductance and susceptance between generators i and j as the system reduced to generator internal nodes

δ_i : rotor angle of generator i.

ω_i : rotor speed of generator i with respect to a synchronous reference frame.

ω_S : synchronous speed

Then x_2 can be expressed by

$$x_2^T = [\omega_{m+1}, \delta_{m+1}, \cdots, \omega_n, \delta_n] \tag{3.14}$$

3.3 **Power System Stabilizer (PSS) Modeling**

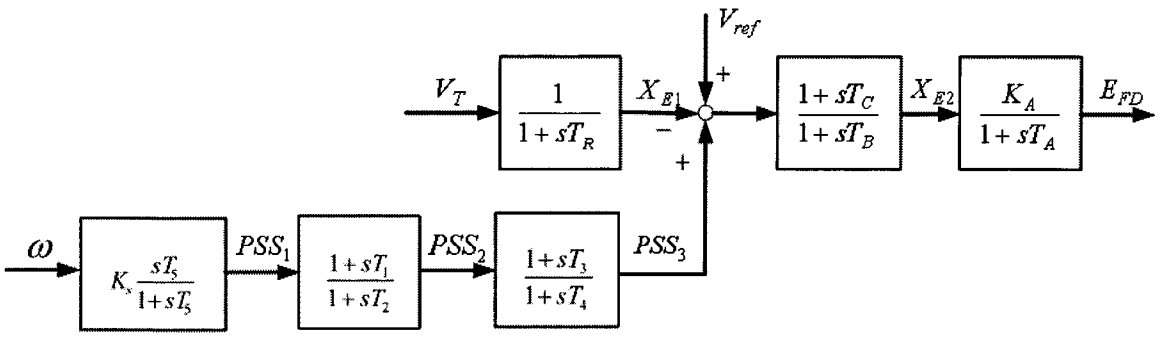

Figure 3.2 Block diagram of the PSS (IEEE Type PSS1A) and excitation system

Figure 3.2 shows the block diagram of the PSS and exciter used in this work. The general form of the system dynamic equations can be expressed by

$$\dot{\tilde{x}} = \tilde{f}(\tilde{x}) \tag{3.15}$$

where $\tilde{x}^T = [x_1^T, x_2^T, x_3^T]$ is the vector of system states. x_1 is the vector of the system states with generators represented by the two-axis model and equipped with exciters, x_2 is the vector of the system states with generators represented by the classical model, and x_3 is the vector of the system states with a PSS. For the PSS shown in Figure 3.2, the states vector x_3 is given by

$$x_3^T = [PSS_{11}, PSS_{21}, PSS_{31}, \cdots, PSS_{1m}, PSS_{2m}, PSS_{3m}] \tag{3.16}$$

Based on the system equations shown in 3.1, the new system can be expressed by changing system equations for X_{E2i} as follows:

$$\dot{X}_{E2i} = \frac{1}{T_{Bi}}(\frac{T_{Ci}}{T_{Ri}} - 1)X_{E1i} - \frac{1}{T_{Bi}}X_{E2i} - \frac{T_{Ci}}{T_{Bi}T_{Ri}}V_{Ti} + \frac{1}{T_{Bi}}V_{REFi} + \frac{T_C}{T_B}P\dot{S}S_{3i} \tag{3.17}$$

The system equations with PSSs can be expressed by

$$P\dot{S}S_{1i} = -\frac{1}{T_{5i}}PSS_{1i} + K_{si}\frac{1}{120\pi}\dot{\omega}_i \tag{3.18}$$

$$P\dot{S}S_{2i} = -\frac{1}{T_{2i}}PSS_{2i} + \frac{1}{T_{2i}}PSS_{1i} + \frac{T_{1i}}{T_{2i}}P\dot{S}S_{1i} \tag{3.19}$$

$$P\dot{S}S_{3i} = -\frac{1}{T_{4i}}PSS_{3i} + \frac{1}{T_{4i}}PSS_{2i} + \frac{T_{3i}}{T_{4i}}P\dot{S}S_{2i} \tag{3.20}$$

4 NORMAL FORMS OF VECTOR FIELDS

The method of Normal form of vector fields, a well-known mathematical tool of nonlinear analysis techniques, has in the past few years been applied to power systems to investigate various local aspects of system nonlinear behavior in the neighborhood of a stationary or equilibrium point [5, 6, 30]. The application of normal form analysis to power system requires describing the system's dynamics by a series expansion of nonlinear differential equations.

$$\dot{x} = f(x) = Ax + X_2 + X_3 + \ldots, \qquad x(0) = x_0 \tag{4.1}$$

where $x \in R^n$ is the vector of system states, $A = [\partial f / \partial x]_{EP}$ is the Jacobian matrix, and X_i contains polynomial terms of order i.

Poincaré's normal-form theorem [51] states that under non-resonance conditions the series expansion of the system equations may be reduced to a linear equation by a polynomial change of variable. In recent work, the problem of near resonance between modes has been addressed by Dobson et al. [10]. Additionally, the occurrence of second-order near resonance has been evidenced in a number of studies [5, 6, 11].

4.1 Introduction of Normal Forms of Vector Fields

In system analysis it is well known that the Jordan-form Transformation consisting of the linear change of coordinates

$$x = Uy$$

transforms a set of linear differential equations

$$\dot{x} = Ax, \; x(0) = x_0$$

into the form

$$\dot{y} = (U^{-1}AU)y = Jy$$

where $y \in C^n$ is the vector of Jordan form variables, U is the matrix of right

eigenvectors of matrix A, and J is diagonalized with the eigenvalues of matrix A on the diagonal.

Applying the Jordan-form transformation to nonlinear differential equations (4.1), the Jordan form series expansion can be derived:

$$\begin{aligned}\dot{y} &= U^{-1}AUy + U^{-1}X_2(Uy) + U^{-1}X_3(Uy) + \ldots \\ &= Jy + Y_2(y) + Y_3(y) + \ldots\end{aligned} \tag{4.2}$$

Therefore the case in which A is in its Jordan form can be studied without changing the topological structure of the orbits. With a similar procedure the simplest possible form can be obtained by a suitable nonlinear change of coordinates. This simplest form can be derived by removing as many higher order terms as possible. In practice, this is usually done order by order. The second-order normal form transformation is defined as [51, 52]

$$y = z + h_2(z) \tag{4.3}$$

where $z \in C^n$ is the vector of normal form variables and $h_2(z)$ is a complex-valued vector field of polynomial terms of degree 2 in z to be determined.

By differentiating (4.3) along the trajectory of the system states, obtain

$$\dot{y} = \dot{z} + \frac{\partial h_2(z)}{\partial z}\dot{z} = \{I + D_z[h_2(z)]\}\dot{z} \tag{4.4}$$

where $Dh_2(z)$ is the Jacobian of the nonlinear transformation and I is the $n \times n$ identity matrix.

Using (4.4) and (4.3) in (4.2) and including up to second-order terms, obtain

$$\dot{z} = Jz + Jh_2(z) + Y_2[z + h_2(z)] - \{D_z[h_2(z)]\}\dot{z} \tag{4.5}$$

Since Y_2 contains polynomial terms of order 2, $Y_2[z + h_2(z)]$ can be expressed in the form $Y_{2iab}[z_a + h_{2a}(z)][z_b + h_{2b}(z)]$. Thus, $Y_2[z + h_2(z)]$ contains second and higher order terms, so $Y_2(z)$ can be used to express second-order terms.

With straightforward computation, equation (4.5) becomes

$$\dot{z} = Jz + F_2(z) + O(\|z\|^3) \tag{4.6}$$

where

$$F_2(z) = Jh_2(z) + Y_2(z) - \{D_z[h_2(z)]\}Jz \tag{4.7}$$

and $O(\|z\|^3)$ contains third and higher order terms.

The nonlinear transformation given by (4.3) has two important properties:

1. The transformation leaves the linear part of (4.2) invariant.
2. The nonlinear coordinates y and z agree to the first degree.

Given (4.6), the goal of the nonlinear coordinate transformation (4.3) is to choose the coefficients of $h_2(z)$ such that in the new coordinate framework, the second-order terms can be annihilated.

From (4.6) and (4.7) it is clear that nonlinear terms of degree 2 can be annihilated if the homological equation

$$Y_2(z) = Jh_2(z) - \{D_z[h_2(z)]\}Jz \tag{4.8}$$

is satisfied. The coefficients of $h_2(z)$ are given by [19]

$$h_{2jkl} = \frac{Y_{2jkl}}{(\lambda_k + \lambda_l - \lambda_j)} \tag{4.9}$$

where Y_{2jkl} are the coefficients of Y_2 in (4.2). Equation (4.9) shows that mapping (4.8) is possible if the no resonance conditions $\lambda_k + \lambda_l - \lambda_j \neq 0$ are met.

It then follows that the original system in (4.2) can be expressed in the normal form space as

$$\dot{z} = Jz + O(\|z\|^3) \tag{4.10}$$

Excluding third and higher order terms, (4.10) can be rewritten as

$$\dot{z} = Jz \tag{4.11}$$

In the more general case, in which $\lambda_a + \lambda_b - \lambda_i = 0$, the system in (4.6) can be expressed as

$$\dot{z} = Jz + F_{r2} + O(\|z\|^3) \tag{4.12}$$

where F_{r2} represents resonance terms that cannot be removed and must remain in simplified normal form.

Essentially, the normal-form approximation in (4.11) yields a simplified representation in which nonessential terms are removed. A critical aspect in determining the normal form transformation coefficients and hence in linearizing the system is the resonance condition $\lambda_a + \lambda_b - \lambda_i = 0$. Two cases are of special interest when the system in (4.2) cannot be transformed to its simplest expression (4.11) [53, 54]:

1. Resonance. There is at least one modal combination such that $\lambda_a + \lambda_b - \lambda_i = 0$. In general there is no formal power series transformation that can linearize the vector field.
2. Quasi-resonance. In this case there exists an increasing sequence of modal combinations such that $\lambda_a + \lambda_b - \lambda_i \to 0$. The vector field can either be linearized by a divergent series, or analytically transformed to a vector field that contains all the quasi-resonant monomial terms [53].

This latter condition is of great theoretical and practical interest in the study of power system behavior under stressed operating conditions and will be studied in the following.

Figure 4.1 provides an overview of the transformation from the original system to the normal form system.

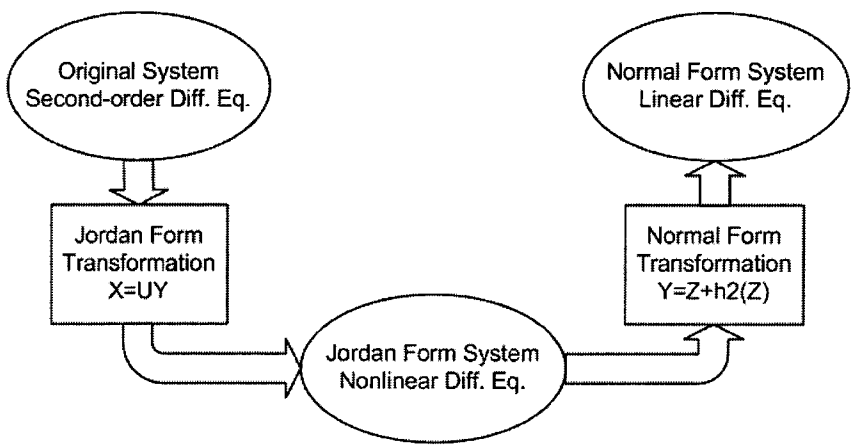

Figure 4.1 Overview of system transformation

4.2 Structural Properties of the Normal Form Transformation

The structural properties of the nonlinear transformation are central to the proposed approach. To clarify the importance of this aspect, let the coordinate change in (4.3) be expressed as

$$y = \varphi(z) = z + h_2(z) \tag{4.13}$$

Using center manifold theory, approximate $\varphi^{-1}(y)$ by a truncated power series expansion [51]

$$z = \varphi^{-1}(y) = y - h_2(y) + O(\|y\|^3) \quad \text{as} \quad \|y\| \to 0 \tag{4.14}$$

where $\varphi^{-1}(y) : C^n \to C^n$ is a homogeneous polynomial map of degree r and $O(\|y\|^3)$ accounts for higher-order terms. In general, $\varphi(y)^{-1}$, cannot be computed exactly. However, several approximations can be made as outlined below. These approximations will now be used to determine the initial conditions in the different coordinate frames.

Let $y_o = U^{-1}x_o$ be the vector of initial conditions in the Jordan space. If the initial values of y are small enough such that higher order terms become negligible [55], then (4.14) reduces to

$$z_0 \approx y^0 - h_2(y_0) = U^{-1}x_0 - h_2\left(U^{-1}x_0\right) \tag{4.15}$$

where x_o represents the initial conditions in physical space.

For the jth component, obtain

$$z_{jo} = y_{jo} - \sum_{p=1}^{n}\sum_{q=p}^{n} h_{2jpq}y_{po}y_{qo} \tag{4.16}$$

in which $y_{po} = \sum_{j=1}^{n} v_{pj}x_{jo}$, and v_{pj} is the p,j element of the left eigenvectors matrix. This result can be used to selectively determine the time responses for specific inputs, x_o.

The significance of these expressions becomes evident when the nature of this

transformation is examined around a given initial condition, y_0, z_0. To this end, let the *jth* component of (4.13) be written as

$$y_{jo} = z_{jo} + (z_o)^T H_j z_o = z_{jo} + \sum_{k=1}^{n}\sum_{l=1}^{n} h_{2jkl} z_{ko} z_{lo} \tag{4.17}$$

where H_j is the *jth* matrix of nonlinear interaction coefficients:

$$H_j = \begin{bmatrix} h_{2j_{11}} & h_{2j_{12}} & \cdots & h_{2j_{1n}} \\ h_{2j_{21}} & h_{2j_{22}} & \cdots & h_{2j_{2n}} \\ \vdots & \vdots & \ddots & \vdots \\ h_{2j_{n1}} & h_{2j_{n2}} & \cdots & h_{2j_{nn}} \end{bmatrix}, \quad \mathrm{j} = 1,\ldots,\mathrm{n} \tag{4.18}$$

Matrix H_j is full, complex-valued and symmetric. Nonlinear coupling between modal and NF coordinates is characterized by two key parameters: strength of nonlinearity, $h_{2jkl} z_{ko} z_{lo}$, and coupling density. The former represents the ratio of magnitudes of nonlinear terms; the latter can be conceptually defined by the number of interactions between two coordinate variables with significant magnitudes.

For a simple one-dimensional system, (4.17) defines a nonlinear curve in the $y - z$ complex plane. For low stress conditions the system behaves linearly and the relationship between coordinates can be approximated as $y_{jo} \approx z_{jo}$. At higher loading conditions, the system behaves more nonlinearly, thus requiring a more accurate representation of nonlinear effects as illustrated in Figure 4.2.

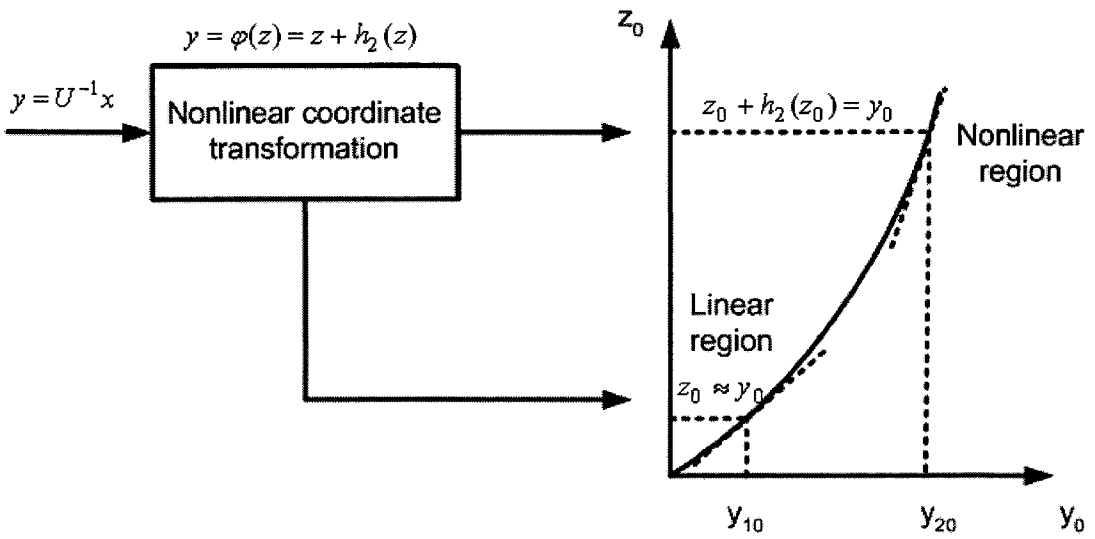

Figure 4.2 Geometrical illustration of the normal form transformation

4.3 Closed-form Analytical Solutions

Discarding third-order and higher terms, $O(\|z\|^3)$, and assuming that no resonance conditions are found, the system in (4.11) can be expressed in the uncoupled form

$$\dot{z}_j = \lambda_j z_j, \qquad j = 1,...,n \tag{4.19}$$

which has solutions

$$z_j(t) = z_{j0} e^{\lambda_j t}, j = 1,...,n \tag{4.20}$$

where z_{j0} is the initial condition of the normal form variable z_j. These equations are the generators of a family of parametric solutions which depend upon the initial excitation z_{j0}.

To determine z_0 in terms of x_0, solve the nonlinear set of equations with complex coefficients

$$z_0 + h_2(z_0) - U^{-1}x_0 = 0 \tag{4.21}$$

for a given excitation x_0.

Having determined the initial conditions in normal form space, z_0 , the approximate solutions to (4.19) can then be converted back to the physical domain by using transformation (4.13).

In terms of modal components, the approximate solutions in the Jordan space are given by

$$y_j(t) = z_{jo}e^{\lambda_j t} + \sum_{k=1}^{n}\sum_{l=k}^{n} h_{2jkl} z_{ko} z_{lo} e^{(\lambda_k+\lambda_l)t} \tag{4.22}$$

and

$$x_i(t) = \sum_{j=1}^{N} u_{ij} z_{jo} e^{\lambda_j t} + \sum_{j=1}^{n} u_{ij}\left[\sum_{k=1}^{n}\sum_{l=k}^{n} h_{2jkl} z_{ko} z_{lo} e^{(\lambda_k+\lambda_l)t}\right] \tag{4.23}$$

Equations (4.22) and (4.23) allow the computation of the contribution of particular modes of oscillation to the system states and permit direct comparison between linear and nonlinear analysis techniques.

As noted in [5], nonlinear effects arise in the NF solution both in the linear part (in terms $u_{ij} z_{j0} e^{\lambda_j t}$), and in the nonlinear part (in the terms $u_{ij}\sum_{k=1}^{N}\sum_{l=k}^{N} h_{2jkl} z_{ko} z_{lo}$). Large values of the product $h_{2jkl} z_{ko} z_{lo}$ compared to z_{jo} indicate that, in principle, strong interaction between mode j and modes k,l and can be used to assess various aspects of nonlinear system performance. Usually only the largest interaction coefficient ($\max_{k,l} h_{2jkl} z_{ko} z_{lo}$) is considered, assuming other contributions to be negligible [6, 11]. This, however, may lead to inaccurate estimates near critical operating conditions.

A more useful measure of the nonlinear interaction that takes into account both the structural properties of the nonlinear transformations and the initial conditions excited by the fault may be obtained from the analysis of approximate time-domain solutions. Defining the second-order contribution factors as $\sigma_{2ij} = u_{ij} z_{jo}$ and $\sigma_{22ikl} = z_{ko} z_{lo}[\sum_{k=1}^{N} u_{ij} h_{2jkl}]$, the time-domain solution of the ith state becomes

$$x_i(t) = \sum_{j=1}^{N} \sigma_{2ij} e^{\lambda_j t} + \sum_{k=1}^{N} \sum_{l=k}^{N} \left[\sigma_{22ikl} e^{(\lambda_k + \lambda_l)t} \right] \tag{4.24}$$

where the coefficient σ_{2ij} represents the second-order contribution of the *jth* single mode to the *ith* state. Accordingly, σ_{22ikl} represents the contribution of the mode combination $\lambda_k + \lambda_l$ to the *ith* state.

Equation (4.24) can be used to predict how intermodulation and harmonic terms can arise in the output response of nonlinear systems following a fault. Further simplifications of these formulae follow from a consideration of the structural properties of the system and may be used to assess various aspects of system performance as discussed below.

The entire process for obtaining a closed-form solution in the original space is shown in Figure 4.3.

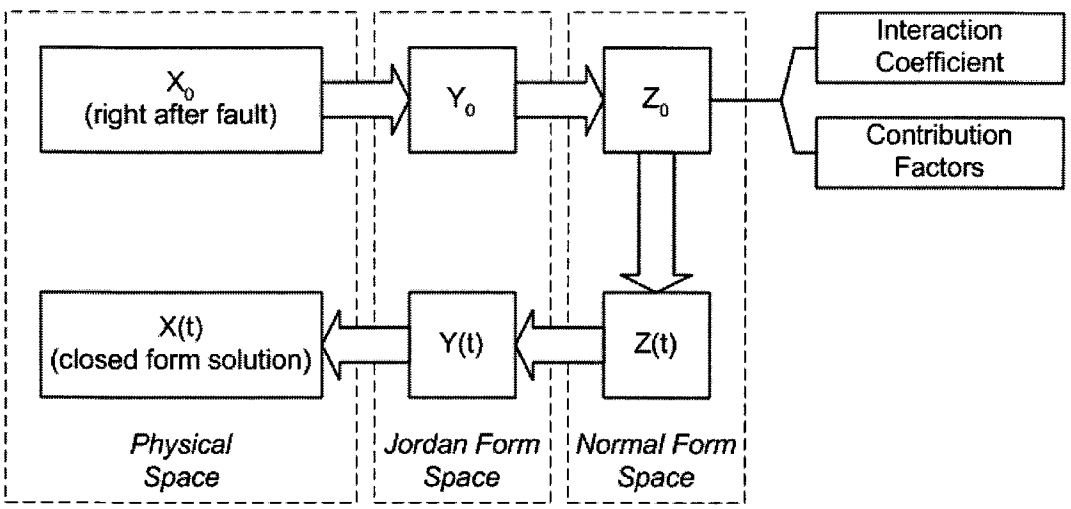

Figure 4.3 Overview of closed-form solution

4.4 Analytical and Numerical Estimates of Mode-State Participations

According to the derivation above, nonlinear fault-independent measures may be computed to determine nonlinear measures of mode-state participations. The key to dealing with nonlinear participations in the suggested approach relies upon finding initial conditions in the normal form space for an arbitrary excitation in real coordinates. This is

a problem for which few analytical results have been presented up to this time.

An interesting special case of (4.16) is that when the initial condition vector $x_0 = \alpha e_i$ is applied[1]. Use of this condition in (4.16) gives

$$z_{jo} = y_{jo} - \sum_{p=1}^{n}\sum_{q=p}^{n} h_{2jpq} y_{p0} y_{q0} = \alpha v_{ji} + \alpha^2 v_{2jii},\ j = 1,\ldots,n \tag{4.25}$$

where $y_{jo} = \alpha v_{ji}$ and $v_{2jii} = -\sum_{p=1}^{n}\sum_{q=p}^{n} h_{2jpq} v_{pi} v_{qi}$.

In the following, the choice of the initial conditions of the system states to determine the influence of excitation control in the dynamics of interest will be discussed.

It should be observed, however, that (4.16) is a very special case of the model (4.14), in that higher-order terms are neglected.

Inserting (4.25) into (4.23) and simplifying yields

$$x_i(t) = \sum_{j=1}^{n} p_{2ij} e^{\lambda_i t} + \sum_{k=1}^{n}\sum_{l=1}^{n} p_{2ikl} e^{(\lambda_k + \lambda_l)t} \tag{4.26}$$

where

$$p_{2ij} = u_{ij}(\alpha v_{ji} + \alpha^2 v_{2jii}) = p_{2ij_L} + p_{2ij_{NL}},\ p_{2ikl} = u_{2ikl}(\alpha v_{ki} + \alpha^2 v_{2kii})(\alpha v_{li} + \alpha^2 v_{2lii})$$

and $u_{2ikl} = \sum_{j=1}^{n} u_{ij} h_{2jkl}$, $v_{2mii} = -\sum_{p=1}^{n}\sum_{q=1}^{n} h_{2mpq} v_{pi} v_{qi}$, $m = k, l$.

The first term in (4.26), p_{2ij}, represents the second-order participation of the *jth* single-eigenvalue mode in the *ith* state, and the second term p_{2ikl} represents the second-order participation of the *ith* state in the mode formed by the combination of the eigenvalues λ_k and λ_l. Observe that $p_{2ij_L} = u_{ij} v_{ji}$ is the linear participation factor (PF) and $p_{2ij_{NL}} = u_{ij} v_{2jii}$ may be interpreted as a correction term to the linear participation.

By selectively including residual terms in (4.14) up to the desired order of

[1] Here e_i is the unity vector and α is an arbitrary scalar (normally unity) chosen to provide the desired degree of excitation of a given state [56].

approximation, second and higher order *analytical estimates* of PFs can be defined. The validity of this approximation is limited by the size of the higher-order terms, $O(\|y\|^3)$, which may limit the region in the operating space where this approach can be applied.

In the context of the analysis of stressed, nonlinear systems, a more precise measure of the nonlinear mode-state participations can be obtained by exciting a given state of interest, x_i, and solving numerically for the normal form initial conditions, z_0, in (4.13). To achieve this, a Newton-based iterative technique that enables the determination of both the initial conditions arising from a specific fault scenario and the initial conditions associated with exciting a specific set of states (modes) has been implemented.

Given a set of states of interest, $x_0 = [\alpha_1 x_{10} \quad \alpha_2 x_{20} \quad \cdots \quad \alpha_n x_{n0}]^T$, the following approach is used to determine nonlinear mode-state relationships:

1. Determine the modes excited in modal coordinates using the relationship $y_0 = U^{-1} x_0$.

2. Solve (4.13) using a Newton-based iterative algorithm for z_0. This requires the solution of a series of complex algebraic equations of the form

$$J_r \Delta z_r = -F_r(z)$$

where Δz_r is the *rth* Newton update and $F_r(z_r) = [f_1(z) \quad f_2(z) \quad \cdots \quad f_n(z)]^T$ is the vector of residuals with $f_j(z) = z_{j0_r} - y_{j0} + \sum_{k=1}^{n}\sum_{l=1}^{n} h_{2jkl} z_{k0_r} z_{l0_r}$, $j = 1,2,...,n$ and $J_r = \left(DF_r(z)\right)\Big|_{z=z_r}$ is the Jacobian matrix with elements

$$\frac{\partial f_j(z)}{\partial z_j} = 1 + \sum_{\substack{k=1 \\ k\neq j}}^{n} h_{2j_{kj}} z_k + \sum_{\substack{l=1 \\ l\neq j}}^{n} h_{2_{jjl}} z_l + 2h_{2_{jjj}} z_j$$

$$\frac{\partial f_j(z)}{\partial z_p} = \sum_{\substack{k=1 \\ k\neq p}}^{n} h_{2j_{kp}} z_k + \sum_{\substack{l=1 \\ l\neq p}}^{n} h_{2_{jpl}} z_l + 2h_{2_{jpp}} z_p \quad , p \neq j$$

3. With this selection for $\mathbf{z}_o$, the approximate solution (4.23) can be written as

$$x_i(t) = \sum_{j=1}^{n} p'_{2ij}\, e^{\lambda_i t} + \sum_{k=1}^{n}\sum_{l=1}^{n} p'_{2ikl}\, e^{(\lambda_k+\lambda_l)t} \tag{4.27}$$

where $p'_{2ij} = u_{ij} z_{jo}$ and $p'_{2ikl} = z_{ko} z_{lo} [\sum_{j=1}^{n} u_{ij} h_{2jkl}]$.

The above steps have been implemented in the NF procedure and have the advantage of allowing systematic calculation of various measures of mode-state participation. Thus, for example, by setting $x_0 = \alpha_i e_i$, where α_i is an appropriate scaling factor, fault-independent numerical approximations to PFs in (4.27) can be obtained. Conversely, fault-dependent contribution factors in (4.24) can be calculated using $y_o = U^{-1}(x_{cl} - x_o)$, where x_o is the post-disturbance equilibrium point and x_{cl} is the system condition at the end of the disturbance. This latter algorithm is more accurate than currently-used approaches, especially for highly stressed conditions, and it may be used to define more general measures of nonlinear mode-state participations.

Both of the approaches to calculate approximate and numerical nonlinear participation factor are shown in Figure 4.4.

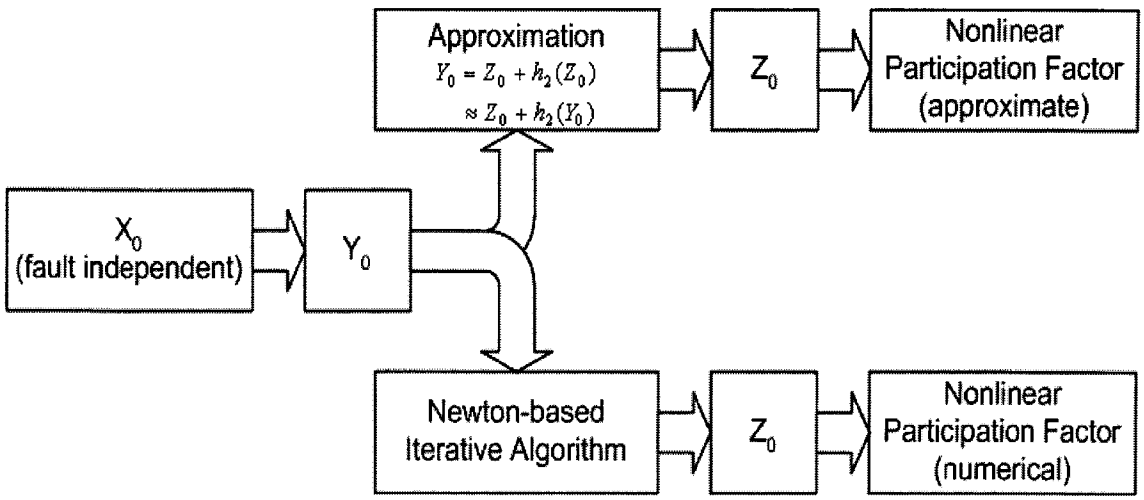

Figure 4.4 Overview of approximate and numerical nonlinear participation factor

4.5 Nonlinear Modal Interaction

Previous work [6, 7, 11] shows that the presence of nonlinear modal interaction has strong impact on system performance. To quantify the extent to which modes interact nonlinearly, use the interaction index (II) defined in previous work [7]. The relative amount of the second-order nonlinearity at mode j can be computed by $\left|y_j(t)/z_j(t)\right|$. By inserting (4.20) and (4.22),

$$\left|\frac{y_j(t)}{z_j(t)}\right| = \left|\frac{z_{j0}e^{\lambda_j t} + \sum_{k=1}^{n}\sum_{l=k}^{n} h_{2jkl} z_{k0} z_{l0} e^{(\lambda_k+\lambda_l)t}}{z_{j0}e^{\lambda_j t}}\right| \qquad j = 1,2,...,N \tag{4.28}$$

Since a time-domain solution scales the initial distances z_{j0}, $h_{2jkl}z_{k0}z_{l0}$, with exponential functions of time variable $e^{\lambda_j t}$ and $e^{(\lambda_k+\lambda_k)t}$, the initial distances can be used to express the relative amount of second-order nonlinearity.

$$\left|\frac{y_j(t)}{z_j(t)}\right| \approx \left|\frac{z_{j0} + \sum_{k=1}^{n}\sum_{l=k}^{n} h_{2jkl} z_{k0} z_{l0}}{z_{j0}}\right| = \left|1 + \frac{\sum_{k=1}^{n}\sum_{l=k}^{n} h_{2jkl} z_{k0} z_{l0}}{z_{j0}}\right| \le 1 + \left|\frac{\sum_{k=1}^{n}\sum_{l=k}^{n} h_{2jkl} z_{k0} z_{l0}}{z_{j0}}\right| \tag{4.29}$$

In (4.29), the summation term $\sum_{k=1}^{n}\sum_{l=k}^{n} h_{2jkl} z_{ko} z_{lo}$ adds a heavy computational burden for fast calculation, especially in large systems, so usually only the largest term or at most a few largest terms are calculated to represent the relative size of the nonlinearity in the initial value.

$$II^1(j) = \left|\frac{\max_{k,l} h_{2jkl} z_{k0} z_{l0}}{z_{j0}}\right|, \quad II^2(j) = \left|\frac{\underline{\sec}\max_{k,l} h_{2jkl} z_{k0} z_{l0}}{z_{j0}}\right|,$$

$$II^3(j) = \left|\frac{\underline{third}\max_{k,l} h_{2jkl} z_{k0} z_{l0}}{z_{j0}}\right|, \quad ... \tag{4.30}$$

where $\underline{\sec}\max_{k,l} h_{2jkl} z_{k0} z_{l0}$ and $\underline{third}\max_{k,l} h_{2jkl} z_{k0} z_{l0}$ are the complex form when the

second and the third largest values of $| h_{2jkl} z_{k0} z_{l0} |$ $(k = 1:n, \quad l = k:n)$ occurs.

The indices shown in (4.30) are also measures of normalized magnitude of nonlinear interaction.

5 MODAL RESONANCE AND POWER SYSTEM OSCILLATIONS

Two pairs of complex conjugate eigenvalues are exactly in resonance when they have exactly the same frequency and damping. Exact resonance is an unusual occurrence, but if it does occur, then the eigenvalues can be very sensitive to system changes [10].

5.1 Exact Strong Resonance of Two Complex Pairs

Consider a 4×4 matrix A_C

$$M=\begin{pmatrix} a & b & 0 & 0 \\ u & a & 0 & 0 \\ 0 & 0 & a^* & b^* \\ 0 & 0 & u^* & a^* \end{pmatrix}=\begin{pmatrix} M_U & 0 \\ 0 & M_U^* \end{pmatrix} \tag{5.1}$$

where u is a complex parameter moving smoothly, a and b are constant complex numbers, $b\neq0$.

The eigenvalues of M_U are given by

$$\lambda_1=a+\sqrt{ub},\ \lambda_2=a-\sqrt{ub} \tag{5.2}$$

and the eigenvalues of M_U^* are given by

$$\lambda_1^*=a^*+\sqrt{u^*b^*},\ \lambda_2^*=a^*-\sqrt{u^*b^*} \tag{5.3}$$

Since the eigenvalues of M are λ_1, λ_2, λ_1^*, and λ_2^*, detailed analysis of M_U will reveal the mode characterization of matrix M.

As $u=0$, two eigenvalues of M_U coincide at a and exact strong resonance condition occurs.

In order to predict the movement of eigenvalues as u moves through 0, the sensitivity of eigenvalues to u must be analyzed.

$$\frac{\partial \lambda_1}{\partial u} = \frac{1}{2\sqrt{ub}}, \quad \frac{\partial \lambda_2}{\partial u} = -\frac{1}{2\sqrt{ub}} \tag{5.4}$$

As $u \to 0$, the eigenvalues sensitivity tends toward positive and negative infinity and the eigenvalues' movements will change their directions toward 90^o.

To verify the prediction of the eigenvalues' movment characteristics, a real example can be considered. With $a = -1 + j3$, $b = 1 + j$, the matrix M in (5.1) can be expressed by

$$M = \begin{pmatrix} -1+j3 & 1+j & 0 & 0 \\ u & -1+j3 & 0 & 0 \\ 0 & 0 & -1-j3 & 1-j \\ 0 & 0 & u & -1-j3 \end{pmatrix} \tag{5.5}$$

where u is a real-valued parameter.

Figure 5.1 shows the movement of the eigenvalues of the matrix M as u varies from -2 to +2.

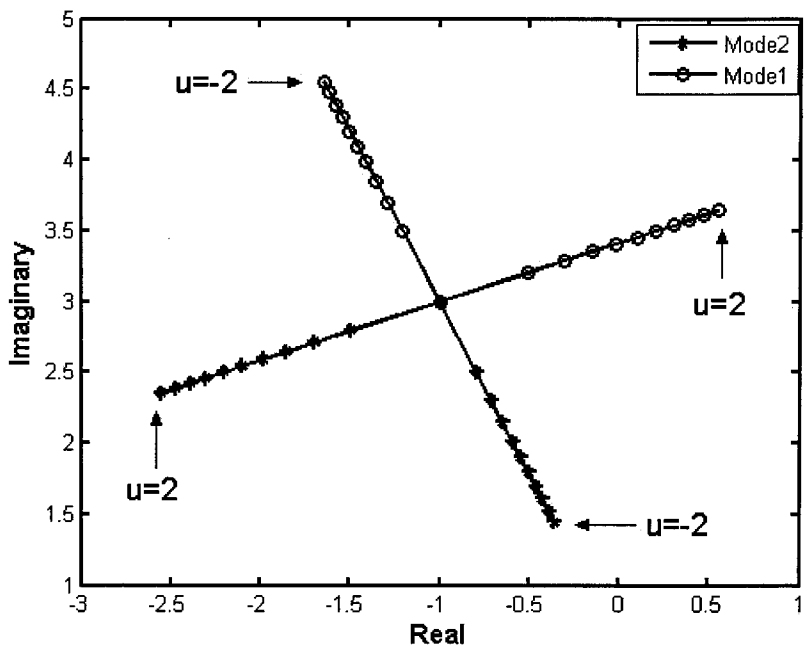

Figure 5.1 Exact strong resonance of two complex pairs

Exact strong resonance of the two modes occurs at $u = 0$ as the two modes coincide at $-1 + j3$. As u increases through 0, the movement of the eigenvalues change

their directions around 90^o. Mode 1 becomes unstable after the resonance.

In a real system, this kind of exact strong-resonance condition is an unusual occurrence. A near-resonance condition is more typical.

5.2 Near Strong Resonance of Two Complex Pairs

Now add a perturbation to matrix M in 5.5.

$$M' = M + \Delta M = \begin{pmatrix} -1+j3 & 1+j & 0 & 0 \\ u & -1+j3 & 0 & 0 \\ 0 & 0 & -1-j3 & 1-j \\ 0 & 0 & u & -1-j3 \end{pmatrix} + \begin{pmatrix} 0 & 0 & 0 & 0 \\ 0 & 0 & 1 & 0 \\ 0 & 0 & 0 & 0 \\ 2 & 0 & 0 & 0 \end{pmatrix} \quad (5.6)$$

As u varies from -2 to +2, the two modes of matrix M' come close together and then quickly move beyond each other. Similarly to the movement as that for exact resonance, the movement of eigenvalues change directions around 90^o as u increases through 0 and mode 1 becomes unstable after resonance.

Figure 5.2 shows the movement of the eigenvalues of matrix M' as u varies from -2 to +2.

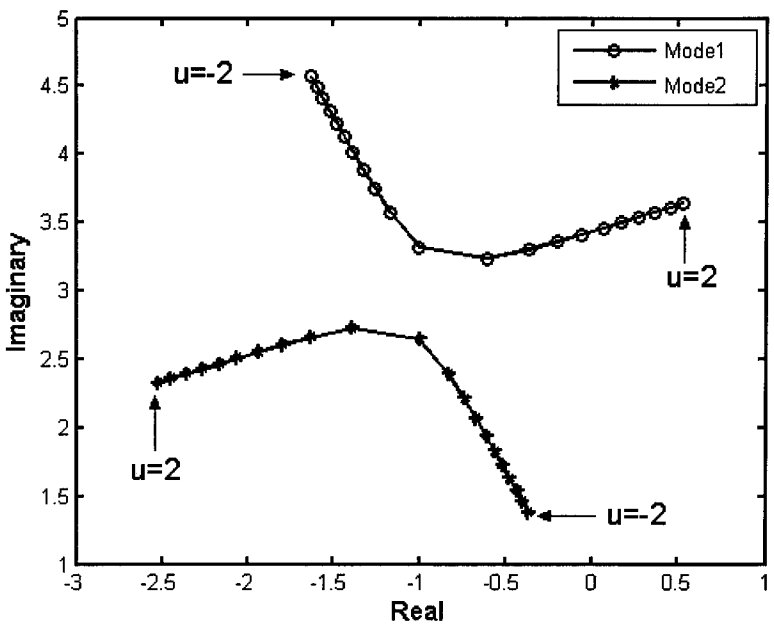

Figure 5.2 Near resonance of two complex pairs

The characteristics of near-resonance conditions are summarized in [10]

If the system is near strong resonance, then the following conditions are typical:

1. The eigenvalues and eigenvectors are very sensitive to parameter variations.
2. A general parameter variation causes the direction of eigenvalue movement in the complex plane to turn quickly through an approximate right angle.
3. The right and left eigenvectors are nearly orthogonal.
4. The right eigenvectors of the two modes are nearly aligned. This implies that the pattern of oscillation of the two modes is similar.

5.3 Strong Resonance of Critical Modes in Power Systems

As parameter $u \Rightarrow 0$, exact strong resonance occurs and the matrix in (5.1) becomes

$$M_{SR} = \begin{pmatrix} a & b & 0 & 0 \\ 0 & a & 0 & 0 \\ 0 & 0 & a^* & b^* \\ 0 & 0 & 0 & a^* \end{pmatrix}, \quad b \neq 0 \tag{5.7}$$

Matrix M_{SR} is nondiagonalizable. The occurrence of exact strong resonance requires two independent parameters, the real and imaginary part of complex parameter u to be zero. Nondiagonalizable resonance will typically not be encountered when varying only one parameter, but it is still possible to pass close to nondiagonalizable resonance and in that case this close proximity would have a significant effect on system behavior. [10]

Modern power systems are increasingly expected to be operated at a variety of operating conditions as the demand on such systems keeps increasing and power prices vary geographically. As a result, variations in power system parameters could change system operating conditions and cause troublesome dynamic oscillations. Since the frequencies of critical oscillation modes are typically in the range of 0.2 to 2.5 Hz, the region of interest in the complex plane shrinks. This increases the possibility of encountering strong resonances in power systems. Although exact strong resonances are

always neglected in electric power systems analysis [57, 58, 59, 60], near strong resonance conditions may occur as a parameter is varied with the system operating under different conditions. When two eigenvalues pass the near strong resonance condition, one of the eigenvalue reduces its damping and becomes unstable. Therefore, instead of only tracing the movement of a single mode, the nearness of two critical modes also needs to be considered in order to fully understand the cause of the oscillation. The occurrence of near strong resonance conditions in 3-bus and 9-bus power systems are discussed in [10].

In Chapter 7, a 2-area, 4-machine test system from [25] is analyzed over a wide range of operating conditions to fully characterize modal resonance in power systems. In addition to the near strong linear resonance condition as described in this Chapter, the nonlinear resonance conditions expressing the interaction of the three modes is also presented in this discussion. The occurrence of near strong linear and nonlinear resonance leads to complex behavior and requires nonlinear analysis methods to more accurately describe system dynamic behavior.

6 ASSESSING PLACEMENT AND EFFECT OF CONTROLLERS IN POWER SYSTEM

Many power systems encounter the problem of troublesome dynamic oscillations in the range of 0.2 to 2.5 *Hz* associated with some poorly damped swing modes [47]. Power system damping controllers such as power system stabilizers and FACTS (Flexible AC Transmission Systems)-based stabilizers may be used to damp these oscillations and increase damping of the swing modes. In considering application of such controllers to a multimachine power system the first step is to assess the best location for the controllers. It is not difficult to choose the location of controllers to damp local modes since these modes are confined to a specific area with a few machines, but for the interarea mode it can become very complicated since several machines are typically involved in this type of modal oscillation.

6.1 Conventional Techniques

During the last three decades, many techniques have been applied to analyze and determine the location of power system damping controllers [46, 47, 61, 62]. For the commonly-used PSS (Power System Stabilizer), the mode shape, participation factor, and residue methods have been the most effective and popular techniques.

6.1.1 Mode Shape

The right eigenvector gives the mode shape, i.e., the relative activity of the state variables when a particular mode is excited [1]. Using PSS input (for instance machine speeds) as state variables, the best PSS location can be identified by comparing the relative amplitude of right eigenvectors.

6.1.2 Participation Factor

Since the elements of the eigenvectors are dependent on units and scaling associated with the state variables, there is a problem in using right eigenvectors individually to identify the relationship between the states and the modes. Participation factor, which combines both the right and left eigenvectors, is proposed as a possible solution to this problem.

For a linear system,

$$\begin{aligned} \dot{X} &= AX + Bu \\ y &= CX \end{aligned} \tag{6.1}$$

where u is the output of PSS and y is the feedback signal of the PSS.

Referring to equation (6.1), the right and left eigenvector of the oscillation mode, $\lambda_i = -\sigma_i + j\omega_i$ are given by

$$U_i = \begin{bmatrix} u_{i1} \\ u_{i2} \\ \cdots \\ u_{in} \end{bmatrix}, \quad V_i = [v_{i1} \quad v_{i2} \quad \cdots \quad v_{in}] \tag{6.2}$$

The participation of the *kth* state in this *ith* oscillation mode can be expressed as follows [63]:

$$p_{ki} = u_{ik} v_{ik} \tag{6.3}$$

Choosing a PSS input (such as machine speeds) as the state variables, the best PSS location can be identified by the largest magnitude of the participation factor.

6.1.3 Residue

For a linear system (6.1), the controllability and observability index of the PSS associated with oscillation mode $\lambda_i = -\sigma_i + j\omega_i$ are

$$\begin{aligned} b_i &= V_i B \\ c_i &= C U_i \end{aligned} \tag{6.4}$$

where U_i and V_i are the right and left eigenvectors of the oscillation mode λ_i in (6.1).

The residue of λ_i is the product of the controllability and observability indices [46]

$$R_i = b_i c_i \tag{6.5}$$

Comparing the magnitudes of the residue, the placement of the PSS can be determined.

6.1.4 Conclusion

Although mode shape, participation factor, and residue are the most popular approaches proposed so far, they only include linear information about dynamic systems, so none of them may provide complete characterization of the system performance, especially under heavy stress or near the onset of unstable behavior. With normal form theory, it is possible to consider information related to higher order terms and express the whole set of system equations in the simplest form. The results produced by linear techniques and nonlinear indices will be compared in future case studies.

6.2 Nonlinear Participation Factor

The approach outlined in section 4.4 was used to determine nonlinear participation factors (PFs). To provide a basis of comparison with the results obtained from linear analysis, the speed deviations of system generators were expressed in the form of

$$\begin{aligned}
\Delta\omega_1(t) &= \sum_{j=1}^{n} u_{1j} z_{jo} e^{\lambda_j t} + \sum_{j=1}^{n} u_{1j} \sum_{k=1}^{n} \sum_{l=k}^{n} h_{21_{kl}} z_{ko} z_{lo} e^{(\lambda_k+\lambda_l)t} \\
\Delta\omega_2(t) &= \sum_{j=1}^{n} u_{2j} z_{jo} e^{\lambda_j t} + \sum_{j=1}^{n} u_{2j} \sum_{k=1}^{n} \sum_{l=k}^{n} h_{22_{kl}} z_{ko} z_{lo} e^{(\lambda_k+\lambda_l)t} \\
&\vdots \\
\Delta\omega_{ng}(t) &= \sum_{j=1}^{n} u_{ngj} z_{jo} e^{\lambda_j t} + \sum_{j=1}^{n} u_{ngj} \sum_{k=1}^{n} \sum_{l=k}^{n} h_{2ng_{kl}} z_{ko} z_{lo} e^{(\lambda_k+\lambda_l)t}
\end{aligned} \tag{6.6}$$

By properly choosing a fault-independent initial value x_0 in physical space, the

initial value z_0 can be calculated in two different ways, the approximate (analytical) estimate or the numerical estimate, as shown in Section 4.4. Then (6.6) can be rewritten as

$$\Delta\omega_i(t) = \sum_{j=1}^{n} p_{2ij} e^{\lambda_j t} + \sum_{p=1}^{n} \sum_{q=p}^{n} p_{2ipq} e^{(\lambda_p+\lambda_q)t} \tag{6.7}$$

where p_{2ij} represents the second-order participation of the *ith* speed state in the *jth* single-eigenvalue mode, and p_{2ipq} represents the second-order participation of the *ith* speed state in the mode formed by the combination of the eigenvalues λ_p and λ_q.

By including second-order information, the nonlinear participation factor provides the participation of one state with a single mode of oscillation in a more accurate way than the linear participation factor. It can also uncover the participation of one state with the combination of two modes. Both these kinds of information will be helpful in improving the assessment of the PSS location and analyzing system behavior.

When determining the best location to place a PSS using nonlinear participation factors, both approximate and numerical estimates should be calculated. For low-stress conditions these two kinds of estimates may provide similar results, but for high-stress conditions the numerical estimate may give more precise information than the approximate estimate.

It should be observed, however, that nonlinear PFs as defined in (6.7) represent open-loop measures. Since a PSS on a machine is a closed-loop controller, both its input and its control effect on a system should be taken into account, especially for the case when the critical modes have a large participation in the exciter's states.

6.3 Nonlinear PSS Sensitivity Index

Assuming that both the structure and parameters of the PSS are known, closed-loop nonlinear participation factors can be computed by using the procedure in section

4.3. This is a computationally intensive problem since the choice of each PSS alternative modifies the structure and numerical values of the normal form representation. Because the decision regarding PSS location should be done prior to the design of the PSS, the detailed PSS blocks cannot be included directly in the analysis. A useful alternative approach to assess the effect of control action on the system response can obtained from the analysis of structural properties of the NF solution.

Within the framework of the above interpretation, assume now that the speed ω of machine i is perturbed by an amount $\omega_{\Delta 0}$, and that the speed deviation is used to modulate the excitation system of the generator i through a PSS as shown in Figure 6.1. This development can be extended without loss of generality to any other variable used to modulate the excitation and will not alter the basic premise of the approach.

It should be observed that in assessing the effect of an initial excitation on the modal oscillations, two primary dynamic loops are of interest:

1. A direct open-loop, involving the effect of the perturbation $\omega_{\Delta 0}(i)$ on the speed deviation of the *ith* machine.
2. An indirect feedback loop through control action in which the output of the PSS modifies the modal oscillation of the *ith* machine.

To assess the effect of a PSS on system behavior, both the direct and indirect loops must be accurately represented.

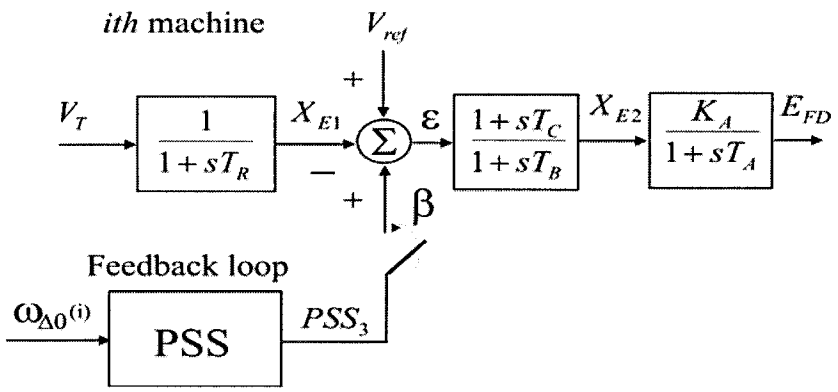

Figure 6.1 Block diagram of the excitation system with PSS

From the block diagram of the PSS, it can be clearly seen that the output of the PSS can be considered as an equivalent change in ε of magnitude $\beta = -X_{E1}$, where $\varepsilon = V_{ref} - X_{E1} + PSS_3$. A nonlinear functional relationship involving the feedback loop would be extremely difficult to obtain. Since no assumptions are made on the structure or parameters of the supplemental modulation control, a useful approximation to include the effect of the PSS is to perturb both the speed deviation of the *ith* machine and the output of the supplemental circuit. This preserves the normal form structural information thus reducing the problem to one of computation of initial conditions in NF space. By transforming the initial conditions in physical space to the NF space, a nonlinear functional relationship between the input and output of the PSS is then obtained, as explained below.

Letting

$$x_0 = [0,\cdots,0,\omega_{\Delta 0}(i),0\cdots,0,X_{E10}(i),0,\cdots,0]^T \tag{6.8}$$

the effect of excitation modulation can be estimated. Assuming that $\omega_{\Delta 0} = \alpha$, the vector of initial conditions can be written as

$$\begin{matrix} x_0 = [0,\cdots,0,\alpha,0\cdots,0,-\beta,0,\cdots,0]^T \\ \qquad\qquad\quad \uparrow \qquad\quad \uparrow \\ \qquad\qquad\quad i^{th} \qquad n^{th} \end{matrix} \tag{6.9}$$

Then the initial conditions in Jordan space become

$$\hat{y}_{j0} = y_{jo} + \Delta y_{jo} \tag{6.10}$$

where $y_{jo} = v_{ji}\alpha$, and $\Delta y_{jo} = -v_{jn}\beta$.

Further, noting that z_{jo} is given by (4.25), write

$$\hat{z}_{j0} = z_{jo} + \Delta z_{jo} \tag{6.11}$$

in which

$$\Delta z_{jo} = (-v_{jn}\beta) + \sum_{p=1}^{n}\sum_{q=p}^{n} h_{2jpq}[\alpha\beta(v_{pi}v_{qn} + v_{pn}v_{qi}) - \beta^2(v_{pn}v_{qn})] \tag{6.12}$$

Physically, Δy_{jo} and Δz_{jo}, represent corrections due to the effect of supplemental control action to open-loop initial conditions. Clearly, Δy_o and Δz_o are zero when $\beta = 0$. This suggests that the degree of excitation β could be used to assess the effect of control action on system behavior as discussed in the sequel.

Having determined initial conditions in NF space, this information can be used to estimate the contribution of the generator PSS to the modal oscillations. Substitution from (6.11) into (6.6) yields

$$\Delta\omega_i(t) = \sum_{j=1}^{n} u_{ij}(z_{j0} + \Delta z_{jo})e^{\lambda_j t} + \sum_{j=1}^{n} u_{ij}[\sum_{k=1}^{n}\sum_{l=k}^{n} u_{2ikl}(z_{k0} + \Delta z_{ko})(z_{l0} + \Delta z_{lo})e^{(\lambda_k+\lambda_l)t}] \tag{6.13}$$

Additional insight is obtained by noting that $p_{2\omega ij} = u_{ij} z_{jo}$ and $p_{2\omega ipq} = u_{2ikl} z_{po} z_{qo}$. Then, the speed deviation of machine i may be expressed as

$$\Delta\omega_i(t) = \sum_{j=1}^{n} (P_{2\omega ij} + \Delta P_{2\omega ij})e^{\lambda_j t} + \sum_{k=1}^{n}\sum_{l=k}^{n} (P_{2\omega ikl} + \Delta P_{2\omega ikl})e^{(\lambda_k+\lambda_k)t} \tag{6.14}$$

where $\Delta P_{2\omega ij} = u_{ij}\Delta z_{jo}$ and $\Delta P_{2\omega ikl} = u_{2ikl}(z_{ko}\Delta z_{lo} + z_{lo}\Delta z_{ko} + \Delta z_{ko}\Delta z_{lo})$.

In interpreting these results notice that, $P_{2\omega ij}$ and $P_{2\omega ikl}$ are the open-loop participation factors whilst $\Delta P_{2\omega ij}$ and $\Delta P_{2\omega ikl}$ provide a measure of the extent to which control actions modifies the modal oscillations.

A more meaningful interpretation of (6.14) can be obtained by defining the nonlinear PSS sensitivity indices (NPSI) $PSI_{ij} = u_{ij}\hat{z}_{j0}$ and $PSI_{ikl} = u_{2ikl}\hat{z}_{k0}\hat{z}_{l0}$. Then (6.14) may be rewritten as

$$\Delta\omega_i(t) = \sum_{k=1}^{n} PSI_{ij} e^{\lambda_j t} + \sum_{k=1}^{n}\sum_{l=k}^{n} PSI_{ikl} e^{(\lambda_k+\lambda_l)t} \tag{6.15}$$

where $PSI_{ij} = P_{2\omega ij} + \Delta P_{2\omega ij}$ and $PSI_{ikl} = P_{2\omega ikl} + \Delta P_{2\omega ikl}$.

Equation (6.15) allows the contribution of the generator PSS to be singled out and quantified. It also provides an estimate of the effect of control action on nonlinear modal interaction. By analogy to the notion of conventional nonlinear PFs, the nonlinear index PSI_{ij}, represents the second-order participation of the jth single-eigenvalue mode in the ith state when a PSS is added to machine i. Similarly, the second term PSI_{ikl} represents the second-order participation of the ith state in the mode formed by the combination of the eigenvalues λ_k and λ_l for the case with the PSS.

Compared with linear techniques, the nonlinear PSS sensitivity index provides more complete characterization of the PSS performance, especially under heavy stress conditions.

Compared with nonlinear participation factors, the nonlinear PSS sensitivity index includes both PSS input and its control effort. The best PSS location can be predicted by this index under more general conditions, especially for the case when the critical modes have large participation with the states of the exciter.

6.4 Input Value to PSS Sensitivity Index

Practical use of the above technique requires recognition of the nonlinear nature of the problem. Set $\alpha = 1.0$, this means $\alpha = 1.0 rad/\sec$. Since the input of the PSS should be the speed deviation (p.u.), α should be changed to per unit value, i.e. $\alpha/(2\pi f) = \alpha/(2*60\pi)$.

Since the nonlinear participation factor of the inter-area mode for X_{E1} expresses the participation of inter-area modes in the state X_{E1}, it also expresses the response of X_{E1} corresponding to inter-area modes when only X_{E1} is excited. Therefore, a practical value of β is estimated from

$$\beta = \alpha/(2*60\pi)*K*PF(X_{E1}) \tag{6.16}$$

where $PF(X_{E1})$ is the nonlinear participation factor of the inter-area mode for X_{E1}. K is the gain of the PSS, and it can be set to 20 as a representative value of the gain of the PSS. It must be emphasized that, when considering a wide range of operating conditions, the value of β may very widely. In some situations β will be too small, and the effect of the PSS will be ignored. In other situations β will be too large. Since normal form analysis is a local nonlinear technique, large initial values will influence the accuracy of the results. Hence the value of β should be limited to a range such as, for example, 0.01 to 1.0. If the smallest β among all the generators is smaller than 0.01, it can be set to 0.01 and the values of β for the other generators is then normalized to this smallest β. If, on the other hand, β is larger than 1.0, it can be set to 1.0. It has been found that this basic technique works well for practical studies.

6.5 Numerical Considerations

The computation of nonlinear sensitivity indices requires the calculation of initial conditions in different coordinate frames. Given an initial excitation x_o, the initial conditions in normal form space can be estimated using (4.15).

Alternatively, for a given x_o, a better approximation of initial conditions in normal form space can be obtained from (4.13) by solving the set of nonlinear algebraic equations

$$\min_{z_o} (z_o + h_2(z_o) - V x_o)^2 \tag{6.17}$$

Reference [56] provides a more detailed account of the numerical implementation of this algorithm. Analytical formulations have the advantage of providing a more in-depth analysis of structural factors influencing the initial conditions in NF space. On the other hand numerically-constructed formulations based on (6.17), may yield a more

accurate estimate of the initial conditions.

Judicious choice of the initial excitation is a key step in obtaining meaningful results. The importance of these indices is discussed in the section on numerical studies.

6.6 PSS Model and Effect of Control Action on Modal Interactions

6.6.1 Nonlinear Participation Factors with PSS

Using the nonlinear functional relationships involving the feedback loop being obtained in section 3.3

$$\dot{\tilde{x}} = \tilde{f}(\tilde{x}) = A\tilde{x} + \tilde{X}_2 + \tilde{X}_3 + \ldots \tag{6.18}$$

the nonlinear participation factors with PSS can be derived.

The vector of initial conditions can be written as

$$\tilde{x}_0 = [0,\cdots,0,\alpha,0\cdots,0]^T \quad \begin{matrix} \uparrow \\ i^{th} \end{matrix} \tag{6.19}$$

Then, the initial conditions in Jordan space become

$$\tilde{y}_{j0} = \tilde{v}_{ji}\alpha \tag{6.20}$$

Furthermore, noting that $\tilde{z}_{jo}$ is given by (4.16), write

$$\tilde{z}_{jo} = \tilde{y}_{jo} - \sum_{p=1}^{N}\sum_{q=1}^{N} \tilde{h}_{2jpq}\tilde{y}_{p0}\tilde{y}_{q0} = \tilde{v}_{ji} + \tilde{v}_{2jii} \qquad j = 1,\ldots,N \tag{6.21}$$

where $\tilde{y}_{jo} = \tilde{v}_{ji}$, $\tilde{v}_{2jii} = -\sum_{p=1}^{N}\sum_{q=1}^{N}\tilde{h}_{2jpq}\tilde{y}_{p0}\tilde{y}_{q0} = -\sum_{p=1}^{N}\sum_{q=1}^{N}\tilde{h}_{2jpq}\tilde{v}_{pi}\tilde{v}_{qi}$, and N is number of states representing the new system.

With initial values $\tilde{x}_0$, the time-domain evolution in physical space can be expressed by

$$\tilde{x}_i(t) = \sum_{j=1}^{N} p_{2ij}e^{\tilde{\lambda}_j t} + \sum_{k=1}^{N}\sum_{l=1}^{N} p_{2ikl}e^{(\tilde{\lambda}_k + \tilde{\lambda}_l)t} \tag{6.22}$$

where

$$p_{2ij} = \tilde{u}_{ij}(\tilde{v}_{ji} + \tilde{v}_{2jii}) = p_{2ij_L} + p_{2ij_{NL}},\ p_{2ikl} = \tilde{u}_{2ikl}(\tilde{v}_{ki} + \tilde{v}_{2kii})(\tilde{v}_{li} + \tilde{v}_{2lii})$$

and $\tilde{u}_{2ikl} = \sum_{j=1}^{n} \tilde{u}_{ij}\tilde{h}_{2jkl}$, $\tilde{v}_{2mii} = -\sum_{p=1}^{N}\sum_{q=1}^{N} \tilde{h}_{2mpq}\tilde{v}_{pi}\tilde{v}_{qi}$, $m = k,l$.

For this closed-loop system, the first term in (6.22), p_{2ij}, represents the second-order participation of the *jth* single-eigenvalue mode in the *ith* state, and the second term p_{2ikl} represents the second-order participation of the *ith* state in the mode formed by the combination of the eigenvalues $\tilde{\lambda}_k$ and $\tilde{\lambda}_l$. $p_{2ij_L} = \tilde{u}_{ij}\tilde{v}_{ji}$ is the linear PF and $p_{2ij_{NL}} = \tilde{u}_{ij}\tilde{v}_{2jii}$ is obtained by including second-order information, becoming a correction term to the linear participation.

6.6.2 Effect of Control Action on Modal Interaction

To assess the effect of supplemental control on modal interaction define the nonlinearity index for mode j based on the definition presented in 4.5.

$$II^1(j) = \left|\frac{\max_{k,l} \tilde{h}_{2jkl}\tilde{z}_{k0}\tilde{z}_{l0}}{\tilde{z}_{j0}}\right|,\ II^2(j) = \left|\frac{\sec\_\max_{k,l} \tilde{h}_{2jkl}\tilde{z}_{k0}\tilde{z}_{l0}}{\tilde{z}_{j0}}\right|,$$

$$II^3(j) = \left|\frac{third\_\max_{k,l} \tilde{h}_{2jkl}\tilde{z}_{k0}\tilde{z}_{l0}}{\tilde{z}_{j0}}\right| ,\ \ldots \qquad (6.23)$$

where $\sec\_\max_{k,l} \tilde{h}_{2jkl}\tilde{z}_{k0}\tilde{z}_{l0}$ and $third\_\max_{k,l} \tilde{h}_{2jkl}\tilde{z}_{k0}\tilde{z}_{l0}$ are the complex form when the second and the third largest values of $|\tilde{h}_{2jkl}\tilde{z}_{k0}\tilde{z}_{l0}|$ $(k = 1:n,\ l = k:n)$ occurs.

This expression enables an assessment of the extent to which modal interaction of dominant modes is being affected by modulation control of the excitation system.

Compared with linear techniques, the combined use of PSS sensitivity index and modal interaction measures provides a complete characterization of control action on

system performance, especially under heavy stress conditions.

7 CASE STUDY

7.1 Test System – IEEE 4-machine System

The developed procedures will be applied to the 2-area, 4-machine test system from [25], modified to reflect different operating conditions. Figure 7.1 shows a single-line diagram of the system under investigation.

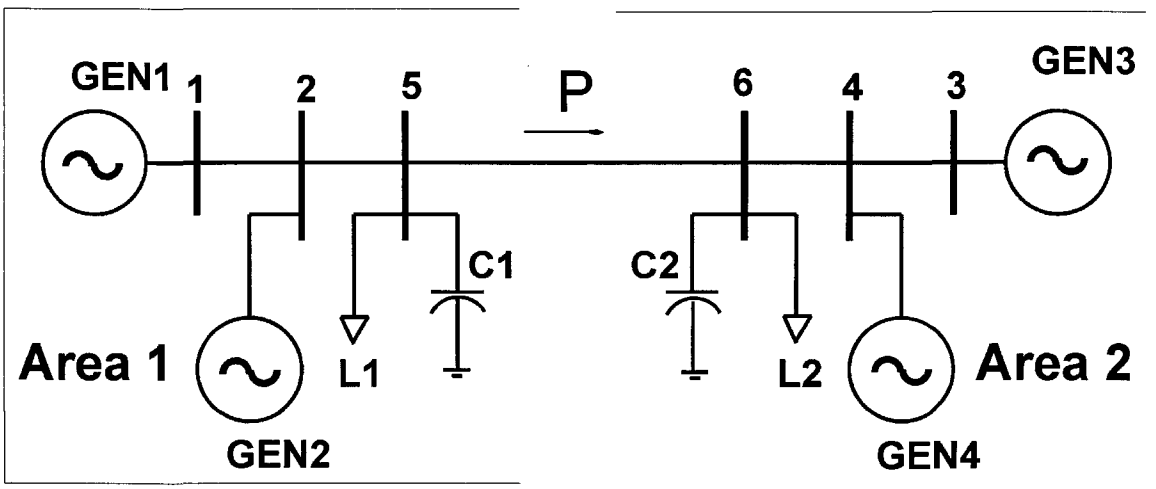

Figure 7.1 Schematic of the study system

For this study, all generators are represented by a fourth-order *d-q* axis model and equipped with an exciter. Loads are modeled as constant impedances. The generator data and system parameters are given in the Appendix A.

7.1.1 Simulated Conditions

An ample range of operating conditions was simulated to fully characterize nonlinear behavior and modal interaction. To stress the system, the load in Area 2 was increased in discrete steps. The load in Area 1 was then modified to achieve a given tie line power transfer.

From this analysis, the following three main operating scenarios to investigate the presence of nonlinear modal interaction were examined: a low-stress case with a 180 MW power transfer between the interconnected areas, a high-stress case obtained by

increasing the level of power transfer to about 410 MW, and an intermediate condition between the first two. Table 7.1 summarizes the operating conditions for these three operating conditions.

Table 7.1 Summary of operating conditions

Operating scenario	Power transfer (MW)	Load Area 1 (MW)	Load Area 2 (MW)
I	180	1120	1180
II	380	920	1380
III	410	890	1410

7.1.2 Linear Analysis

For each operating scenario, detailed eigenvalue-based studies were conducted, with the results providing a basis for comparison with the NF results in subsequent sections. Tables 7.2 to 7.4 show selected modes together with their associated frequency of oscillation, damping ratio, and most dominant states. The two-area system exhibits three electromechanical modes of interest for this study; one oscillatory mode involving the exchange of oscillating energy between Areas 1 and 2 (mode 7 for Scenario I, and mode 9 for Scenario II, III), and two local modes associated with the local dynamics between generators in each area (modes 1 and 3).

Table 7.2 Oscillatory modes of the system – operating scenario I

Mode #	Eigenvalue	Freq. (Hz)	Damping (%)	Dominant states
1,2	-1.113±j7.73	1.23	14.25	Local, Area 1(δ_1, δ_2)
3,4	-1.812±j7.45	1.185	23.64	Local, Area 2 (δ_3, δ_4)
5,6	-0.300±j0.45	0.072	55.22	Controls, GEN1, GEN2
7,8	**-0.427±j3.01**	**0.479**	**14.02**	**Inter-area($\delta_1, \delta_2, \delta_3, \delta_4$)**
9,10	-1.300±j1.12	0.178	75.71	$E'_{d1}, E'_{d2}, E'_{d3}, E'_{d4}, \delta_1, \delta_3, \delta_4$
11,12	-0.945±j1.02	0.162	67.98	E'_{q4}, Exciter GEN4

Table 7.3 Oscillatory modes of the system – operating scenario II

Mode #	Eigenvalue	Freq. (Hz)	Damping (%)	Dominant states
1,2	-1.143±j7.76	1.235	14.58	Local, Area 1(δ_1, δ_2)
3,4	-1.809±j7.54	1.200	23.33	Local, Area 2(δ_3, δ_4)
5,6	-3.685±j0.10	0.016	99.96	$E'_{q1}, E'_{q2}, E'_{q3}, E'_{q4}$
7,8	-1.194±j2.10	0.335	49.39	$E'_{d4}, \omega_4, \delta_4, \omega_3, \delta_3$
9,10	**-0.309±j1.62**	**0.258**	**18.75**	**Inter-area($\delta_1, \delta_2, \delta_3, \delta_4$)**
11,12	-1.071±j0.70	0.116	83.67	Controls unit GEN4

Table 7.4 Oscillatory modes of the system – operating scenario III

Mode #	Eigenvalue	Freq. (Hz)	Damping (%)	Dominant states
1,2	-1.154±j7.72	1.229	14.79	Local, Area 1(δ_1, δ_2)
3,4	-1.802±j7.53	1.199	23.27	Local, Area 2(δ_3, δ_4)
5,6	-3.768±j0.38	0.060	99.50	$E'_{q1}, E'_{q2}, E'_{q3}, E'_{q4}$
7,8	-1.483±j2.09	0.332	57.92	$E'_{d4}, \omega_4, \delta_4, \omega_3, \delta_3$
9,10	**-0.058±j1.31**	**0.209**	**4.40**	**Inter-area($\delta_1, \delta_2, \delta_3, \delta_4$)**
11,12	-1.047±j0.65	0.103	85.08	Controls unit GEN4

Attention in the following analysis is particularly focused on the analysis of nonlinear interaction involving modes 7 and 9. For a certain range of operating conditions, nonlinear coupling of these modes gives rise to complex dynamic behavior involving near first-order resonance and second-order resonance conditions. In the following the strength of these nonlinear interactions in power system behavior will be examined, and their effect on system dynamic performance and problems of control placement and design estimated.

7.1.3 Assessment of Nonlinear Modal Interaction

To quantify the extent to which modes interact nonlinearly, use the interaction index (II), $II(j) = \max_{k,l} | h_{2jkl} z_{k0} z_{l0} / z_{j0} |$, defined in previous work [7]. Tables 7.5 to 7.7 show the interaction indices involving the main modes of concern.

Table 7.5 Nonlinear interaction indices for key modes – operating scenario I

Mode j	II(j)	Mode k	Mode l
1	2.378	1	10
3	4.589	3	10
5	0.354	11	12
7	3.038	11	12
	2.774	11	11
	1.781	9	11
	1.583	7	12
9	2.790	11	12

Table 7.6 Nonlinear interaction indices for key modes – operating scenario II

Mode j	II(j)	Mode k	Mode l
1	5.225	1	12
3	5.643	3	11
5	11.00	5	11
7	8.320	11	11
9	64.09	11	12
	62.87	11	11
	50.37	5	11
	46.10	6	12

Analysis of interaction indices indicates that modes 7 and 9 interact strongly with

mode (11, 12) and to a lesser extent between themselves. Comparing the results in Table 7.5 with those in Table 7.7, it can be seen that for scenario III the magnitude of nonlinear modal interaction increases significantly indicating the importance of nonlinear effects.

Table 7.7 Nonlinear interaction indices for key modes – operating scenario III

Mode j	II(j)	Mode k	Mode l
1	8.04	1	12
3	12.89	11	12
5	9.83	11	12
7	18.24	11	11
9	94.40	11	12
	82.03	11	11
	49.05	12	12
	24.91	7	11

Of particular relevance, a more detailed analysis of these indices in Table 7.7 shows that the system exhibits multiple near second-order frequency resonance conditions in which the frequency sum of two of the modes ($\omega_k + \omega_l$) is close to the frequency of a third mode, ω_j . Namely $|\omega_{11} + \omega_{11} - \omega_9| = 0.003\text{Hz}$, and $|\omega_7 + \omega_{12} - \omega_9| = 0.020Hz$.

In an effort to fully understand the nature of modal interaction leading to strong nonlinear behavior, the trajectory of the system was analyzed for various operating conditions near those of the operating scenarios. Figure 7.2 shows the behavior of mode 9 and mode 7 as a function of system stress. Also of interest, Figure 7.3a) gives the second-order resonance condition for the mode combinations 9,11,11 and 9,7,11 as a function of the inter-tie real power transfer.

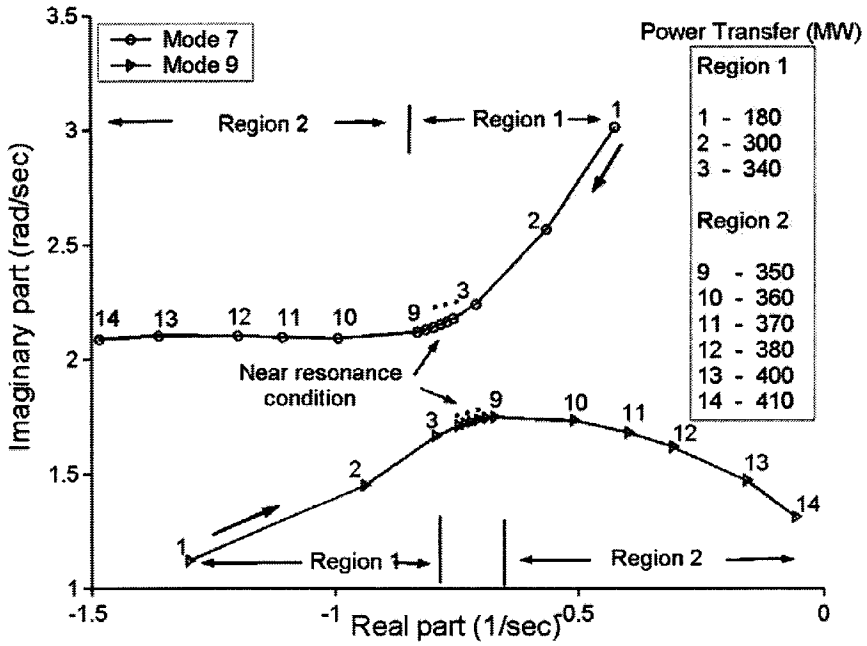

a) Eigenvalue movement

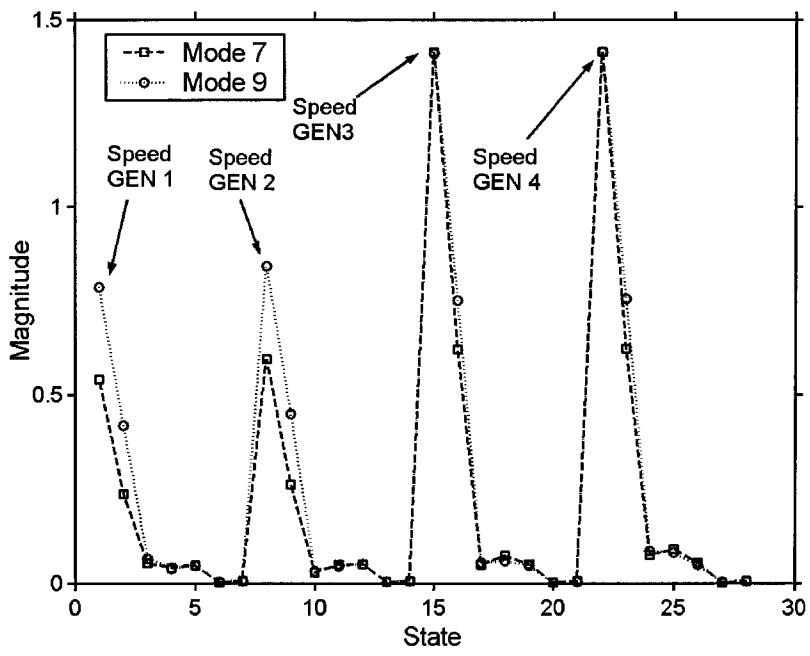

b) Magnitude of right eigenvectors close to first order resonance

Figure 7.2 Schematic illustrating near first order resonance conditions

For the purpose of reference and discussion, the operating space is subdivided into two main stability regions. Region 1 starts at 180 MW, whilst Region 2 depicts the nonlinear behavior near the second-order resonance in the vicinity of scenario II. Region

2 is the most relevant to system analysis since it captures both, first order and second-order resonance of the critical modes. Analysis results in Figure 7.2a), show that as the system is stressed, mode 9 and mode 7 move closer together; a near strong first-order resonance condition is seen to occur at about 350 MW, at which point the damping and frequency of these modes are very close[1]. At this critical point, the right eigenvectors are aligned as shown in Figure 7.2b), thus indicating that both modes have a similar dynamic pattern.

The analysis also suggests that nonlinear effects become important when the system approaches first order resonance. As the system is gradually stressed, the analysis of Region 1 in Figure 7.3a) clearly shows that the frequency resonance conditions $|\omega_7 + \omega_{12} - \omega_9|$, $|\omega_{11} + \omega_{11} - \omega_9|$ drop sharply until a first-order near-resonance condition is met.

As the system is stressed further through resonance, the frequency resonance conditions increase and then decrease sharply near operating scenario II. The damping of mode 7 increases while that of mode 9 decreases. Accordingly, the second-order resonance conditions $|\lambda_7 + \lambda_9 - \lambda_{11}|$, and $|\lambda_9 + \lambda_{11} - \lambda_{12}|$, $|\lambda_9 + \lambda_{11} - \lambda_{11}|$ begin to decrease slowly in the beginning and then drop rapidly for transmission levels in excess of 410 MW (refer to Figure 7.3b)).

This phenomenon leads to complex behavior and has profound implication with respect to the analysis and interpretation of local results near the onset of first and second-order resonances. For operating conditions in Region 1 far from the first order resonance, linear estimates are consistent with NF results. In contrast, NF results lead to a significant improvement in the description of system dynamic behavior for operating scenarios close to linear resonance and within Region 2.

---

[1] If there are two eigenvectors corresponding to a double eigenvalue, the interaction is called weak. In contrast, if there exists only one eigenvector associated with a double eigenvalue the interaction is called strong [64].

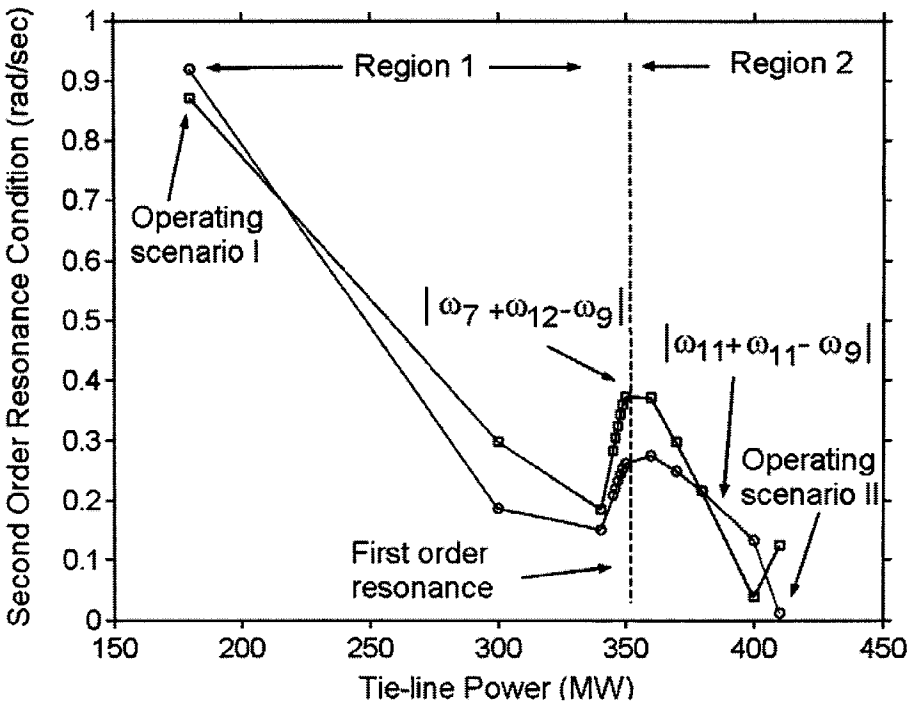

a) Second-order (frequency) resonance condition, $|\omega_k + \omega_l - \omega_j|$

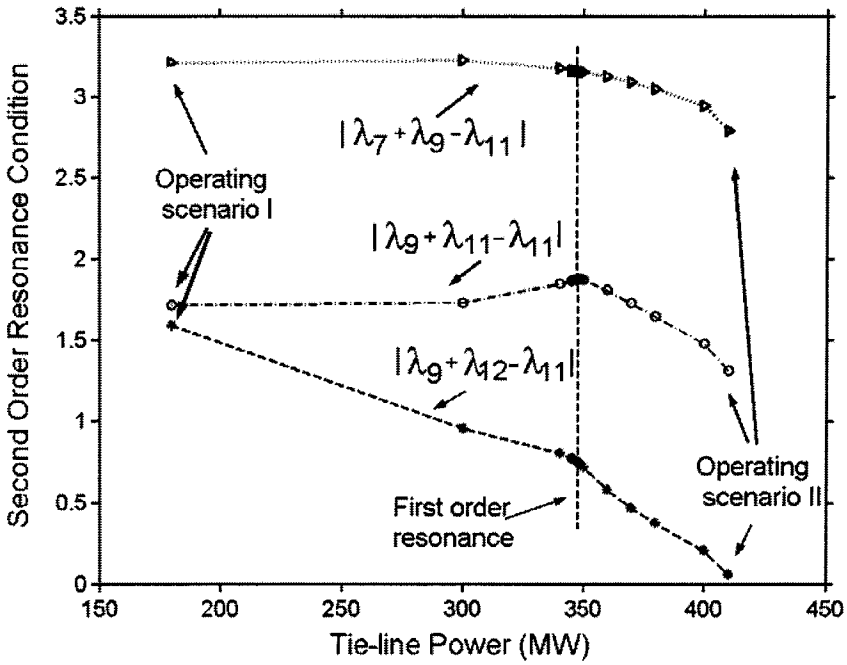

b) Second-order resonance condition, $|\lambda_k + \lambda_l - \lambda_j|$

Figure 7.3 Variation of resonance conditions with system stress

7.1.4 Siting of Controllers; Linear Approach

Conventional analysis techniques were used to site power system stabilizers (PSSs) to enhance damping of the inter-area mode 7 in scenario I and the inter-area mode 9 in scenarios II and III.

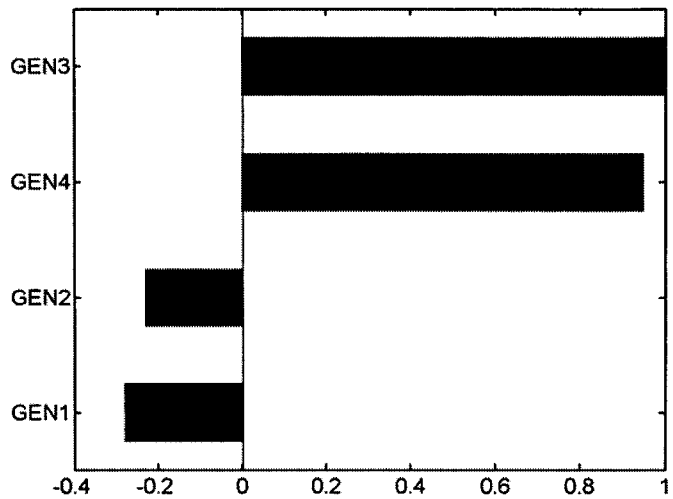

a) Mode shapes

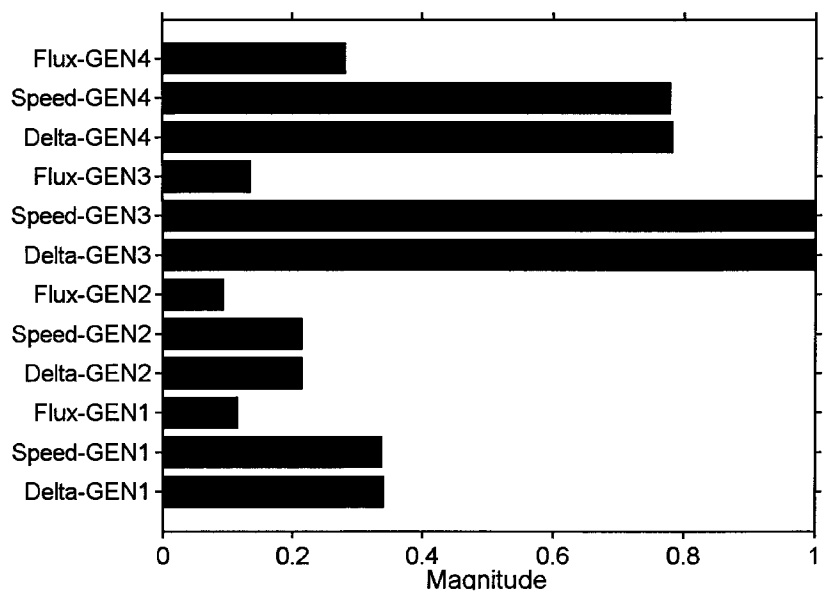

b) Linear participation factors

Figure 7.4 Linear participation factors and mode shapes for inter-area mode 7 - Operating scenario I

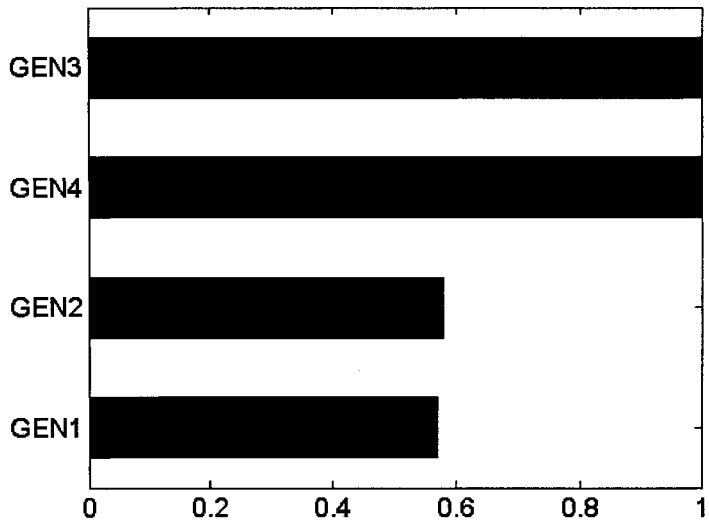

a) Mode shapes

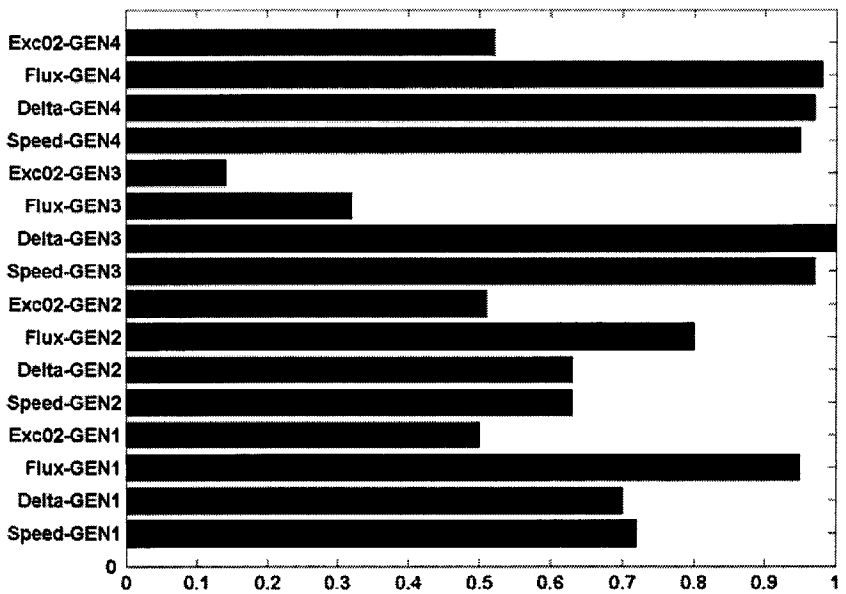

b) Linear participation factors

Figure 7.5 Linear participation factors and mode shapes for inter-area mode 7 - Operating scenario II

Figures 7.4 to 7.6 show linear participation factors and mode shapes for the inter-area modes obtained using the SSAT [65] software. Values are normalized with respect to the largest component.

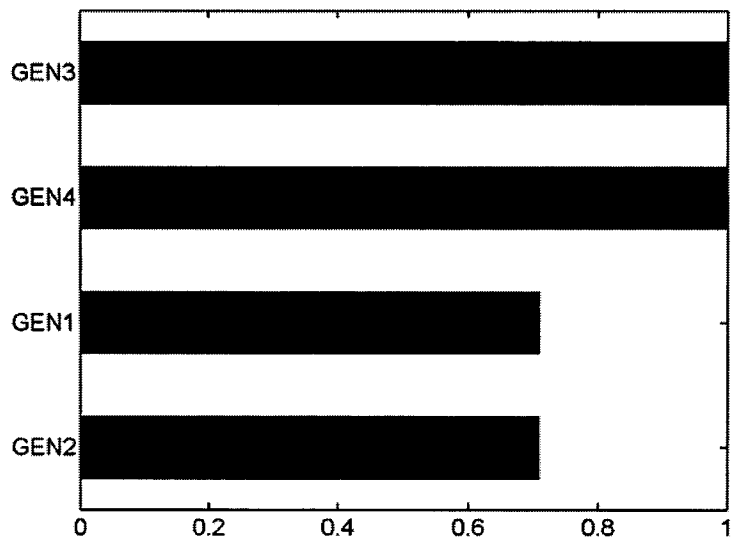

a) Mode shapes

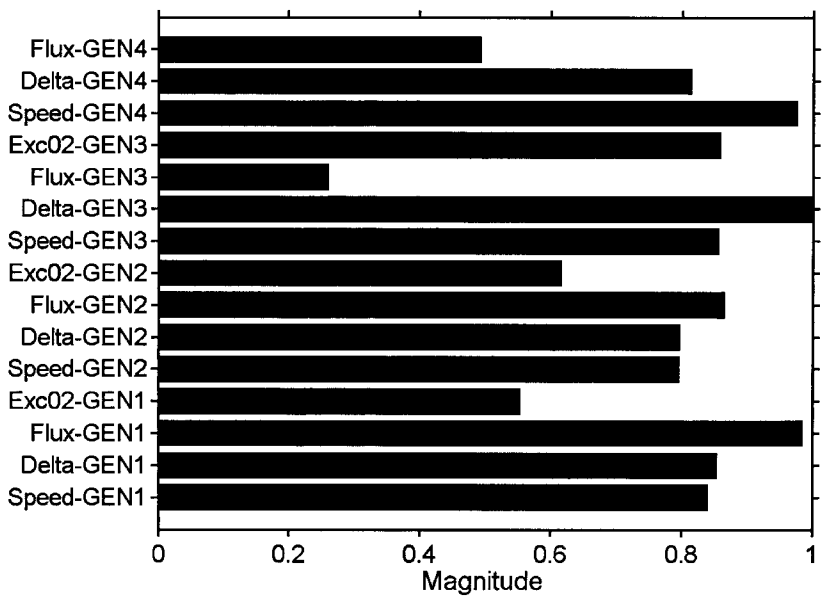

b) Linear participation factors

Figure 7.6 Linear participation factors and mode shapes for inter-area mode 9 - Operating scenario III

Table 7.8 Linear participation factors for inter-area modes

Machine	Operating scenario I	Operating scenario II	Operating scenario III
GEN1	0.3419 (3)	0.7384 (3)	0.9787 (3)
GEN2	0.2170 (4)	0.6537 (4)	0.9257 (4)
GEN3	**1.0000 (1)**	**1.0000 (1)**	0.9976 (2)
GEN4	0.8682 (2)	0.9844 (2)	**1.0000 (1)**

Table 7.8 shows the speed-based linear speed-participation factors for the inter-area modes. Values are normalized with respect to the largest components. The analysis of linear participation factors for scenarios I, II, and III identifies GEN3 and GEN4 in Area 2 as the best locations at which to place PSSs. GEN3 has the largest participation for scenario I and II whilst GEN4 has the largest participation for scenario III. Mode shapes results in Figures 7.4a), 7.5a), and 7.6a) are in good agreement with the analysis of participation factors.

Table 7.9 Residues for inter-area modes

Machine	Operating scenario I	Operating scenario II	Operating scenario III
GEN1	0.2807 (3)	0.5462 (3)	0.7269 (3)
GEN2	0.1942 (4)	0.5479 (2)	0.7295 (2)
GEN3	0.4313 (2)	0.2903 (4)	0.2824 (4)
GEN4	**1.0000 (1)**	**1.0000 (1)**	**1.0000 (1)**

Table 7.9 shows the transfer-function residues for the inter-area modes. Values are normalized with respect to the largest components. The analysis of residues for scenarios I, II, and III identifies GEN4 in Area 2 as the best location at which to place PSSs.

7.1.5 Placement of Controllers Using Nonlinear Participation Factors

The approach outlined above was used to determine nonlinear participation

factors (PFs). To provide a basis of comparison with the results obtained from linear analysis, the speed deviations of system generators were expressed in the form

$$\Delta\omega_i(t) = \sum_{j=1}^{n} u_{ij} z_{jo} e^{\lambda_j t} + \sum_{j=1}^{n} u_{ij} \sum_{k=1}^{n} \sum_{l=k}^{n} h_{2i_{kl}} z_{ko} z_{lo} e^{(\lambda_k+\lambda_l)t}, i = 1,2,3,4 \qquad (7.1)$$

For these states, analytical (From (4.26)) and numerical estimates (From (4.27)) of nonlinear mode-state participations were derived. Figures 7.7 to 7.9 show the top 12 participation factors for machines in the system as a function of the interacting modes. In these plots, the horizontal axis gives the mode (λ_j) or mode combination ($\lambda_k + \lambda_l$) participating in the state, while the vertical axis gives the associated magnitude.

Additionally, numerical estimates for nonlinear participation factors were derived using the procedure outlined in 4.4 and were subsequently used to determine the best location for PSSs. Tables 7.10 to 7.12 show the speed-based nonlinear participation factors computed using these approximations. For comparison, analytical estimates of nonlinear participation factors from (4.26) are also included.

For scenario I, the analysis of participation factors in Figure 7.7 identifies machines in Area 2 as the best places to install PSSs in order to enhance the damping of mode 7. GEN3 has the largest participation in this mode. For Area 1 the analysis of nonlinear participation factors in Figures 7.7a) and 7.7b) shows the presence of local mode 1 and to a lesser extent the inter-area mode 7. In contrast, the analysis of nonlinear participation factors for Area 2 shows that the participation of mode 7 relative to the local mode increases, so the results of this analysis suggest that Area 2 is a better option to place PSSs. These results are in good agreement with linear participation factors in Figure 7.4b).

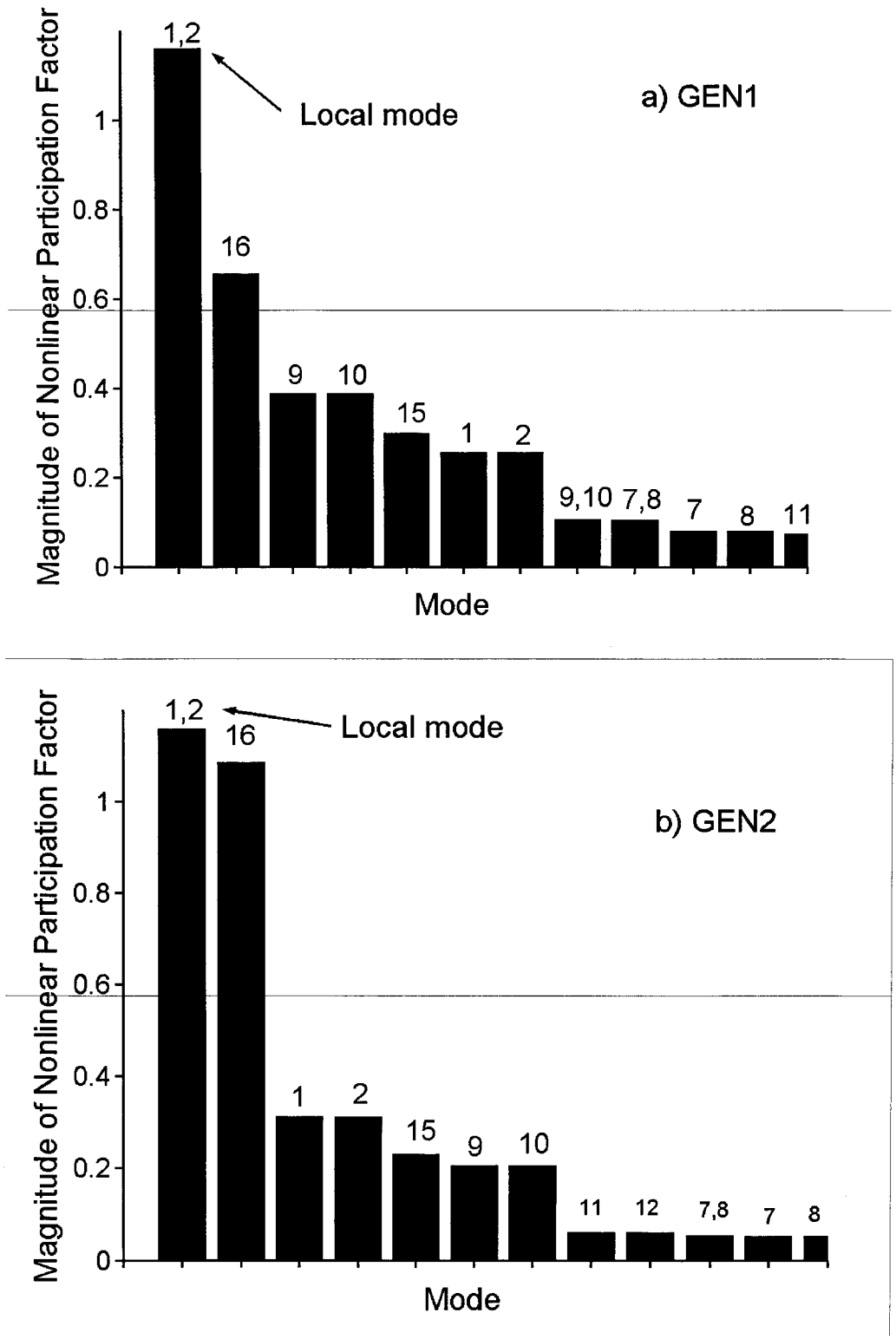

Figure 7.7 Analytical estimates of nonlinear speed PFs - Operating scenario I

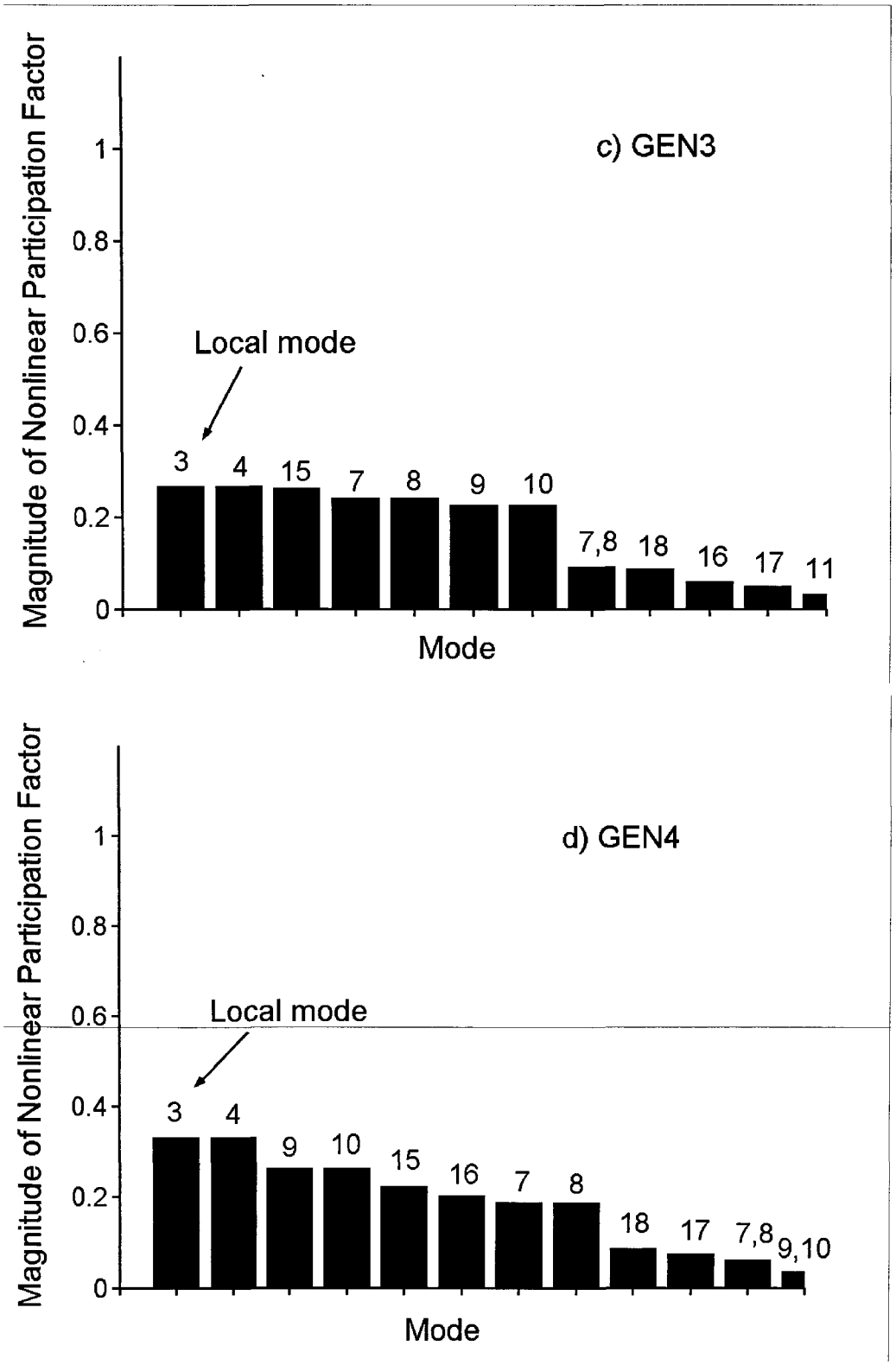

Figure 7.7 (Continued)

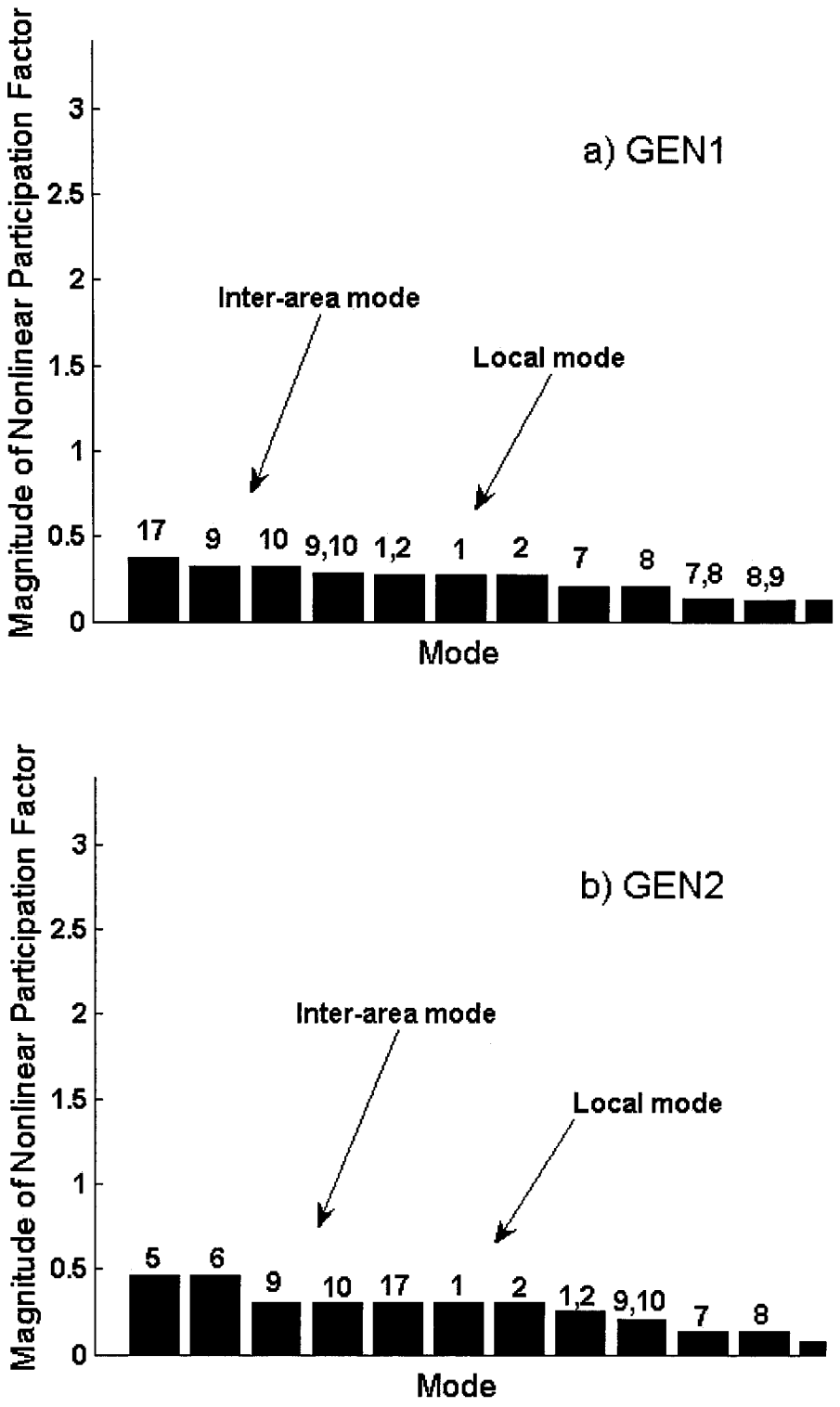

Figure 7.8 Analytical estimates of nonlinear speed PFs - Operating scenario II

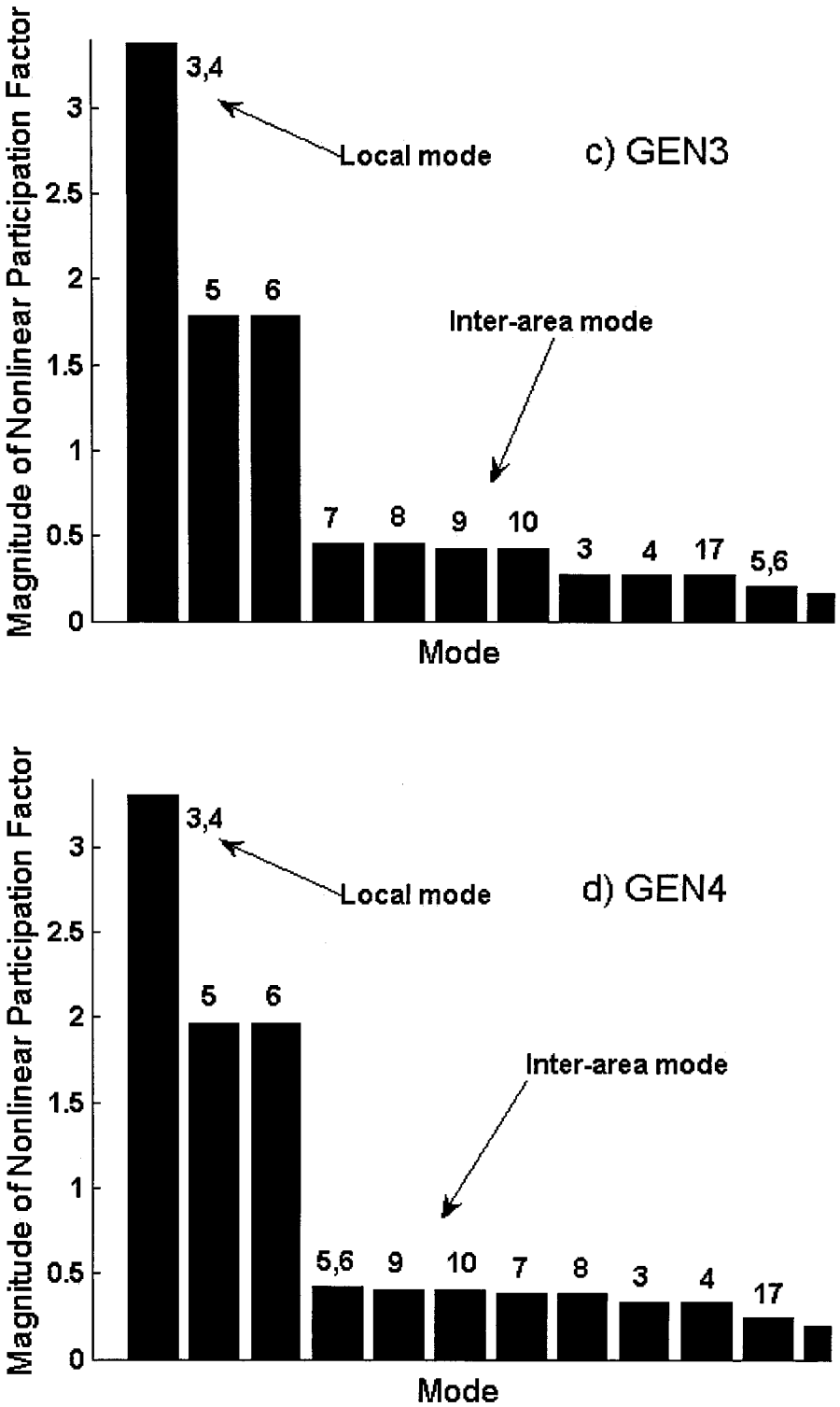

Figure 7.8 (Continued)

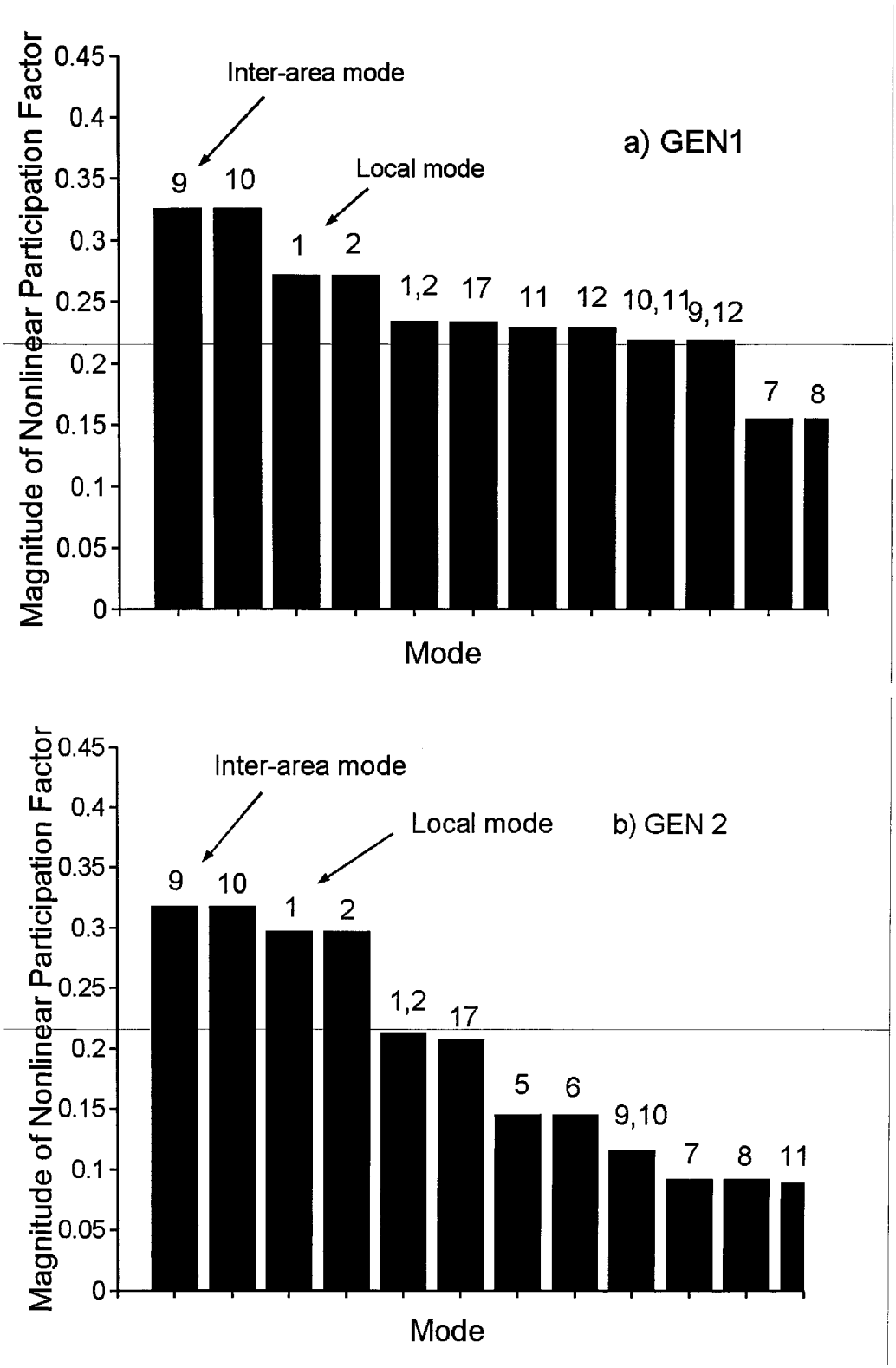

Figure 7.9 Analytical estimates of nonlinear speed PFs - Operating scenario III

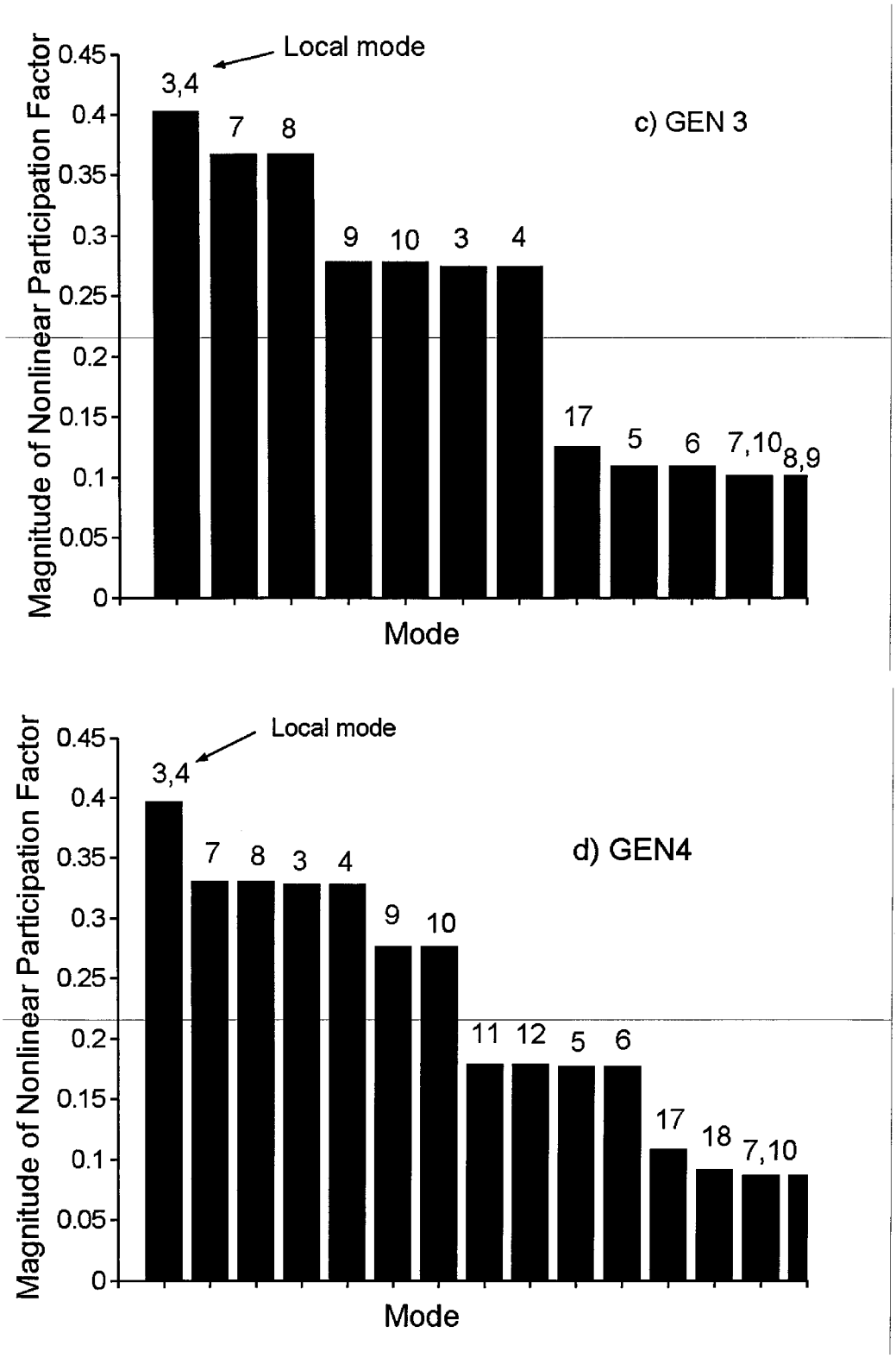

Figure 7.9 (Continued)

As system stress is increased in scenario II, the analysis of participation factors in

Figure 7.8 identifies machines in Area 2 as the best places to install PSSs in order to enhance the damping of inter-area mode 9. GEN3 has the largest participation in this mode. But for Area 1 the analysis of nonlinear participation factors in Figure 7.8a) and 7.8b) shows the presence of inter-area mode 9 and to a lesser extent local mode 1. For Area 2 the analysis of nonlinear participation factors shows that the participation of mode 9 relative to the local mode decreases.

As system stress is increased in scenario III, the analysis of nonlinear participations for machines in Area 1 in Figure 7.9a) shows a dominant presence of inter-area mode 9 suggesting that Area 1 is the best place to install PSSs. By contrast, the analysis of machines in Area 2 indicates the presence of local mode 3 followed by the presence of mode 7 and to a lesser extent inter-area mode 9. Contrary to the result for linear participations in Figure 7.6b), nonlinear participations suggest that Area 1 is a better alternative in which to use PSSs. Furthermore, the large participation of modes (3,4), (7, 8) and (11, 12) in the speed deviations of GEN3 and GEN4 for scenario III suggests a potential for undesirable nonlinear modal interaction arising from coupling between control modes and the inter-area mode (see Figure 7.9c) and 7.9d)). The complexity of this behavior can be appreciated by noting that, for scenario III, the flux deviation (E'_{q4}) of GEN4 has the largest linear participation in mode 7. In turn, the analysis of mode 9 in Figure 7.6b) shows that angle deviation of GEN3 has the largest participation (1.00) followed by the flux state of GEN1 (0.984). Furthermore, the analysis of mode 11 reveals that the state associated with the second block of the AVR of GEN4 has the largest participation in mode 11. This strong participation of electromechanical and voltage states in mode 9 suggests that both voltage control support and PSSs might be used to enhance damping of the modes and, additionally, that control action at GEN4 may interact unfavorably with the mode. Attention here is restricted to the use of PSSs.

For scenario I, comparison of nonlinear participation factors in Table 7.10 confirms that GEN3 is the best candidate to be equipped with PSS, while numerical

estimates for scenario III in Table 7.12 single out GEN2 as the best option. For scenario II, analytical and numerical nonlinear participation factors in Table 7.11 suggest differing areas for placement of a PSS to enhance damping of the inter-area mode. The analytical estimate shows GEN3 in Area 2 is the best PSS location, while the numerical estimate suggests GEN1 in Area 1 is the best location at which to place a PSS.

Table 7.10 Comparison of speed nonlinear PFs p_{2ij} of mode 7 – operating scenario I

Machine	Analytical estimate / Ranking	Numerical estimate / Ranking
GEN1	0.0811 (3)	0.0793 (3)
GEN2	0.0519 (4)	0.0495 (4)
GEN3	**0.2415** (1)	**0.2423** (1)
GEN4	0.1868 (2)	0.1883 (2)

Table 7.11 Comparison of speed nonlinear PFs p_{2ij} of mode 9 – operating scenario II

Machine	Analytical estimate / Ranking	Numerical estimate / Ranking
GEN1	0.3271 (3)	**0.5027** (1)
GEN2	0.3078 (4)	0.4095 (2)
GEN3	**0.4177** (1)	0.2358 (3)
GEN4	0.4049 (2)	0.2314 (4)

Table 7.12 Comparison of speed nonlinear PFs p_{2ij} of mode 9 – operating scenario III

Machine	Analytical estimate / Ranking	Numerical estimate / Ranking
GEN1	**0.3257** (1)	0.3170 (2)
GEN2	0.3174 (2)	**0.3407** (1)
GEN3	0.2786 (3)	0.2845 (3)
GEN4	0.2765 (4)	0.2794 (4)

Based on these results, detailed nonlinear studies were conducted to identify the underlying mechanisms leading to resonance and the assessment of its impact on the

location of system controllers.

Tables 7.13 to 7.15 show the nonlinear speed-participation factors and control-participation factors for the inter-area modes. The analysis of nonlinear speed-participation factors identifies GEN3 in area 2 as the best location to place PSSs for scenario I, and II. GEN1 in area 1 is identified as the best location to place PSSs for scenario III.

The analysis of nonlinear control-participation factors shows that the largest speed participation factor is of the same order of magnitude as the largest participation factor of state Xe_1 for scenario I. By contrast, the largest speed PF for operating scenario II and III is much smaller than the largest participation factor of state Xe_1. In order to determine input values for the PSS sensitivity index, the magnitude of participation of the inter-area mode to state Xe_1 should be considered as discussed above.

Table 7.13 Nonlinear participation factors – operating scenario I

Machine	ω		Xe_1	
	Original	Normalized	Original	Normalized
GEN1	0.08114 (3)	0.3359 (3)	0.06075 (3)	0.1962 (3)
GEN2	0.05192 (4)	0.2149 (4)	**0.30960 (1)**	**1.0000 (1)**
GEN3	**0.24155 (1)**	**1.0000 (1)**	0.02705 (4)	0.0874 (4)
GEN4	0.18689 (2)	0.7737 (2)	0.13660 (2)	0.4412 (2)

Table 7.14 Nonlinear participation factors – operating scenario II

Machine	ω		Xe_1	
	Original	Normalized	Original	Normalized
GEN1	0.32714 (3)	0.7831 (3)	1.47917 (2)	0.2177 (2)
GEN2	0.30780 (4)	0.7368 (4)	**6.79409 (1)**	**1.0000 (1)**
GEN3	**0.41773 (1)**	**1.0000 (1)**	0.11871 (4)	0.0175 (4)
GEN4	0.40409 (2)	0.9673 (2)	0.70660 (3)	0.1040 (3)

Table 7.15 Nonlinear participation factors – operating scenario III

Machine	ω		Xe_1	
	Original	Normalized	Original	Normalized
GEN1	**0.32579 (1)**	**1.0000 (1)**	1.2259 (2)	0.1491 (2)
GEN2	0.31749 (2)	0.9745 (2)	**8.2242 (1)**	**1.0000 (1)**
GEN3	0.27863 (3)	0.8552 (3)	0.0614 (4)	0.0075 (4)
GEN4	0.27652 (4)	0.8488 (4)	0.4086 (3)	0.0497 (3)

7.1.6 Nonlinear PSS Sensitivity Index

Tables 7.16 to 7.18 show the normalized PSS Sensitivity Indices for the inter-area modes. In contrast to conventional techniques, the analysis of nonlinear PSS Sensitivity Index identifies GEN3 as the best PSS location for scenario I and GEN2 as the best location at which to place PSSs for scenarios II and III.

Table 7.16 PSS sensitivity index with mode 7 – operating scenario I

Machine	α	β	PSI
GEN1	1.0	0.0229	0.2904 (3)
GEN2	1.0	0.1171	0.0838 (4)
GEN3	**1.0**	**0.0100**	**1.0000 (1)**
GEN4	1.0	0.0514	0.4764 (2)

Table 7.17 PSS sensitivity index with mode 9 – operating scenario II

Machine	α	β	PSI
GEN1	1.0	0.1246	0.0196 (2)
GEN2	**1.0**	**0.5721**	**1.0000 (1)**
GEN3	1.0	0.0100	0.0085 (4)
GEN4	1.0	0.0595	0.0151 (3)

Table 7.18 PSS sensitivity index with mode 9 – operating scenario III

Machine	α	β	PSI
GEN1	1.0	0.0650	0.0157 (2)
GEN2	**1.0**	**0.4363**	**1.0000 (1)**
GEN3	1.0	0.033	0.0066 (4)
GEN4	1.0	0.0217	0.0080 (3)

7.1.7 Effect of PSSs on System Behavior

To verify the effects of nonlinear behavior on the analysis and design of controllers, PSSs were designed using the approach described in [39, 66]. In this analysis a PSS was designed considering one machine location at a time. Figure 7.10 shows the block diagram of the PSS. The parameters for the designed PSSs are shown in Tables 7.19 and 7.20.

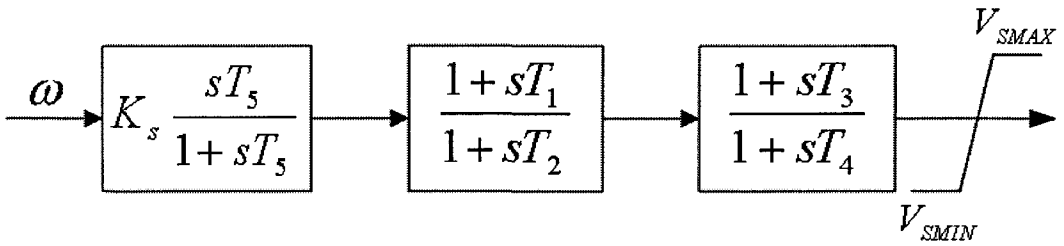

Figure 7.10 Block diagram of the PSS (IEEE Type PSS1A)

Table 7.19 Parameters for the designed PSSs – operating scenario I

PSS location	T_1	T_2	T_3	T_4	T_5	V_{SMAX}	V_{SMIN}
GEN1	0.1	0.01	0.9	0.07	13	0.1	-0.1
GEN2	0.1	0.03	1.5	0.03	10	0.1	-0.1
GEN3	0.1	0.05	1.3	0.03	10	0.1	-0.1
GEN4	0.3	0.05	0.18	0.03	3.0	0.1	-0.1

Table 7.20 Gain for the designed PSSs

PSS location	Scenario I	Scenario II	Scenario III
GEN1	20.0	10.0	2.0
GEN2	20.0	10.0	2.0
GEN3	20.0	10.0	1.4
GEN4	20.0	5.0	1.0

Figures 7.11 to 7.13 show the phase characteristics of generators in different scenarios and including the properly designed PSSs. For all three scenarios, the phase characteristics of properly designed PSSs have appropriate phase compensation for the phase lag between the exciter input and the electrical torque over the large range 0.1 Hz to 2 Hz.

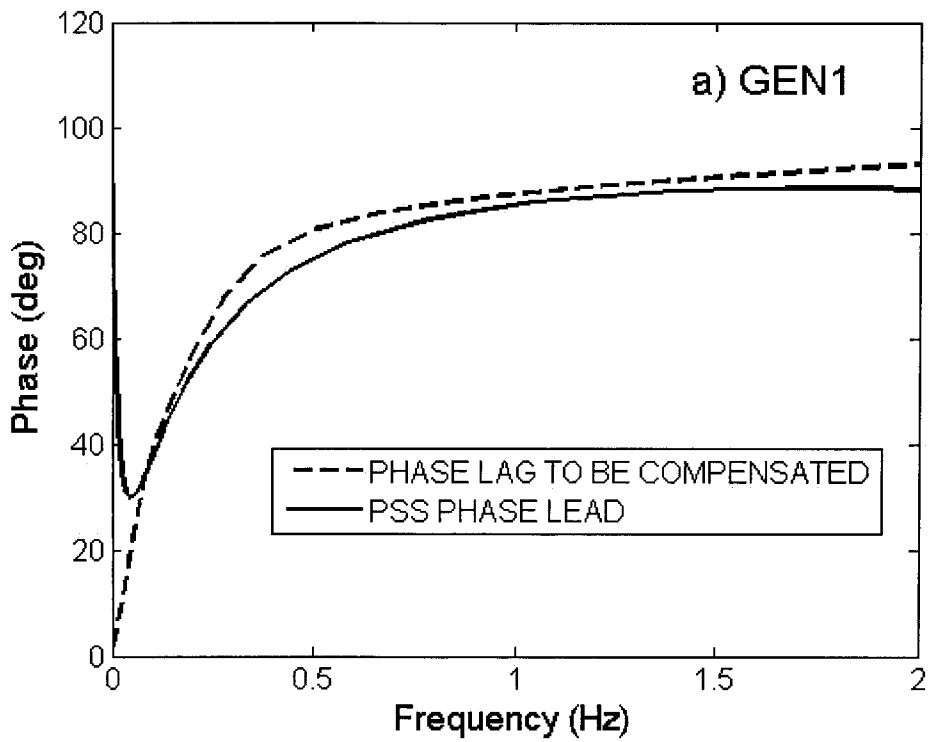

Figure 7.11 Phase characteristics of generators and properly designed PSSs – operating scenario I

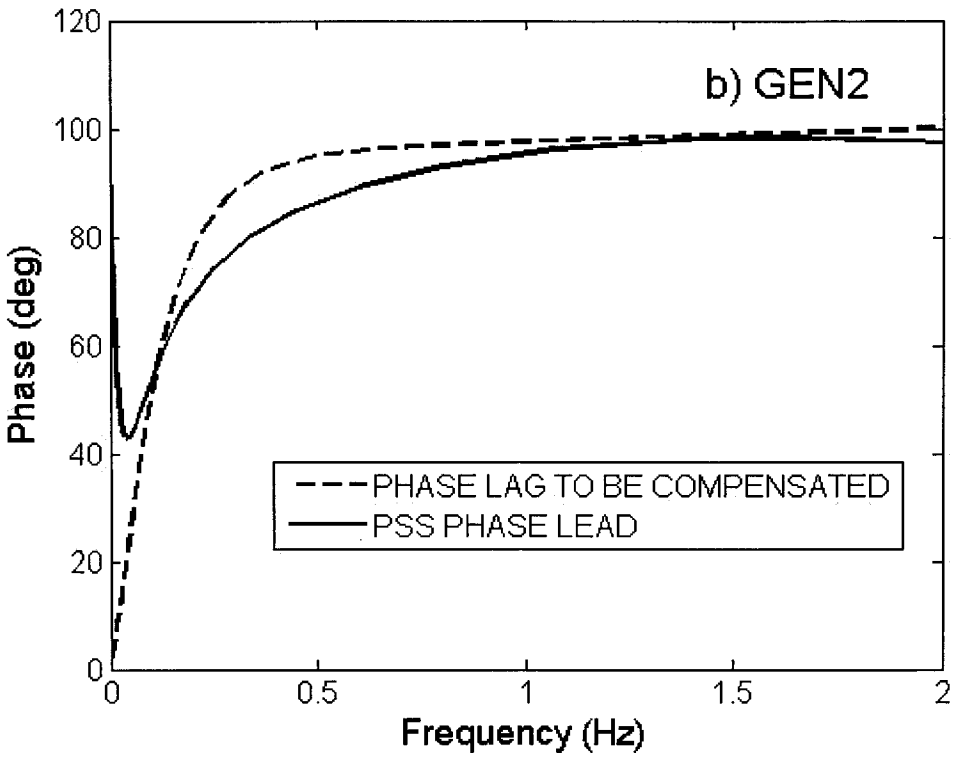

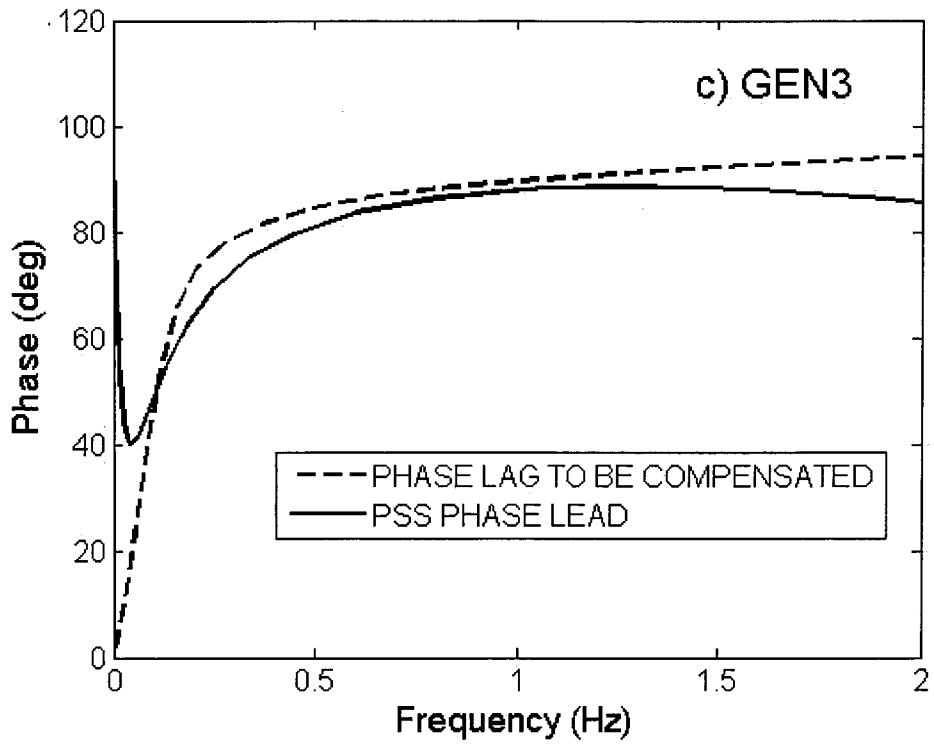

Figure 7.11 (Continued)

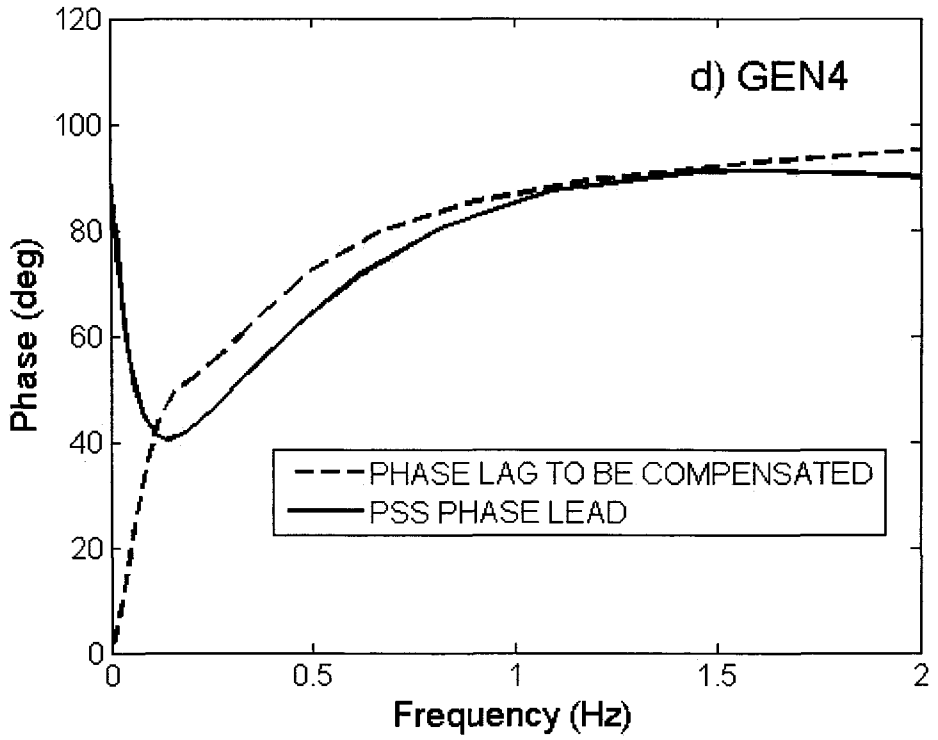

Figure 7.11 (Continued)

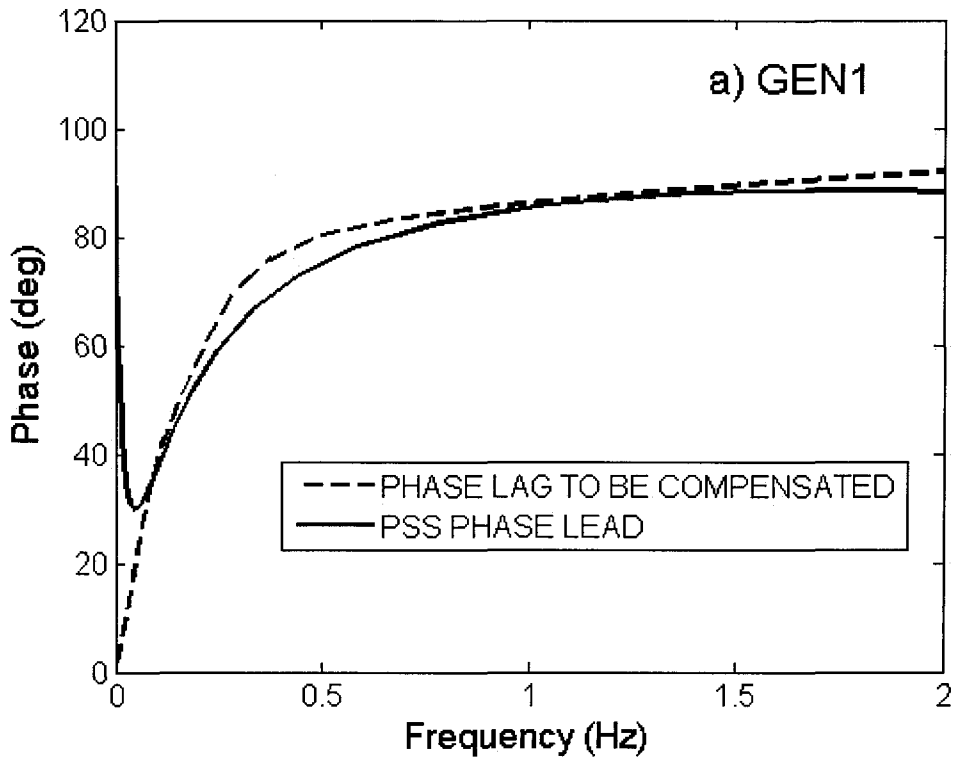

Figure 7.12 Phase characteristics of generators and properly designed PSSs – operating scenario II

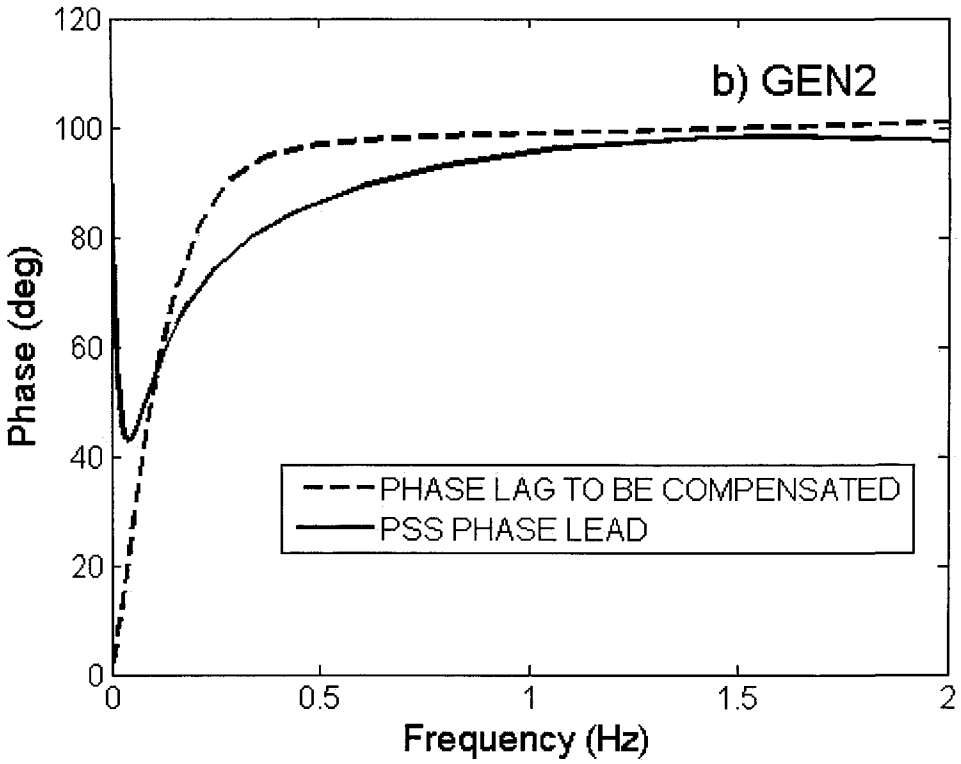

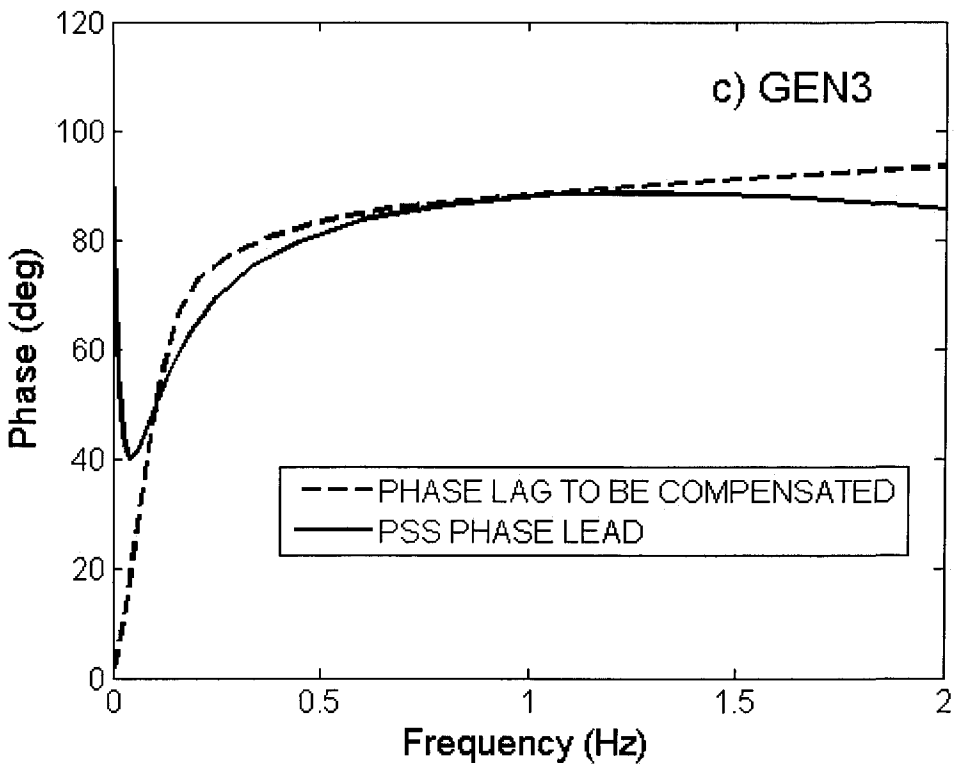

Figure 7.12 (Continued)

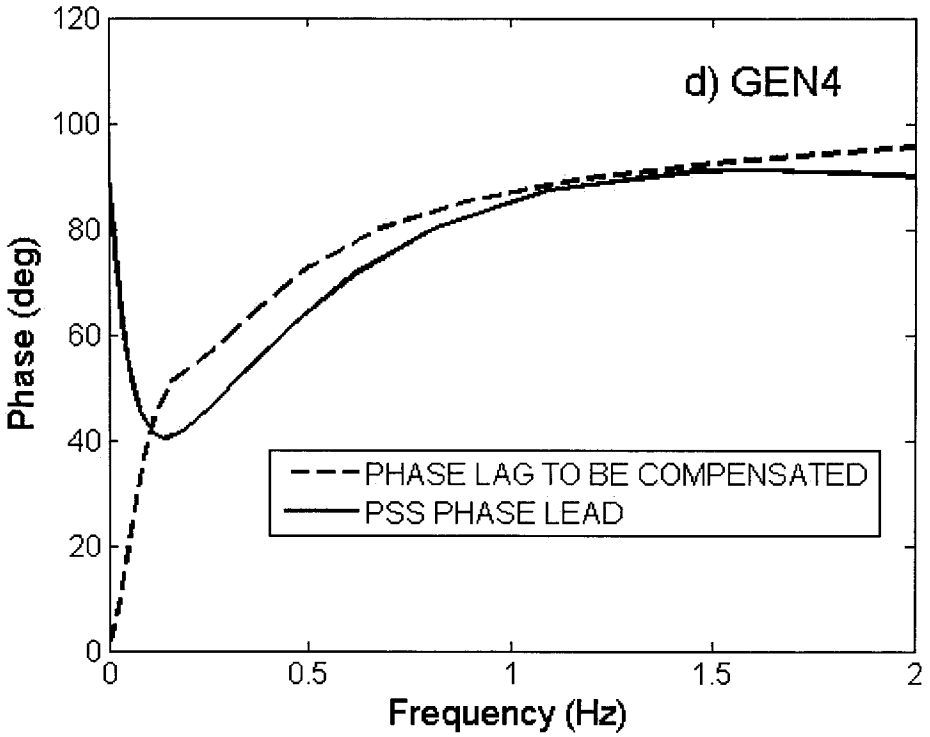

Figure 7.12 (Continued)

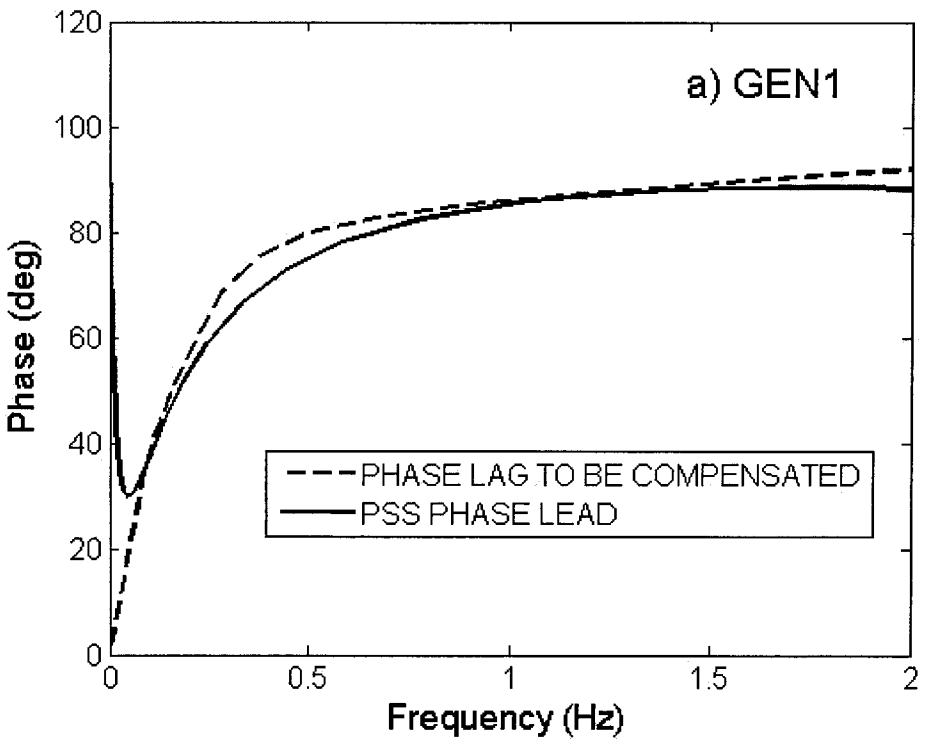

Figure 7.13 Phase characteristics of generators and properly designed PSSs – operating scenario III

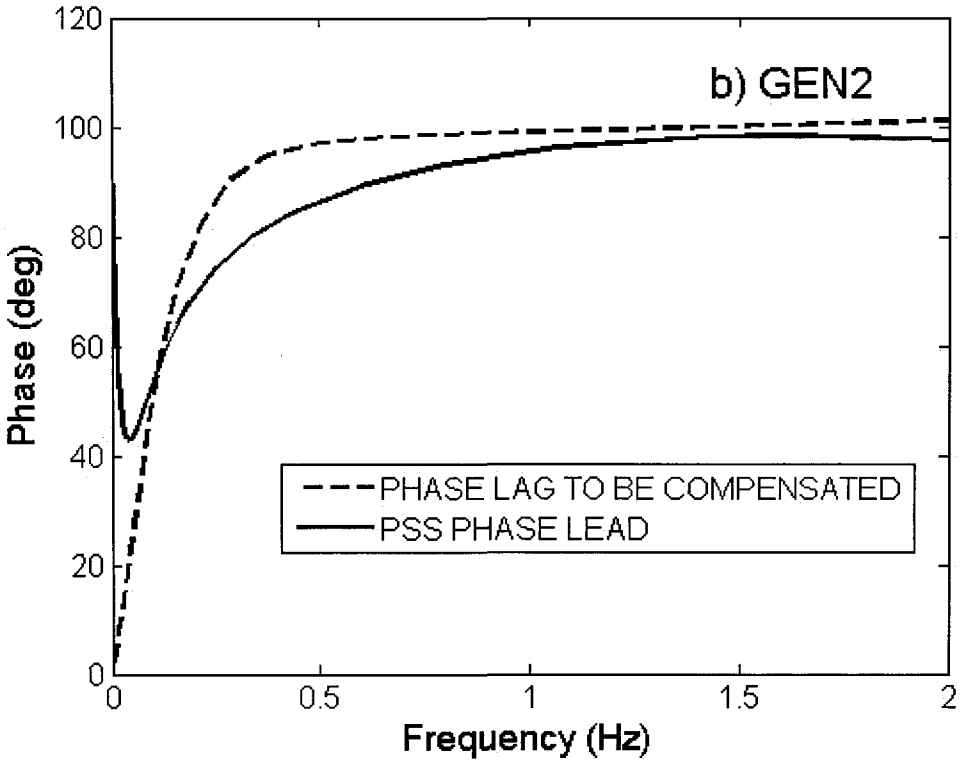

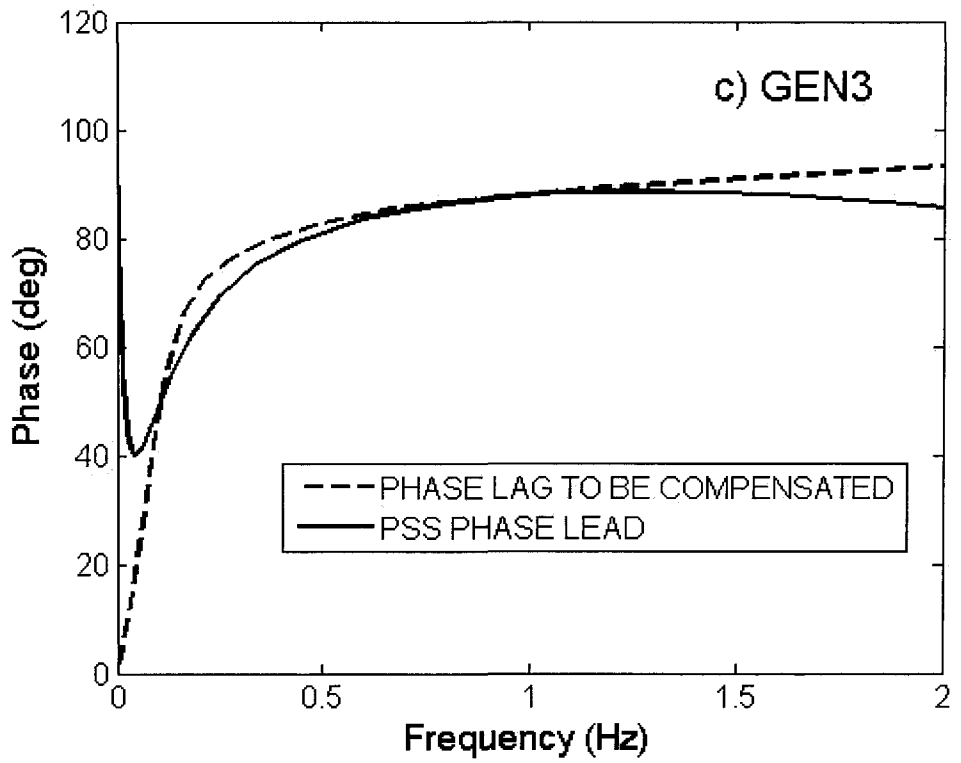

Figure 7.13 (Continued)

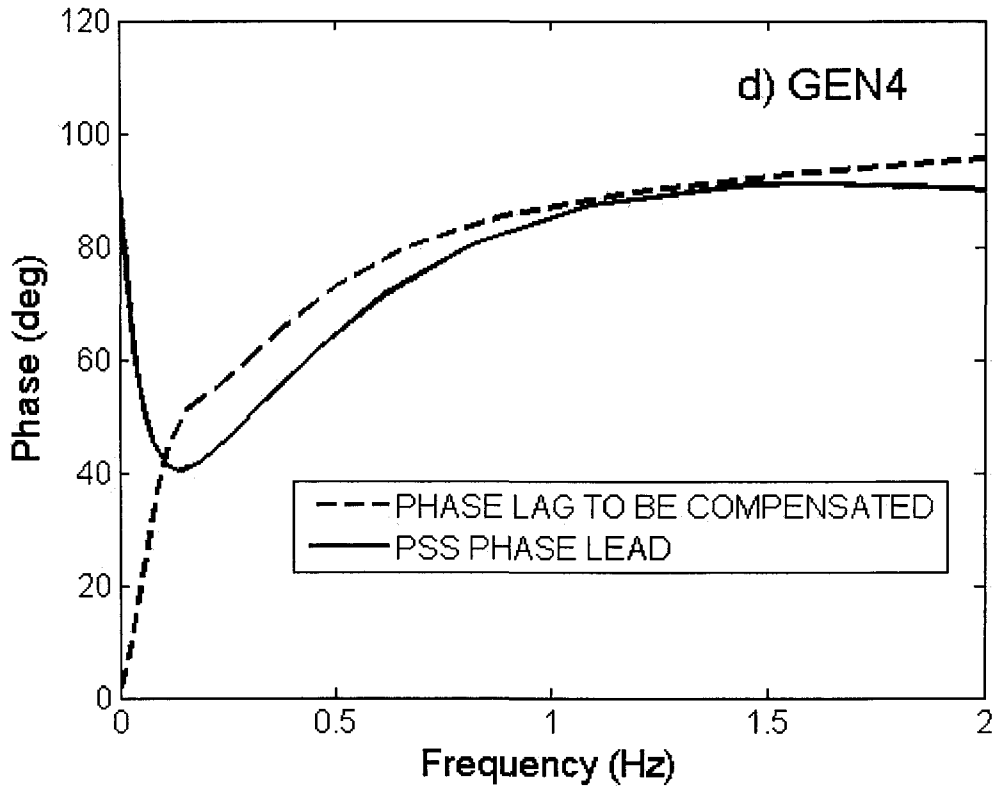

Figure 7.13 (Continued)

Table 7.21 Effect of PSSs on system damping – operating scenario I

PSS location	Eigenvalues	Frequency (Hz)	Damping ratio (%)
GEN1	-0.6765±j3.08 (7)	0.490	21.45
	-2.969±j6.84 (1)	1.088	39.82
GEN2	-0.6587±j3.03 (7)	0.482	21.27
	-2.611±j6.96 (1)	1.108	35.13
GEN3	**-0.9904±j2.58 (7)**	**0.411**	**35.79**
	-3.637±j6.49 (3)	1.033	48.88
GEN4	-0.9765±j2.92 (7)	0.465	31.70
	-2.781±j7.02 (3)	1.117	36.83

Tables 7.21 through 7.23 summarize the effect of selected PSS alternatives on the damping of the local and inter-area modes. For scenario I, the results show that the use of

PSSs significantly improves the damping of both the local and the inter-area modes for all alternatives considered. It can be seen from Table 7.21 that use of a PSS at GEN3 for scenario I results in the best improvement of damping as suggested by nonlinear and linear participation factors.

Table 7.22 Effect of PSSs on system damping – operating scenario II

PSS location	Eigenvalues	Frequency (Hz)	Damping ratio (%)
GEN1	-0.4315±j2.08 (9)	0.3318	20.27
	-2.1419±j7.52 (1)	1.1964	27.40
GEN2	**-0.5085±j2.27 (9)**	**0.3617**	**21.83**
	-1.8825±j7.62 (1)	1.2126	23.99
GEN3	-0.1289±j1.49 (9)	0.2373	8.61
	-2.8005±j7.29 (3)	1.1598	35.87
GEN4	-0.1651±j1.45 (9)	0.2313	11.28
	-2.0390±j7.49 (3)	1.1920	26.27

Table 7.23 Effect of PSSs on system damping – operating scenario III

PSS location	Eigenvalues	Frequency (Hz)	Damping ratio (%)
GEN1	-0.1151±j1.38 (9)	0.220	8.30
	-1.355±j7.71 (1)	1.227	17.30
GEN2	**-0.1534±j1.43 (9)**	**0.223**	**10.87**
	-1.303±j7.73 (1)	1.231	16.61
GEN3	-0.0354±j1.30 (9)	0.206	2.73
	-1.940±j7.54 (3)	1.199	24.93
GEN4	-0.0371±j1.28 (9)	0.203	2.90
	-1.846±j7.54 (3)	1.200	23.78

For scenarios II and III, the use of PSSs in machines in Area 1 results in more damped behavior. Thus, for example, in the case with a PSS at GEN2 in scenario III

(refer to Table 7.23), the damping ratio is increased to 10.87%. By contrast, adding PSSs at machines in Area 2 may actually decrease the damping of the inter-area mode 9 from 4.4% to 2.73% and 2.90% for the cases with a PSS added to GEN3 and GEN4, respectively.

To verify the effect of PSSs, system transient stability was also analyzed for scenario III. Figure 7.14 shows the tie line real power under the condition in which a three phase fault applied at Bus 6 is cleared in 0.034 seconds with no line switching. For this case, 0.034 s is the critical clearing time which is the longest clearing time to keep the system stable after the fault is cleared.

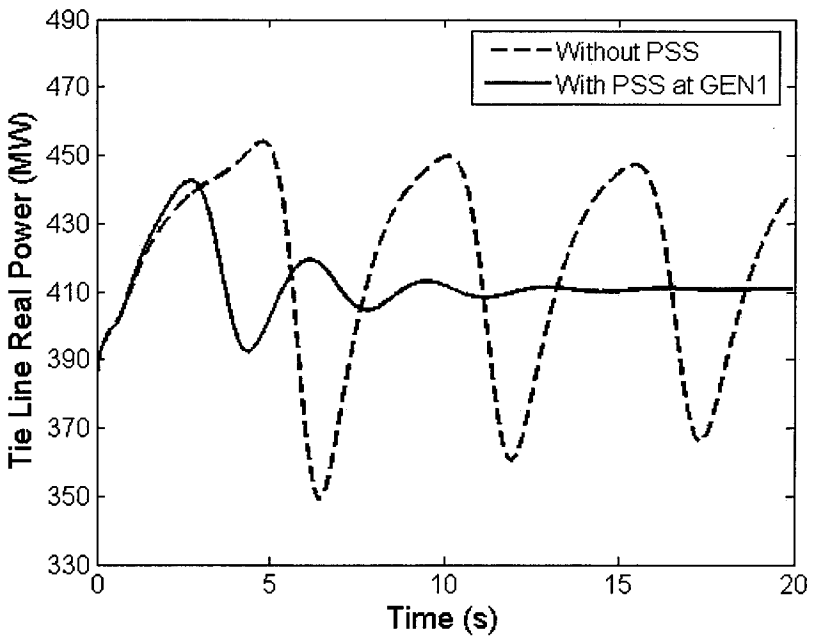

a) Tie line real power with and without PSS at GEN1 (PSS Gain K=15)

Figure 7.14 Tie line real power

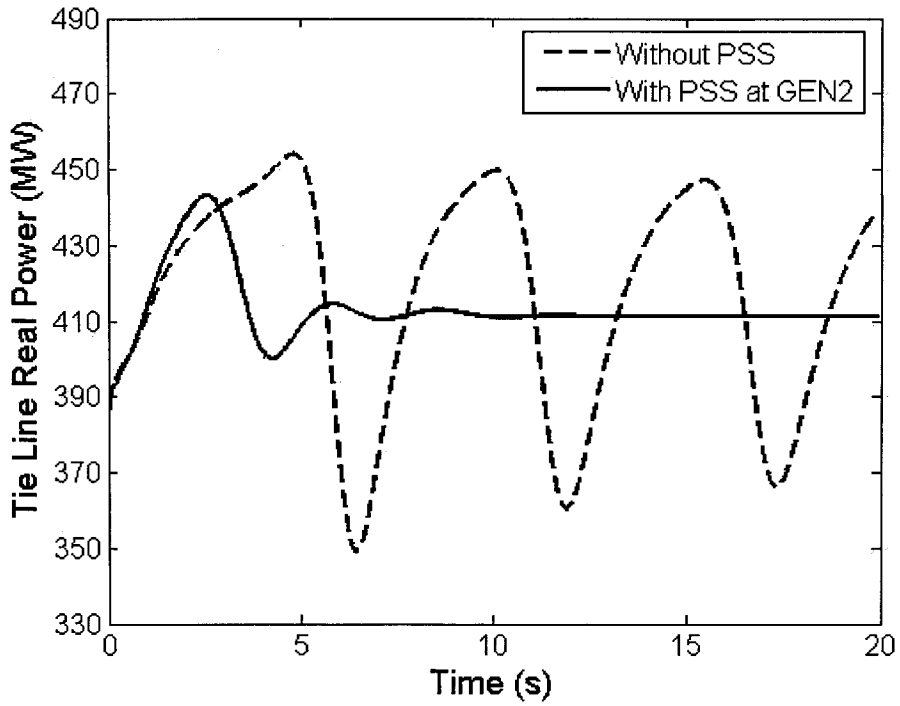

b) Tie line real power with and without PSS at GEN2 (PSS Gain K=15)

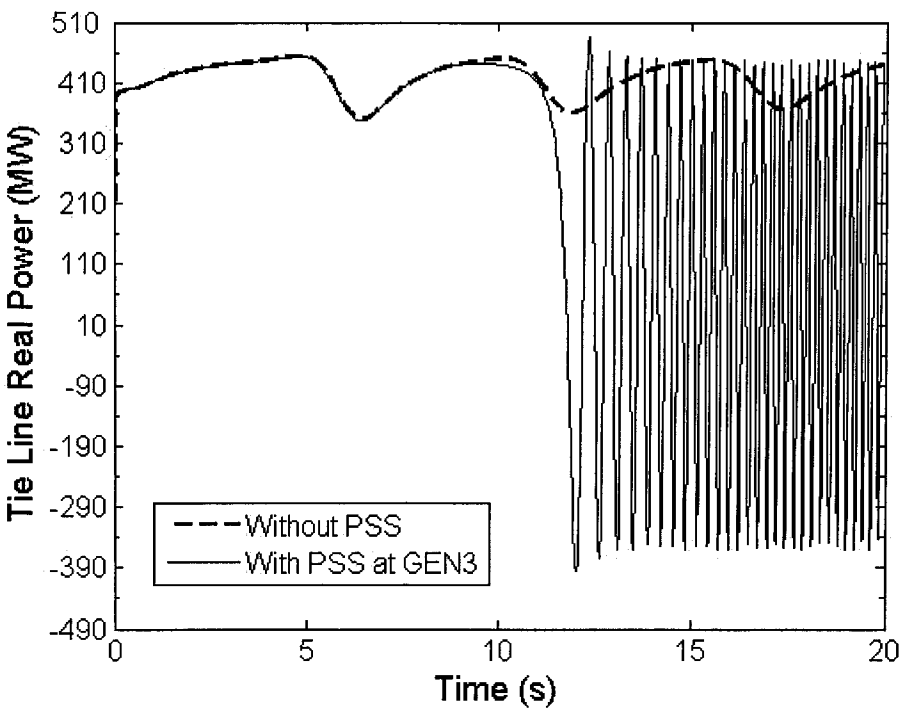

c) Tie line real power with and without PSS at GEN3 (PSS Gain K=1.4)

Figure 7.14 (Continued)

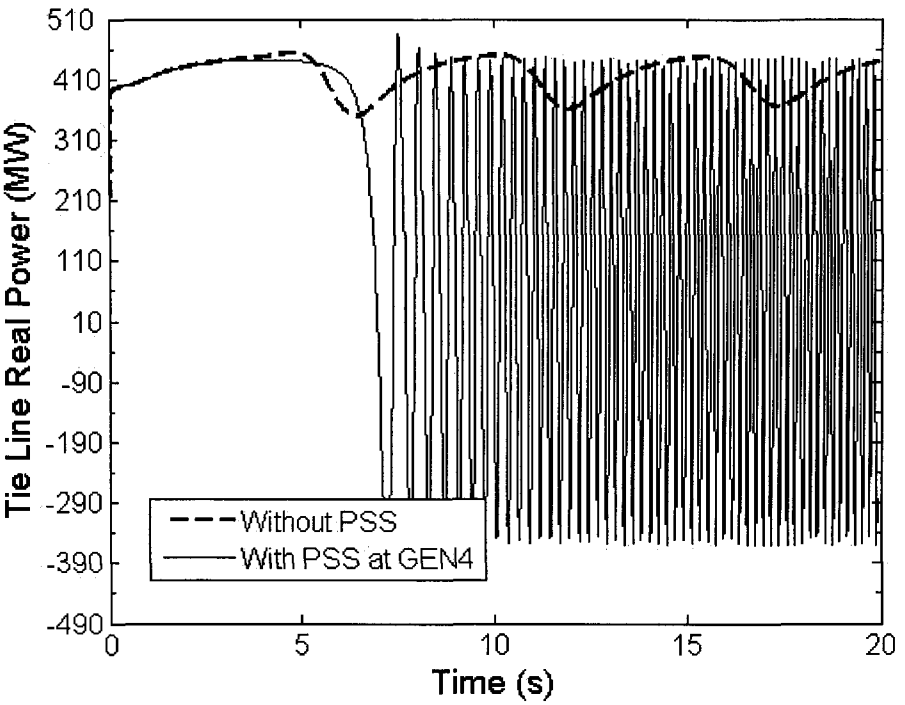

d) Tie line real power with and without PSS at GEN4 (PSS Gain K=1.0)

Figure 7.14 (Continued)

The analysis results enable us to confirm that the use of PSSs at the locations suggested by nonlinear PSS sensitivity index for different scenarios leads to better dynamic performance. For scenarios II and III, increasing the PSS gains in Area 2, three times beyond the values given in Table 7.20 results in an unstable system, and increasing the gain of the PSS in Area 1 results in higher damping. This follows the procedure outlined in [67]. The values of gain were reduced to make a fair comparison between gains in Areas 1 and 2. Comparing these results with the analysis of linear participation factors in Table 7.8 and residues in Table 7.9, one can see that modal interaction is not properly captured by linear analysis. As a result, conventional techniques do not identify the ideal location for system controllers.

7.1.8 Participation Factors with PSSs Designed using the Approach in [67]

Tables 7.24 and 7.25 show the results of linear and nonlinear analysis of scenario III with PSSs designed using the approach in [67]. Observe that the nonlinear

participation factors provide different information from that of the linear participation factors.

Table 7.24 Linear participation factors with PSSs in the system

PSS location	Eigenvalues	Participation factors
GEN1	-0.1151±j1.38	0.8604
		0.8148
		1.0000
		0.9981
GEN2	-0.1534±j1.43	0.8247
		0.7593
		1.0000
		0.9967
GEN3	-0.0354±j1.30	**1.0000**
		0.9499
		0.9487
		0.9604
GEN4	-0.0371±j1.28	**1.0000**
		0.9531
		0.9092
		0.9231

This analysis reveals that with a properly tuned PSS at GEN1, the nonlinear participation factor for speed deviation of GEN1 to inter-area mode becomes the largest. With a properly designed PSS at GEN2, the speed deviation of GEN2 has the largest participation in the inter-area mode. These studies demonstrate that with a properly located and designed PSS, the participation of critical generators in the inter-area mode will increase. Furthermore, this will improve the effectiveness of the PSS in damping critical modes. In particular, this information confirms that the use of PSSs at GEN1 or GEN2 can improve the damping of inter-area mode more effectively.

Table 7.25 Nonlinear participation factors with PSSs in the system

PSS location	Eigenvalues	Participation factors	Normalized PFs
GEN1	-0.1151±j1.38	**0.9745**	**1.0000**
		0.2727	0.2798
		0.3766	0.3865
		0.3564	0.3658
GEN2	-0.1534±j1.43	0.7542	0.1318
		5.7205	**1.0000**
		0.0227	0.0040
		0.3835	0.0670
GEN3	-0.0354±j1.30	**0.2982**	**1.0000**
		0.2938	0.9853
		0.2446	**0.8203**
		0.2680	0.8987
GEN4	-0.0371±j1.28	0.1720	0.3200
		0.5374	**1.0000**
		0.0311	0.0578
		0.0156	**0.0290**

It is also interesting to observe that with a well-designed PSS at GEN3, the nonlinear participation factor for speed deviation of GEN3 in the inter-area mode becomes very small. A similar situation occurs when a properly designed PSS is located at GEN4. This shows that with an improperly located PSS, the participation of certain generators in the inter-area mode will drop; this will influence the behavior of the PSS. These results confirm the poor performance of the PSS at GEN3 and GEN4. The PSS in area 2 can't improve the damping of the inter-area mode.

7.1.9 Effect of Control Action on Modal Interaction

Based on the above results, a detailed investigation was undertaken to consider the effect of control action on modal interaction for Scenario III. The gains of the PSS

were set to a value of 4.0 pu to clearly demonstrate the contribution made by each PSS.

Table 7.26 Nonlinear interaction indices for key modes – PSS at GEN1

Without PSS				With PSS			
Mode j	II(j)	Mode k	Mode l	Mode j	II(j)	Mode k	Mode l
1	0.744	1	12	1	0.630	1	17
3	1.058	11	12	3	0.946	5	13
5	2.003	11	12	5	2.084	5	17
7	2.106	9	11	7	16.92	5	13
9	0.816	11	12	9	**13.15**	9	17
	0.709	11	11		**10.50**	13	13
	0.705	9	12		**9.553**	5	13
	0.686	9	11		**9.361**	5	14
11	0.933	9	12	11	18.57	11	17

Table 7.27 Nonlinear interaction indices for key modes – PSS at GEN2

Without PSS				With PSS			
Mode j	II(j)	Mode k	Mode l	Mode j	II(j)	Mode k	Mode l
1	0.690	1	12	1	3.047	7	11
3	0.677	3	11	3	2.137	3	12
5	1.088	11	12	5	28.02	7	12
7	2.214	9	11	7	37.53	11	11
9	0.676	11	12	9	**269.2**	7	12
	0.655	9	12		**211.0**	11	11
	0.637	9	11		**191.3**	8	11
	0.587	11	11		**182.1**	7	11
11	0.970	9	12	11	22.56	7	12

Tables 7.26 to 7.29 show the nonlinear interaction indices for key modes with and without a PSS on each unit. The initial values for calculating these indices are $x_0 = e_k$ with the k^{th} element of the vector equal to 1, and all the others zero. The k^{th} element is the speed deviation for the associated unit.

Table 7.28 Nonlinear interaction indices for key modes – PSS at GEN3

Without PSS				With PSS			
Mode j	II(j)	Mode k	Mode l	Mode j	II(j)	Mode k	Mode l
1	1.332	7	9	1	0.531	11	13
3	0.086	3	8	3	0.425	3	17
5	1.516	3	4	5	1.117	3	4
7	0.152	9	11	7	3.264	11	13
9	0.196	9	10	9	2.043	9	17
	0.131	7	10		1.188	11	13
	0.099	9	9		1.075	12	13
	0.077	7	9		1.065	13	13
11	0.689	9	12	11	3.558	11	17

From the analysis of nonlinear interaction indices in Tables 7.26 and 7.27, it is clear that the interaction indices for the inter-area mode are much larger with the designed PSS than without PSSs for units 1 and 2.

The results in Table 7.28 and Table 7.29 show that the interaction indices for the inter-area mode are larger with the designed PSS than without any PSS for Unit 3 and Unit 4. The interaction, however, is not as large as that for Units 1 and 2. These results suggest that a well-designed PSS increases the modal interaction among critical modes. This in turn aids in enhancing the damping of critical modes more effectively, revealing the importance of nonlinear analysis.

Table 7.29 Nonlinear interaction indices for key modes – PSS at GEN4

Without PSS				With PSS			
Mode j	II(j)	Mode k	Mode l	Mode j	II(j)	Mode k	Mode l
1	1.657	7	9	1	9.360	6	7
3	0.082	3	8	3	0.244	3	17
5	1.099	3	4	5	0.700	5	17
7	0.241	9	11	7	0.611	7	17
9	0.193	9	10	9	1.189	9	17
	0.126	7	10		0.830	9	18
	0.097	9	9		0.792	5	6
	0.077	9	12		0.693	3	6
11	0.679	9	12	11	8.368	9	12

7.1.10 Conclusions

The analysis results from the above study enable us to confirm that PSS sensitivity indices provide the best prediction of PSS dynamic performance for every operating scenario. For operating scenario I in which the system is operating under a low-stress condition, nonlinear analysis provides similar results as linear analysis. For operating scenario II and III, the system was more stressed, and the PSS sensitivity index predicted the best PSS location more effectively than linear analysis, which failed to provide the correct information.

Nonlinear participation factors and interaction indices with proper designed PSS were calculated for operating scenario III. With a properly located and designed PSS, the nonlinear participation of critical generators in the inter-area mode and modal interaction among the critical modes will increase. This will also improve the effectiveness of PSSs in damping critical modes. All these analysis results are consistent with the better PSS dynamic performance at GEN1 and GEN2 in area 1.

7.2 Test System – IEEE 50-machine System

7.2.1 Simulated Conditions

The developed procedures were also applied to the IEEE 50-generator system. Figure 7.15 shows a single-line diagram of the area of interest for this study. Six generators (bus 93, 104, 105, 106, 110, and 111) are represented by a fourth-order *d-q* axis model and a fast exciter. The other generators are represented by classical models. Loads are modeled as constant impedances. The overall state model includes 129 states. The generator data and system parameters are given in the Appendix B.

Two main operating conditions were simulated to investigate the presence of nonlinear modal interaction: a low-stress case (operating scenario I), a high-stress condition (operating scenario II). Table 7.30 shows the active power generation of generators represented by the two-axis model for the above operating conditions.

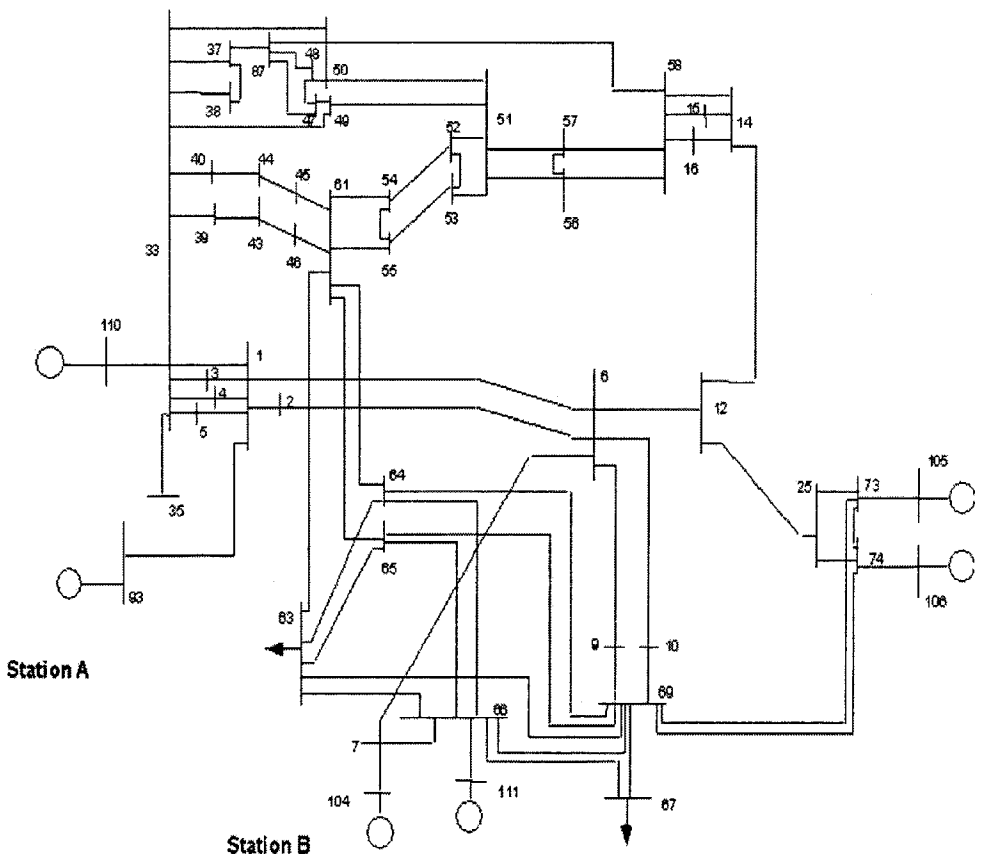

Figure 7.15 IEEE 50-generator system: a single-line diagram of the study area

Table 7.30 Active power generation of generators

Bus #	Active power generation (MW)	
	Operating scenario I	Operating scenario II
93	1080	1080
104	1400	2400
105	620	1620
106	1080	1080
110	980	1080
111	1800	2600

7.2.2 Linear Analysis

Table 7.31 Oscillatory modes of the system– operating scenario I

Mode #	Eigenvalue	Freq. (Hz)	Damping (%)	Dominant states
55,56	-0.391±j10.49	1.67	3.73	Local (111, 104)
73,74	-0.250±j7.52	1.20	3.32	Local (106, 105)
75,76	-0.454±j7.04	1.12	6.43	Local (93, 110)
77,78	-0.052±j7.30	1.16	0.71	Local (104,111)
79,80	-0.461±j7.90	1.26	5.83	Local (105, 106)
85,86	-0.176±j6.41	1.02	2.75	Local (110, 93)
97,98	**-0.023±j2.70**	**0.43**	**0.83**	**Inter-area (110,93) (137,140)**
99,100	-0.630±j0.79	0.13	62.24	Local (104, 111)
101,102	-0.460±j0.63	0.10	59.13	Local (110, 93)
103,104	-0.389±j0.56	0.09	56.92	Local (111, 104)
105,106	-0.328±j0.46	0.07	57.94	Local (93, 110)
107,108	-0.339±j0.39	0.06	65.41	Local (105, 106)
109,110	-0.269±j0.42	0.07	53.74	Local (106, 105)

To provide a basis for comparison with the NF results, detailed eigenvalue-based studies were conducted for each operating condition. Tables 7.31 and 7.32 show selected

modes together with their associated frequencies of oscillation, damping ratio, and the most dominant states. Mode 97 is the critical mode which needs further analysis since it is an inter-area mode and has a negative damping ratio. Conventional analysis techniques were used to site power system stabilizers (PSSs) to enhance damping of the inter-area mode 97.

Table 7.32 Oscillatory modes of the system– operating scenario II

Mode #	Eigenvalue	Freq. (Hz)	Damping (%)	Dominant states
55,56	-0.167±j9.74	1.55	1.71	Local (111, 104)
73,74	-0.316±j7.91	1.26	3.99	Local (106, 105)
75,76	-0.450±j7.10	1.13	6.32	Local (93, 110)
77,78	-0.024±j7.30	1.16	0.33	Local (104,111)
79,80	-0.135±j7.27	1.16	1.86	Local (105, 106)
85,86	-0.144±j6.15	0.98	2.34	Local (110, 93)
97,98	**0.145±j2.14**	**0.34**	**-6.79**	**Inter-area (110,93) (145,136)**
99,100	-1.112±j1.27	0.20	65.92	Local (104, 111)
101,102	-0.484±j0.68	0.11	58.27	Local (110, 93)
103,104	-0.451±j0.68	0.11	55.46	Local (111, 104)
105,106	-0.339±j0.47	0.08	58.38	Local (93, 110)
107,108	-0.305±j0.49	0.08	52.90	Local (105, 106)
109,110	-0.268±j0.40	0.06	55.40	Local (106, 105)

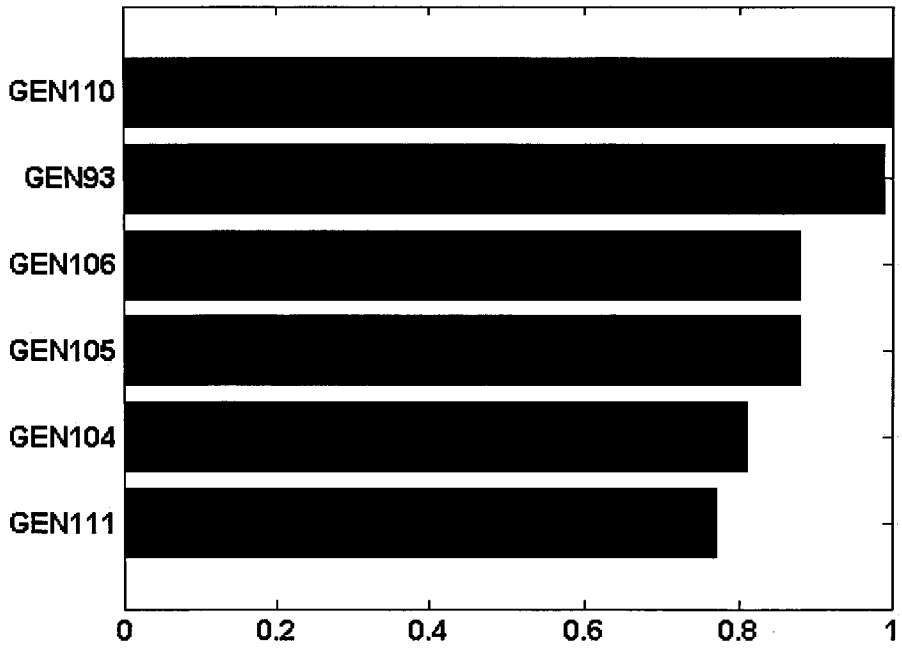

Figure 7.16 Mode shapes of generator speeds with inter-area mode 97 – operating scenario I

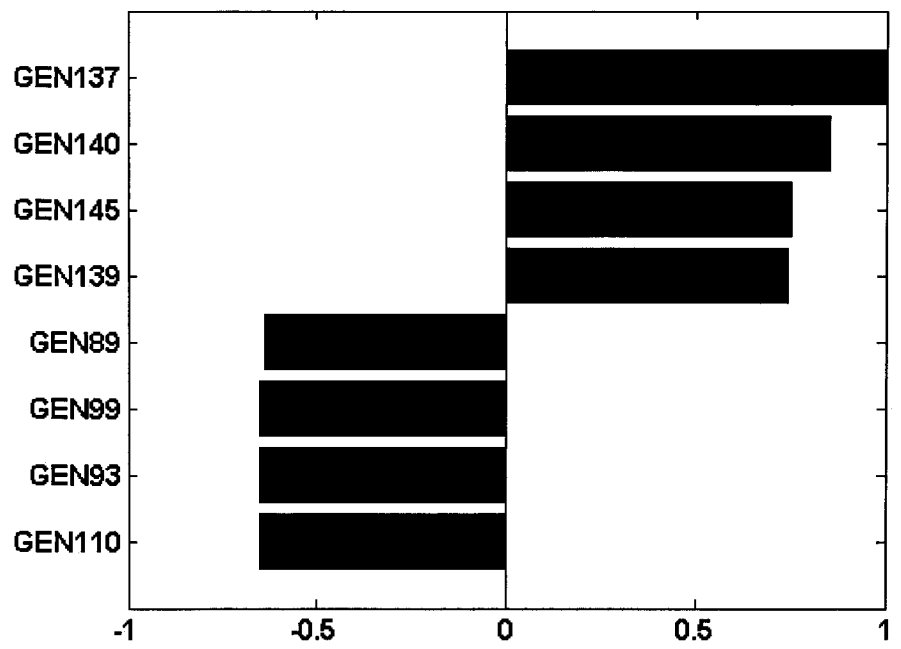

Figure 7.17 Mode shapes of generator speeds with inter-area mode 97 – operating scenario II

Figures 7.16 and 7.17 show the mode shapes of generator speeds for the inter-

area modes obtained using the SSAT [65] software. Values are normalized with respect to the largest component.

Table 7.33 Linear participation factors of generator speeds with inter-area mode 97

Bus #	Operating scenario I	Operating scenario II
93	0.9700 (2)	0.9651 (2)
104	0.4200 (3)	0.8256 (3)
105	0.3720 (5)	0.5930 (5)
106	0.3600 (6)	0.3953 (6)
110	**1.0000 (1)**	**1.0000 (1)**
111	0.3740 (4)	0.6047 (4)

Table 7.33 shows the speed-based linear speed-participation factors for inter-area mode 97. Values are normalized with respect to the largest components. The analysis of linear participation factors identifies GEN110 and GEN93 as the best locations to place PSSs for both two operating conditions. Mode shapes results in Figures 7.16 and 7.17 are in good agreement with those from analysis of participation factors.

Table 7.34 Residues of generator speeds with inter-area mode 97

Bus #	Operating scenario I	Operating scenario II
93	0.9087 (3)	0.4998 (3)
104	0.9690 (2)	**1.0000 (1)**
105	0.4675 (5)	0.3033 (5)
106	0.3319 (6)	0.1993 (6)
110	0.8798 (4)	0.4811 (4)
111	**1.0000 (1)**	0.9536 (2)

Table 7.34 shows the transfer-function residues for the inter-area mode 97. Values

are normalized with respect to the largest components. The analysis of residues identifies GEN111 and GEN104 as the best location to place PSS for damping inter-area mode 97 for operating scenario I and II respectively.

7.2.3 Nonlinear Participation Factors

Tables 7.35 and 7.36 show the nonlinear participation factors of Mode 97 with speed, Xe1 and Xe2 of the six units. Values are normalized with respect to the largest components of speed nonlinear participation factor. The speed nonlinear participation factors show that the generator speed at bus 110 has the largest participation in mode 97 for both operating conditions. However, the generator at bus 111 has large participation factors for mode 97 with exciter states Xe1 and Xe2 for operating scenario II. The generator at bus 104 has similar properties. This makes the analysis both complex and interesting. The PSS sensitivity index will be analyzed in the next section to solve this problem.

Table 7.35 Nonlinear participation factors of mode 97 – operating scenario I

Bus #	Speed		Xe_1	Xe_2
	Original	Normalized	Normalized	Normalized
93	0.0670	0.9721	**0.0385**	0.2041
104	0.0286	0.4154	0.0279	0.0401
105	0.0260	0.3766	0.0115	0.0315
106	0.0249	0.3607	0.0157	0.0517
110	**0.0689**	**1.0000**	0.0360	**0.1906**
111	0.0257	0.3730	0.0340	0.0968

* Values were normalized by the largest speed nonlinear participation factor

Table 7.36 Nonlinear participation factors of mode 97 – operating scenario II

Bus #	Speed		Xe_1	Xe_2
	Original	Normalized	Normalized	Normalized
93	0.0422	0.9736	0.2551	2.9557
104	0.0361	0.8339	0.5690	17.3121
105	0.0262	0.6033	0.3000	3.7648
106	0.0173	0.3978	0.1592	1.6654
110	**0.0434**	**1.0000**	0.2261	2.4384
111	0.0268	0.6226	**1.0185**	**21.3791**

* Values were normalized by the largest speed nonlinear participation factor

7.2.4 PSS Sensitivity Index

Tables 7.37 and 7.38 show the PSS sensitivity indices and corresponding input values. For operating scenario I, the generator at bus 110 has the largest PSS sensitivity index, which confirms with the analysis of linear and nonlinear speed participation factors. The largest PSS sensitivity index occurs on generator at bus 111 for operating scenario II. The index of the generator at bus 104 is also larger than the indices of generators at bus 93 and 110. These indices show different results from linear and nonlinear speed participation factors.

Table 7.37 PSS sensitivity index with mode 97 – operating scenario I

Bus #	α	β	PSI	
			Analytical	Numerical
93	1.0	0.0336	0.9500 (2)	0.9091 (2)
104	1.0	0.0244	0.3667 (5)	0.4622 (3)
105	1.0	0.0100	0.4067 (3)	0.3521 (5)
106	1.0	0.0137	0.3883 (4)	0.3419 (6)
110	1.0	0.0315	**1.0000 (1)**	**1.0000 (1)**
111	1.0	0.0297	0.2883 (6)	0.4545 (4)

Table 7.38 PSS sensitivity index with mode 97 – operating scenario II

Bus #	α	β	PSI	
			Analytical	Numerical
93	1.0	0.0338	0.3583 (4)	0.4844 (3)
104	1.0	0.0755	0.4708 (2)	0.6556 (2)
105	1.0	0.0398	0.2156 (5)	0.3065 (5)
106	1.0	0.0211	0.1573 (6)	0.1845 (6)
110	1.0	0.0300	0.3812 (3)	0.4825 (4)
111	1.0	0.1351	**1.0000 (1)**	**1.0000 (1)**

7.2.5 Effect of PSSs on System Behavior

To verify the effects of nonlinear behavior on the analysis and design of controllers, PSSs were designed using the approach in [39, 66]. In this analysis a PSS was designed considering a single machine location at a time. Figure 7.10 shows the block diagram of the PSS. The parameters for the designed PSSs are shown in Tables 7.39.

Table 7.39 Parameters for the designed PSSs

Bus #	Ks	T_1	T_2	T_3	T_4	T_5	V_{SMAX}	V_{SMIN}
93	50	0.1	0.03	1.5	0.03	10.0	0.1	-0.1
104	50	0.1	0.02	1.0	0.05	10.0	0.1	-0.1
105	50	0.1	0.03	1.5	0.03	10.0	0.1	-0.1
106	50	0.1	0.03	1.5	0.03	10.0	0.1	-0.1
110	50	0.1	0.03	1.5	0.03	10.0	0.1	-0.1
111	50	0.1	0.02	1.0	0.05	10.0	0.1	-0.1

Figures 7.18 and 7.19 show the phase characteristics of generators and the properly designed PSSs for both operating scenarios. The phase characteristics of properly designed PSSs have appropriate phase compensation for the phase lag between the exciter input and the electrical torque over the large range 0.2 Hz to 2 Hz.

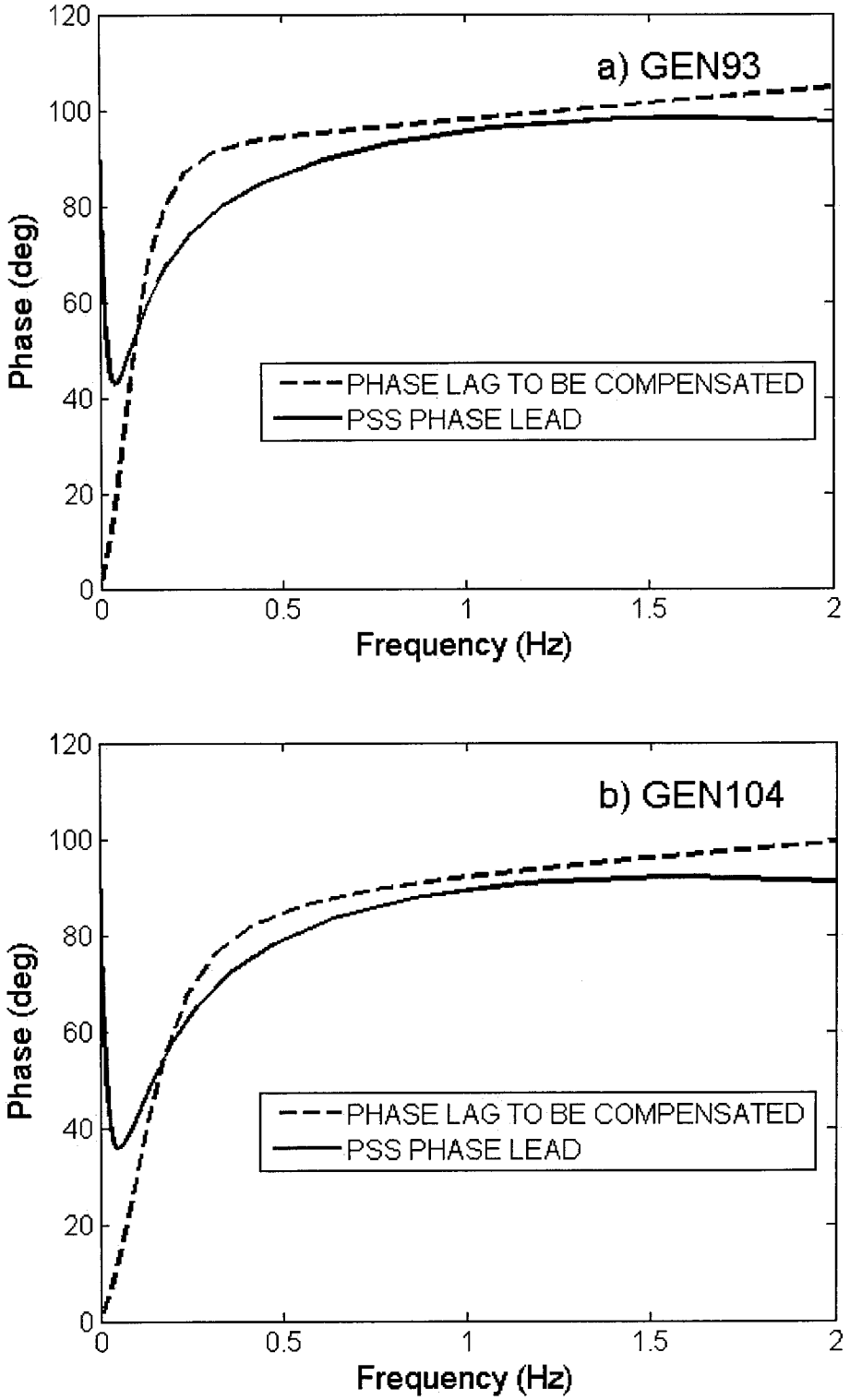

Figure 7.18 Phase characteristics of generators and properly designed PSSs – operating scenario I

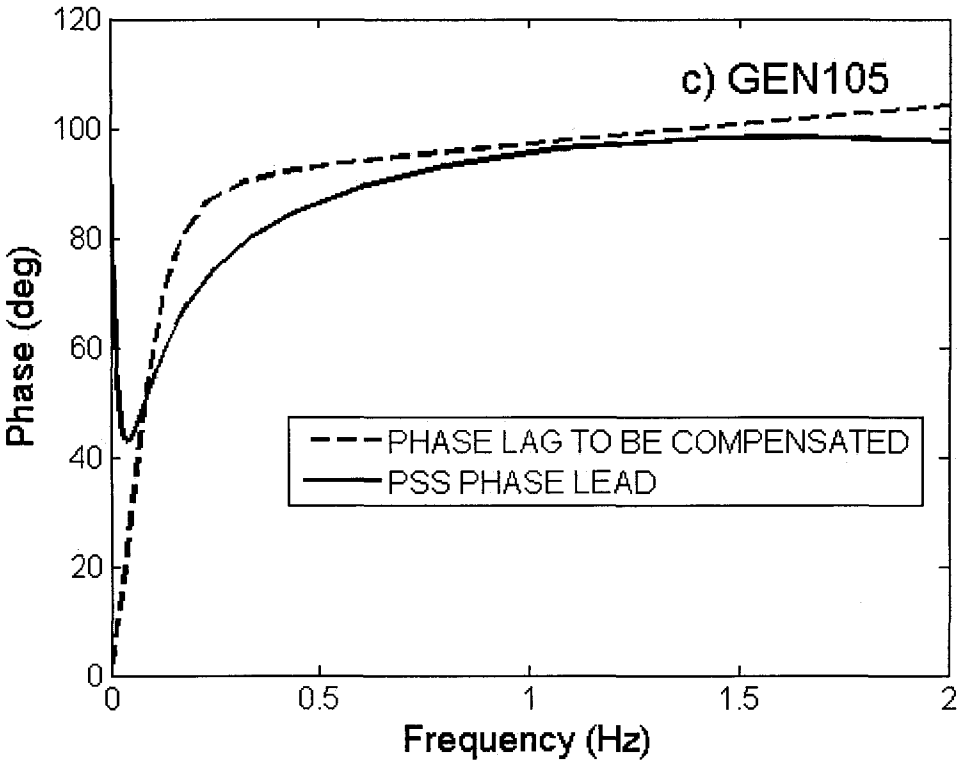

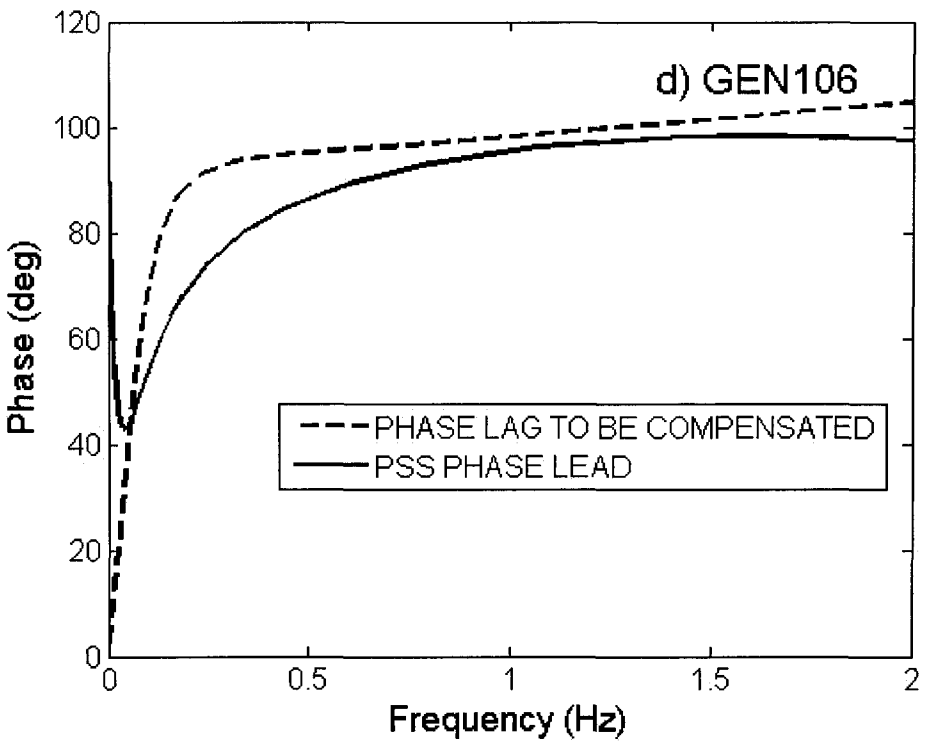

Figure 7.18 (Continued)

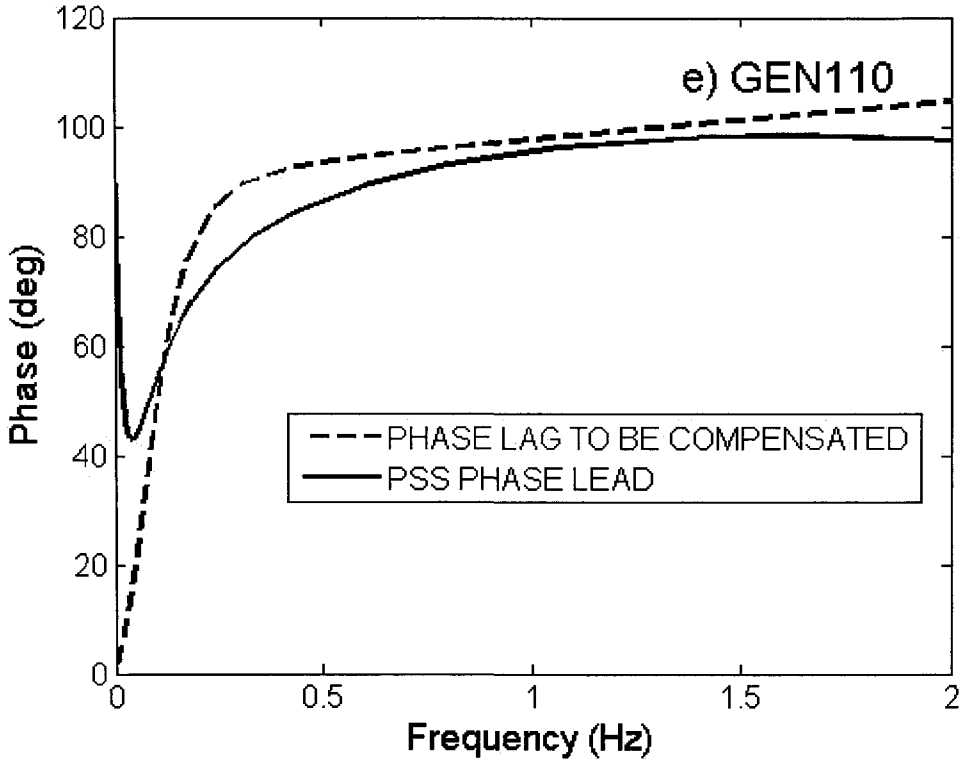

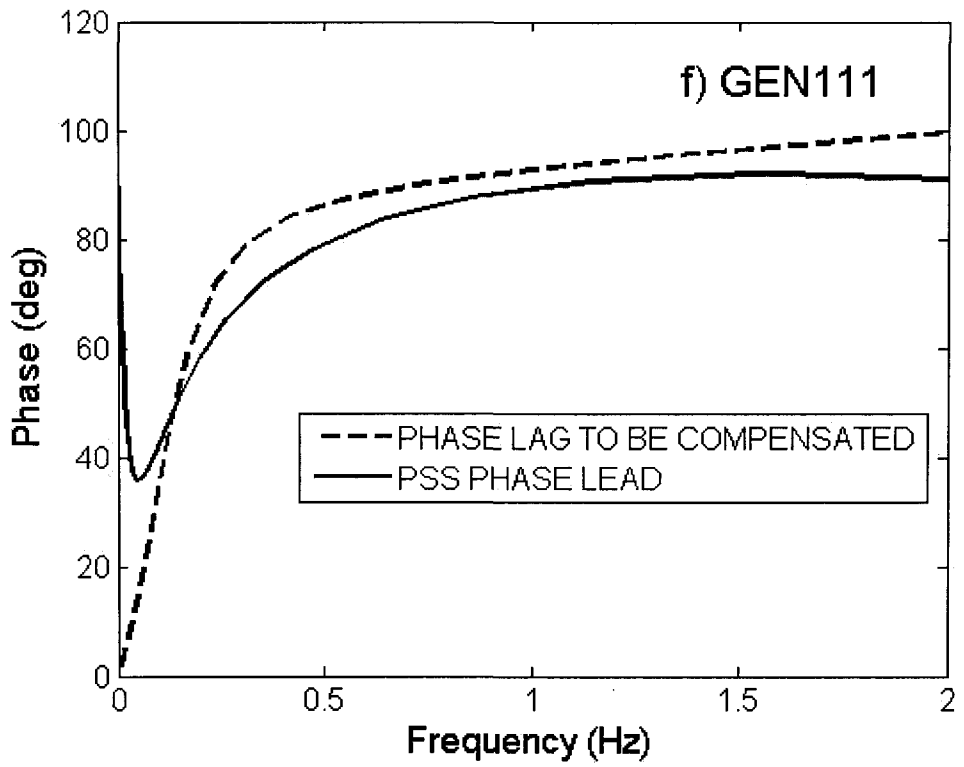

Figure 7.18 (Continued)

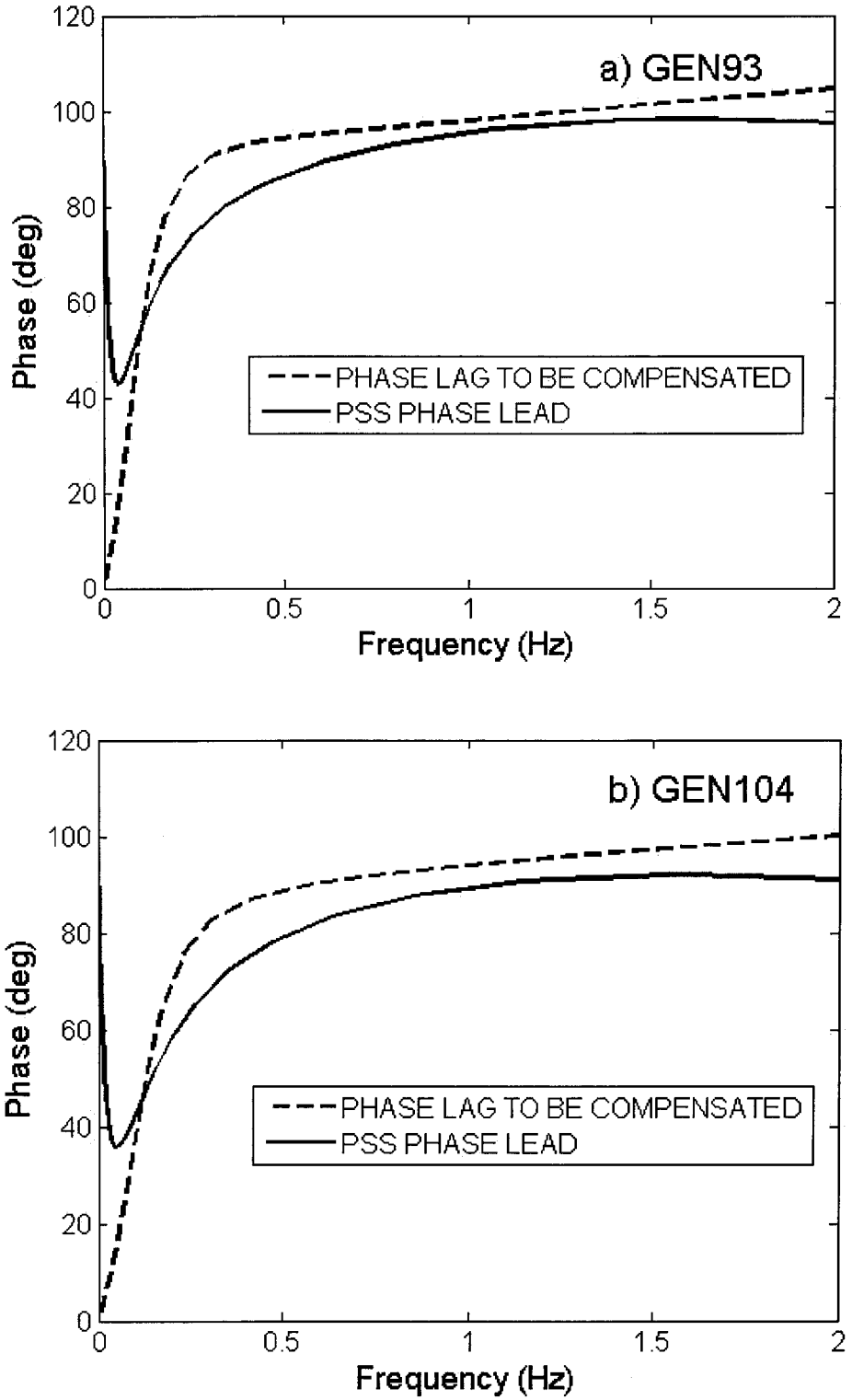

Figure 7.19 Phase characteristics of generators and properly designed PSSs – operating scenario II

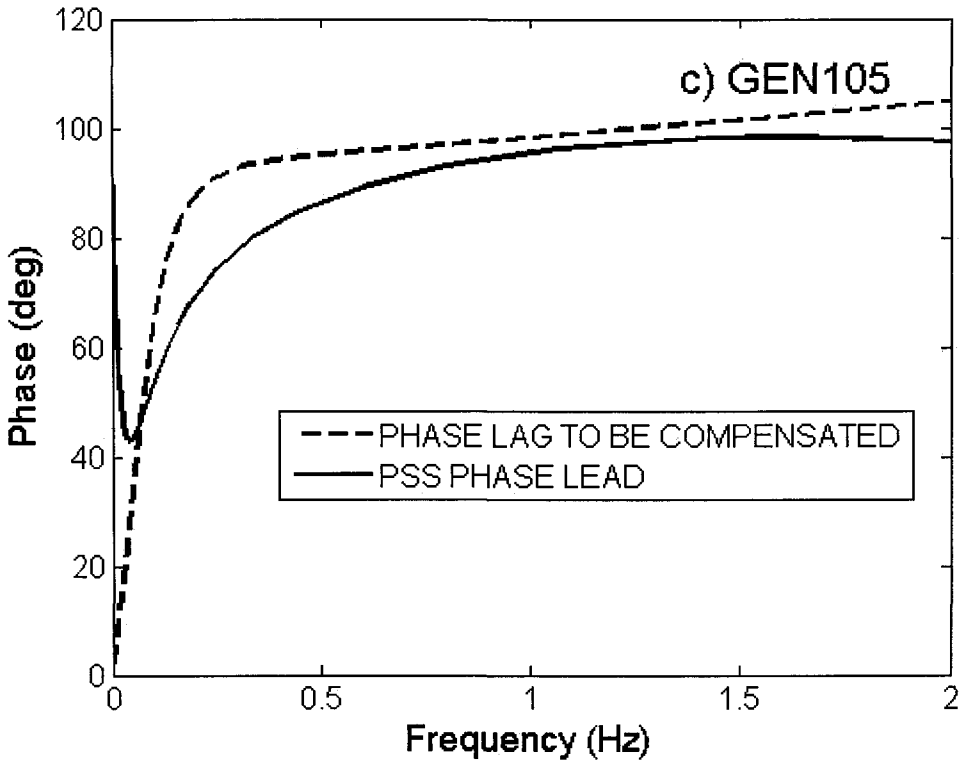

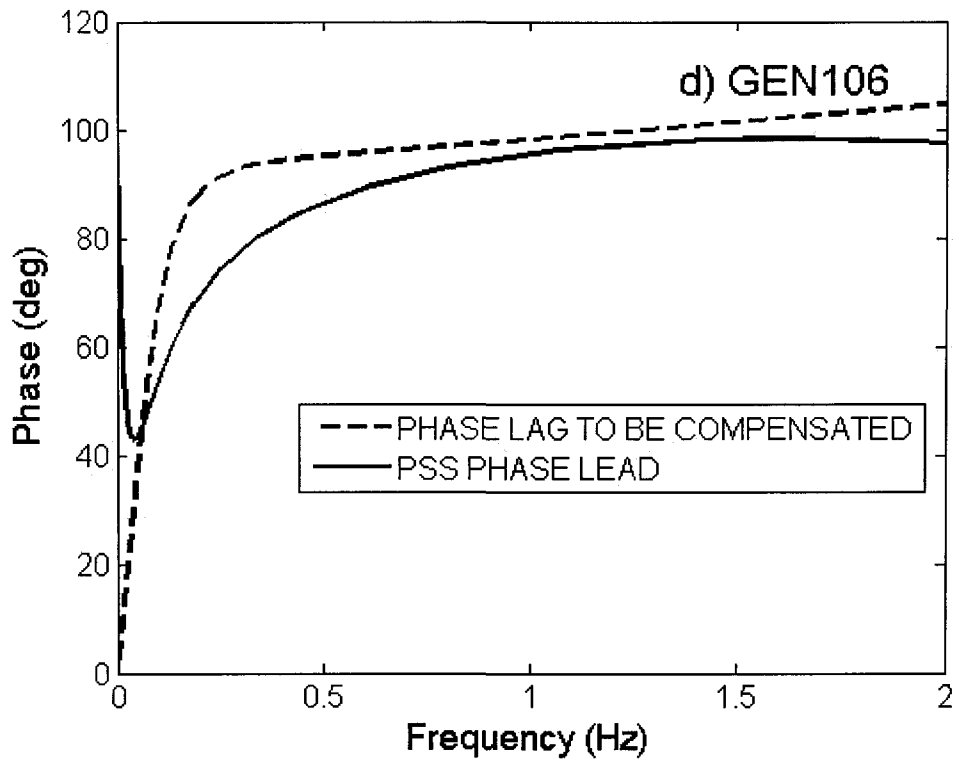

Figure 7.19 (Continued)

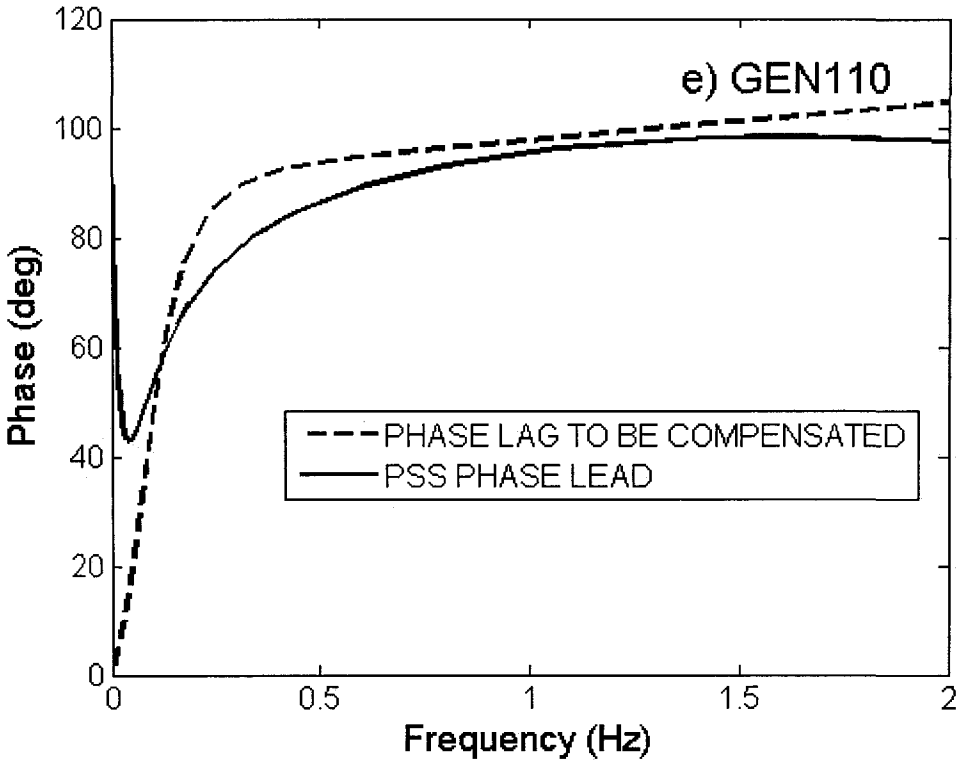

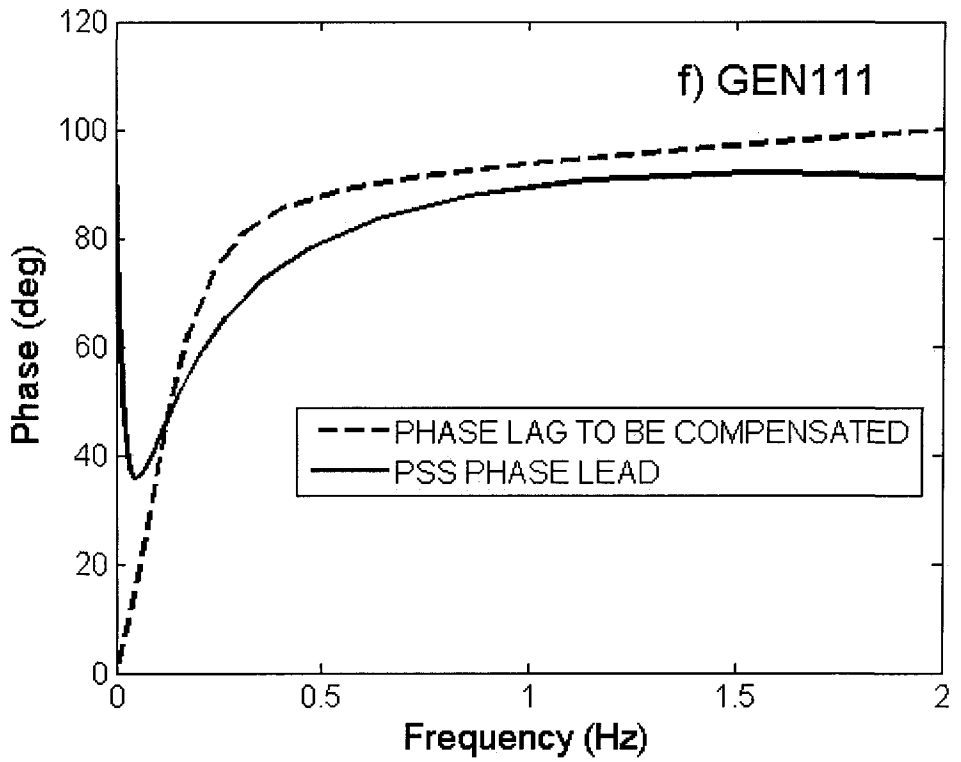

Figure 7.19 (Continued)

Tables 7.40 and 7.41 summarize the effect of selected PSS alternatives on the damping of the inter-area mode.

Table 7.40 Effect of PSSs on system damping (Ks = 50) – operating scenario I

PSS Location	Eigenvalues	Frequency (Hz)	Damping ratio (%)
93	-0.368±j2.93 (97)	0.4671	12.45
	-3.728±j4.75 (75)	0.7558	61.75
104	-0.260±j2.86 (97)	0.4548	9.05
	-5.388±j3.22 (77)	0.5126	85.83
105	-0.253±j2.79 (97)	0.4439	9.02
	-3.013±j6.72 (79)	1.0701	40.90
106	-0.157±j2.79 (97)	0.4438	5.62
	-4.095±j5.54 (73)	0.8813	59.46
110	-0.377±j2.93 (97)	0.4657	12.78
	-3.341±j4.96 (85)	0.7889	55.89
111	-0.256±j2.87 (97)	0.4567	8.87
	-5.535±j2.94 (55)	0.4678	88.32

For operating scenario I, the PSS at GEN110 shows the best improvement for the damping of mode 97 as suggested by nonlinear and linear analysis.

For operating scenario II, the PSS at GEN111 shows the best improvement for the damping of mode 97. PSS at GEN104 has better performance than the PSSs at GEN93 and GEN110. By comparing the results in Table 7.41 and Table 7.38, it is found that the PSS sensitivity indices correctly predict the performance of PSSs at different locations.

Table 7.41 Effect of PSSs on system damping (Ks = 50) – operating scenario II

PSS Location	Eigenvalues	Frequency (Hz)	Damping ratio (%)
93	-0.190±j2.15 (97)	0.3418	8.83
	-3.493±j5.03 (75)	0.8010	57.03
104	-0.384±j2.35 (97)	0.3746	16.11
	-5.186±j1.31 (77)	0.2086	96.94
105	-0.054±j2.19 (97)	0.3491	2.48
	-3.648±j5.55 (79)	0.8838	54.93
106	0.020±j2.18 (97)	0.3471	-0.93
	-3.979±j5.68 (73)	0.9045	57.33
110	-0.181±j2.15 (97)	0.3425	8.37
	-3.229±j4.97 (85)	0.7914	54.45
111	-0.516±j2.12 (97)	0.3375	23.62
	-5.147±j1.74 (55)	0.2771	94.74

Table 7.42 and Table 7.43 show the detailed studies for PSSs at GEN93 and GEN111 with different gains. As PSS gains increase from 20 to 50, PSS performance gets better and better. Since the IEEE Standard indicates that the gain of PSS should be chosen in a range from 0.1 to 50, the gains are set to 50 for all PSSs to obtain best performance.

Table 7.42 Effect of PSSs at GEN93 on system damping – operating scenario II

PSS Gain	Eigenvalues	Frequency (Hz)	Damping ratio (%)
20	-0.0001±j2.1384	0.3403	0.01
30	-0.0652±j2.1410	0.3407	3.04
40	-0.1279±j2.1441	0.3412	5.96
50	-0.1903±j2.1475	0.3418	8.83

Table 7.43 Effect of PSSs at GEN111 on system damping – operating scenario II

PSS Gain	Eigenvalues	Frequency (Hz)	Damping ratio (%)
20	-0.0551±j2.1072	0.3354	2.62
30	-0.1581±j2.0998	0.3342	7.51
40	-0.2811±j2.0944	0.3333	13.30
50	-0.5155±j2.1203	0.3375	23.62

System transient stability was also analyzed for operating scenario II to verify the effect of PSSs. Figure 7.20 shows the tie line real power under a condition in which the three-phase fault applied at Bus 6 is cleared in 0.055 seconds with no line switching.

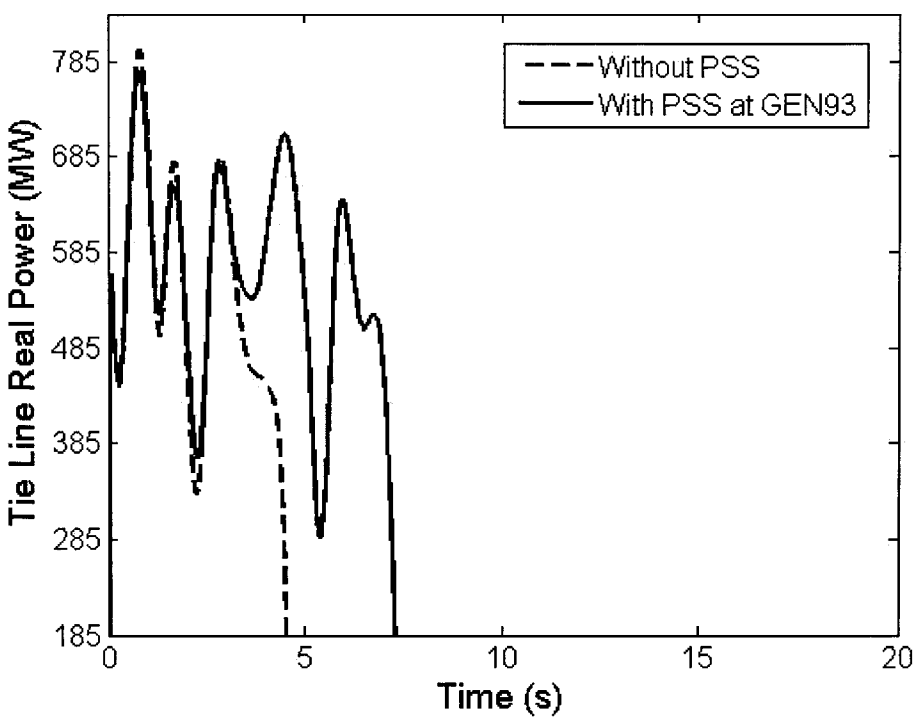

a) Tie line real power with and without PSS at GEN93 (PSS Gain K=50)

Figure 7.20 Tie line real power with three phase fault at bus 6

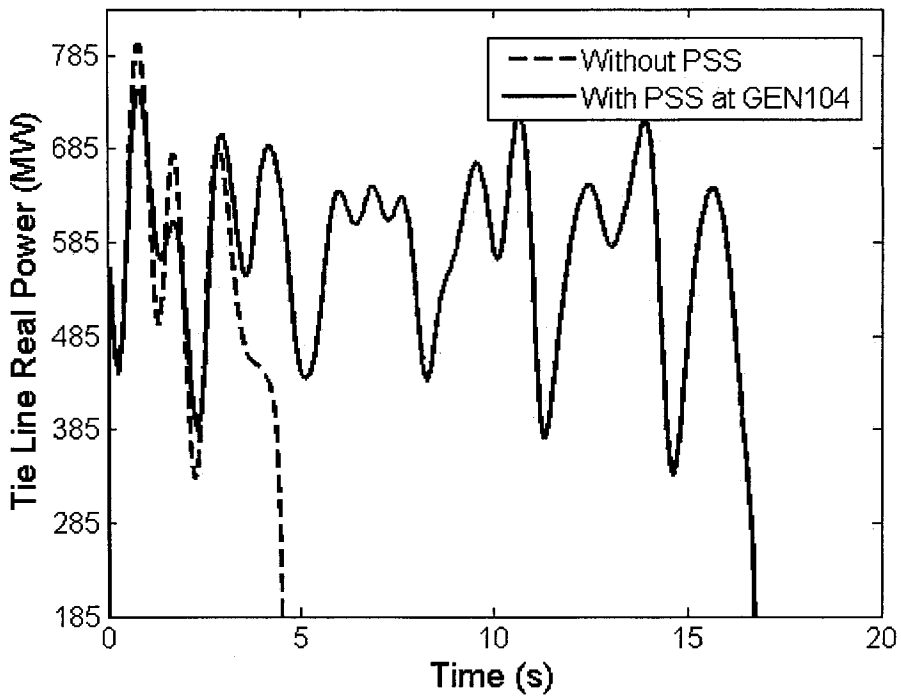

b) Tie line real power with and without PSS at GEN104 (PSS Gain K=50)

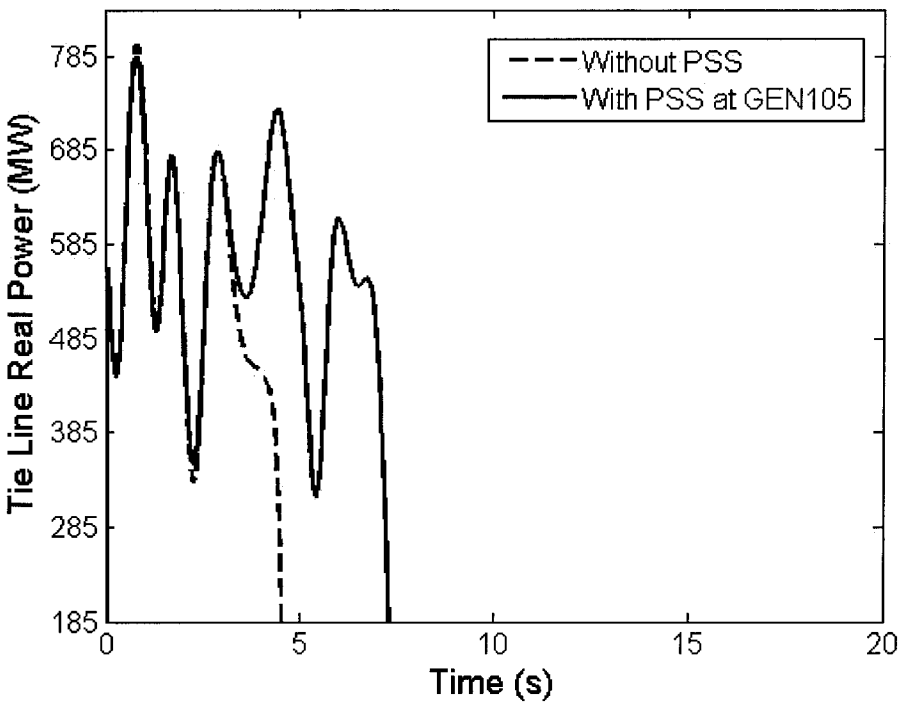

c) Tie line real power with and without PSS at GEN105 (PSS Gain K=50)

Figure 7.20 (Continued)

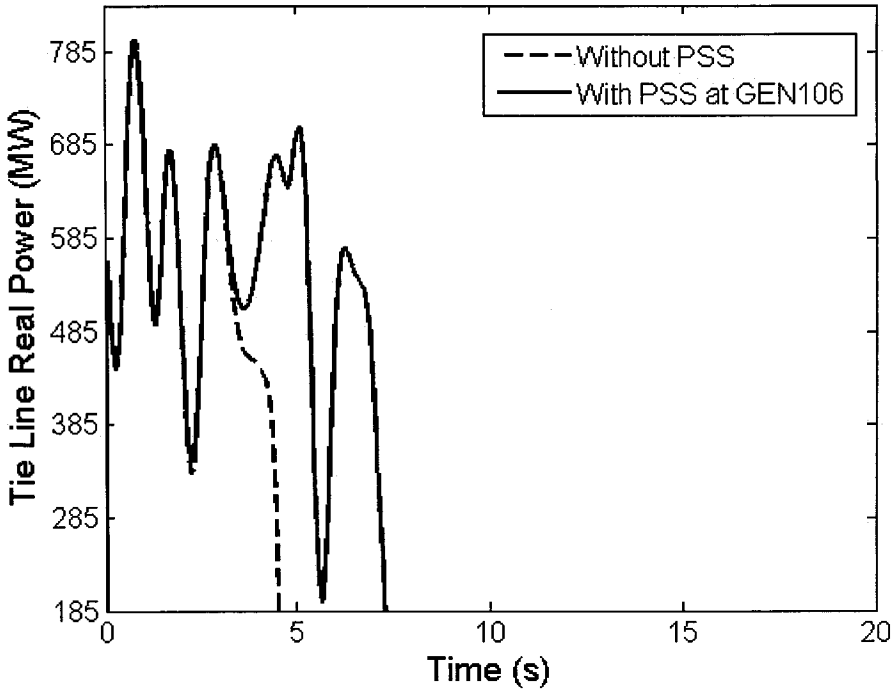

d) Tie line real power with and without PSS at GEN106 (PSS Gain K=50)

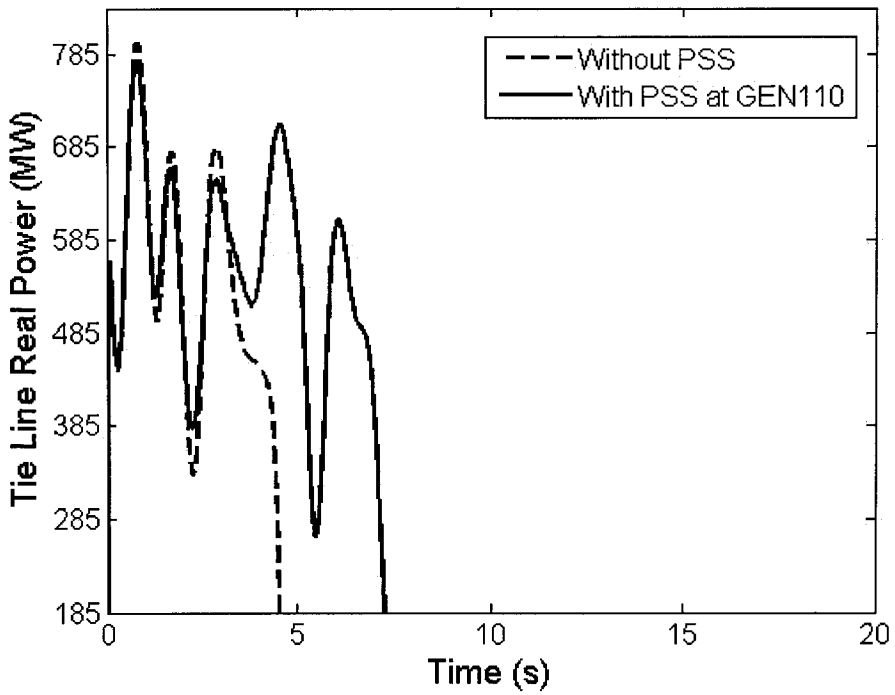

e) Tie line real power with and without PSS at GEN110 (PSS Gain K=50)

Figure 7.20 (Continued)

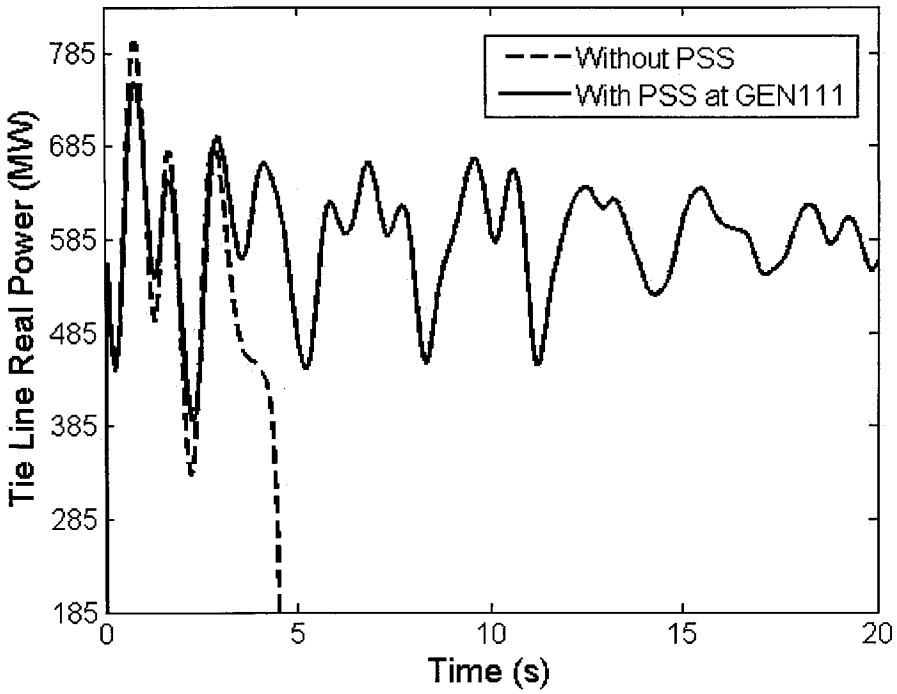

f) Tie line real power with and without PSS at GEN111 (PSS Gain K=50)

Figure 7.20 (Continued)

With such a large disturbance, the system without a PSS becomes unstable due to lack of sufficient damping torque. With properly designed PSSs, system transient stability can be improved. With a PSS at GEN111, the system becomes stable with damped oscillation.

To confirm the effect of PSSs for system transient stability, three-phase fault simulation with variable fault location was chosen for further analysis. Figure 7.21 shows the tie-line real power under a condition in which the three-phase fault applied at Bus 5 is cleared in 0.095 seconds with no line switching.

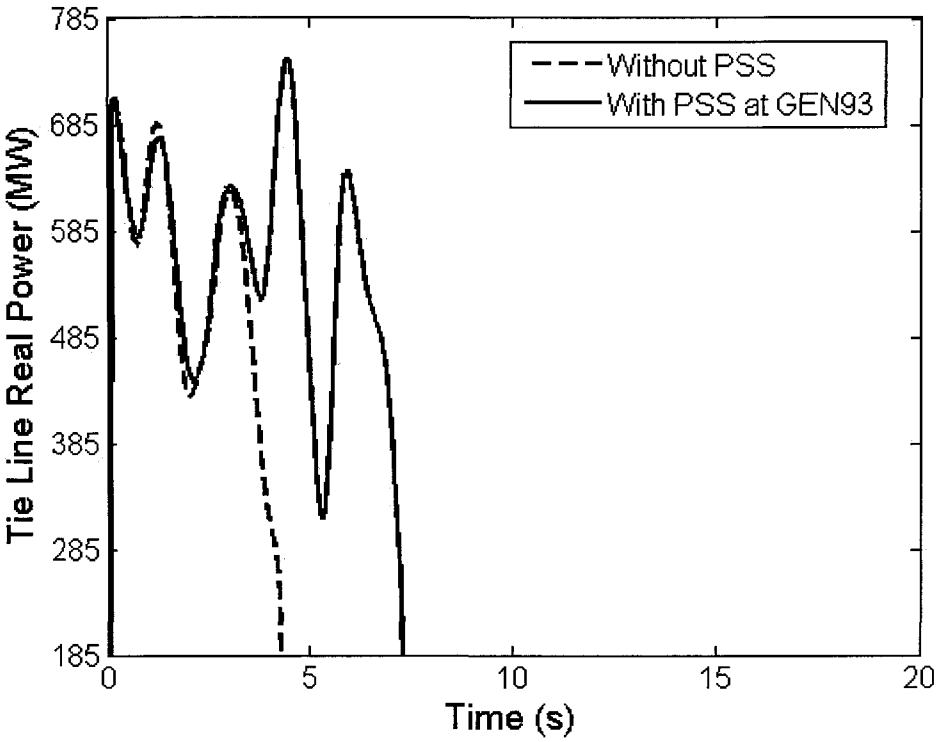

a) Tie line real power with and without PSS at GEN93 (PSS Gain K=50)

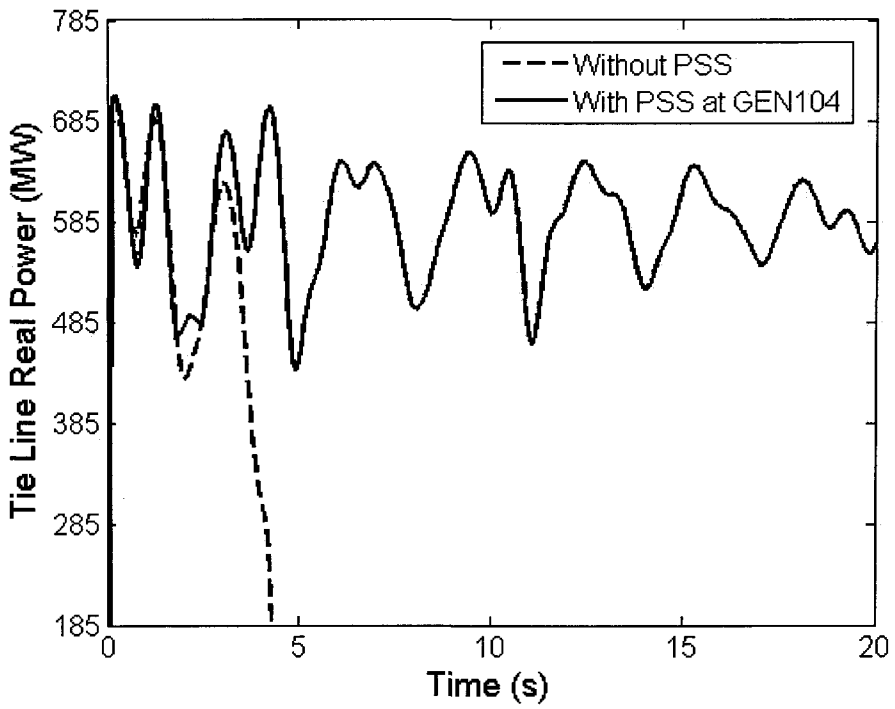

b) Tie line real power with and without PSS at GEN104 (PSS Gain K=50)

Figure 7.21 Tie line real power with three phase fault at bus 5

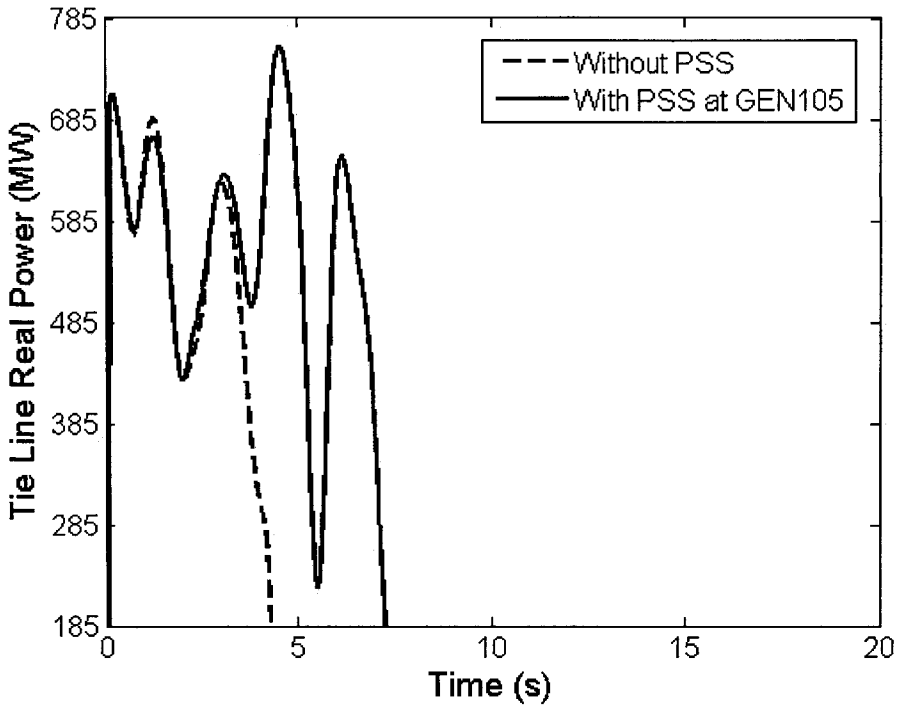

c) Tie line real power with and without PSS at GEN105 (PSS Gain K=50)

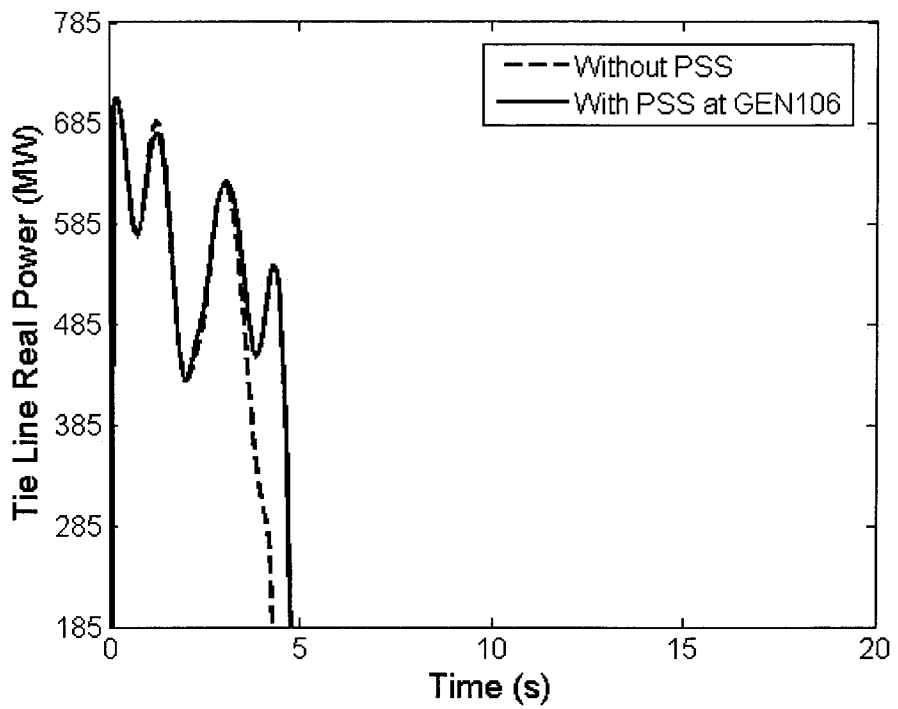

d) Tie line real power with and without PSS at GEN106 (PSS Gain K=50)

Figure 7.21 (Continued)

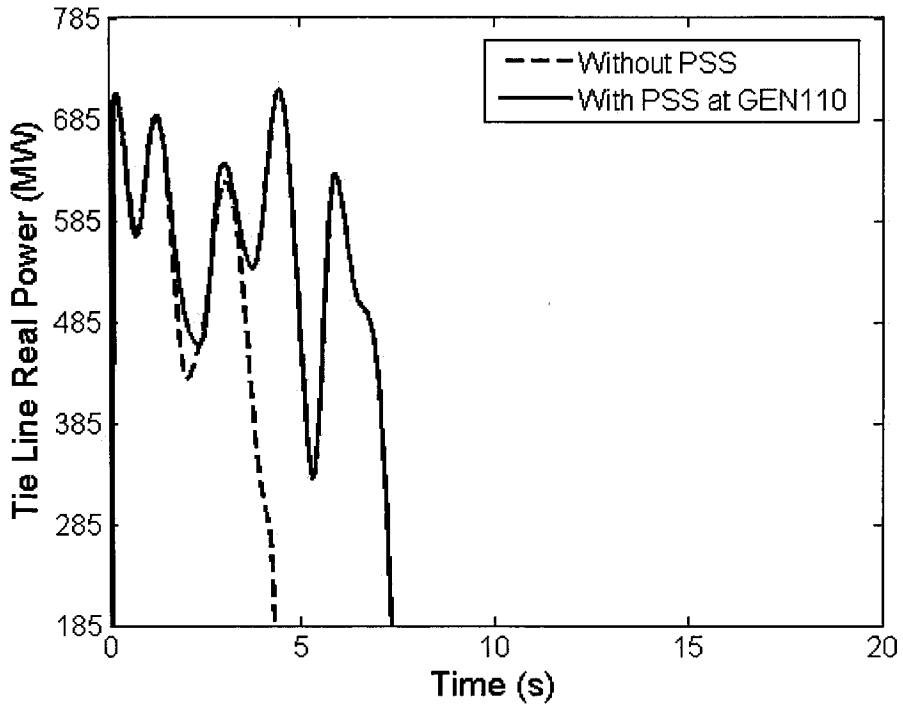

e) Tie line real power with and without PSS at GEN110 (PSS Gain K=50)

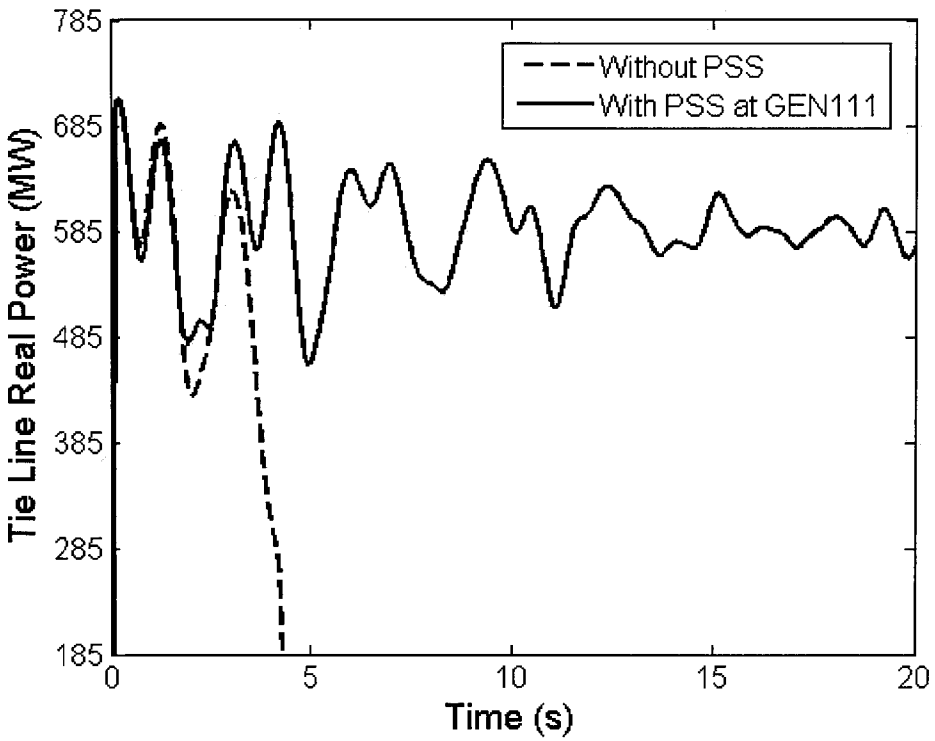

f) Tie line real power with and without PSS at GEN111 (PSS Gain K=50)

Figure 7.21 (Continued)

With a three phase fault at bus 5 for 0.095 seconds, the system without a PSS

becomes unstable with increasing amplitude of oscillation. With properly designed PSSs, system transient stability is improved. With PSSs at GEN104 and GEN111, the system becomes stable with damped oscillation. The PSS at GEN111 shows better transient performance than the PSS at GEN104. The case study shows that GEN111 is the best PSS location for improving small signal stability as well as transient stability. This provides confirmation of the nonlinear analysis.

Comparing these results with the analysis of mode shapes in Figure 7.17, linear participation factors in Table 7.33, and residues in Table 7.34, one can see that modal interaction is not properly represented by linear analysis. As a result, conventional techniques do not identify the ideal location for system controllers to improve small-signal and transient system stability.

7.2.6 Participation Factors with Well Designed PSSs

Tables 7.44 and 7.45 show the linear and nonlinear analysis of operating scenario II with well designed PSSs. Observe that nonlinear participation factors provide different information from linear participation factors.

Comparing the results in Table 7.36 with Table 7.45, it can be seen that with a properly-tuned PSS at GEN93, the nonlinear participation factor for speed deviation of every generator to inter-area mode increases, with the nonlinear participation factor for speed deviation of GEN93 to inter-area mode becoming the largest. Similar situations occur when properly designed PSSs are located at GEN104, GEN105, GEN106, GEN110, and GEN111. A properly tuned PSS at GEN111 increases the nonlinear participation factors most effectively compared with PSSs at other locations. These studies demonstrate that with a properly located and designed PSS, the participation of critical generators in the inter-area mode will increase. Furthermore, the effectiveness of the PSS in damping critical modes will be improved. This information confirms that the use of PSSs at the generators enumerated above can improve the damping of inter-area modes, and that GEN111 is the best PSS location.

Table 7.44 Linear participation factors with PSSs in the system

PSS Location	Eigenvalues	Linear Participation Factors	
		Bus #	Speed PF
93	-0.1903±j2.1475	93	0.58
		104	0.97
		105	0.58
		106	0.38
		110	**1.00**
		111	0.7
104	-0.3843±j2.3538	93	0.96
		104	0.4
		105	0.52
		106	0.35
		110	**1.00**
		111	0.57
105	-0.0544±j2.1937	93	0.96
		104	0.87
		105	0.38
		106	0.36
		110	**1.00**
		111	0.63
106	0.0203±j2.1809	93	0.97
		104	0.86
		105	0.57
		106	0.25
		110	**1.00**
		111	0.63
110	-0.1808±j2.1520	**93**	**1**
		104	**1.00**
		105	0.6
		106	0.4
		110	0.64
		111	0.72
111	-0.5155±j2.1203	93	0.97
		104	0.97
		105	0.52
		106	0.35
		110	**1.00**
		111	0.4

Table 7.45 Nonlinear participation factors with PSSs in the system

PSS Location	Eigenvalues	Nonlinear Participation Factors		
		Bus #	Speed PF	Speed PF (Normalized)
93	-0.1903±j2.1475	**93**	**45.688**	**1.0000**
		104	0.1235	0.0027
		105	0.0712	0.0016
		106	0.0374	0.0008
		110	0.1133	0.0025
		111	0.0713	0.0016
104	-0.3843±j2.3538	93	0.4064	0.0025
		104	**165.31**	**1.0000**
		105	0.2114	0.0013
		106	0.1159	0.0007
		110	0.5215	0.0032
		111	0.4462	0.0027
105	-0.0544±j2.1937	93	0.0606	0.007
		104	0.0547	0.0063
		105	**8.6557**	**1.0000**
		106	0.0288	0.0033
		110	0.0686	0.0079
		111	0.0291	0.0034
106	0.0203±j2.1809	93	0.0454	0.0138
		104	0.0458	0.0139
		105	0.0293	0.0089
		106	**3.2876**	**1.0000**
		110	0.0502	0.0153
		111	0.0275	0.0084
110	-0.1808±j2.1520	93	0.1202	0.0033
		104	0.1203	0.0033
		105	0.0672	0.0019
		106	0.0353	0.001
		110	**35.966**	**1.0000**
		111	0.0697	0.0019
111	-0.5155±j2.1203	93	5.6646	0.0027
		104	4.4139	0.0021
		105	2.499	0.0012
		106	1.1838	0.0006
		110	6.0075	0.0029
		111	**2062.6**	**1.0000**

7.2.7 Effect of Control Action on Modal Interaction

Tables 7.46 to 7.51 show the nonlinear interaction indices for key modes with and without PSSs on each unit. The initial values for calculating these indices are $x_0 = e_k$ with only the k^{th} element of the vector equal to 1, and all the others equal to zeros. The k^{th} element is the speed deviation for the associated unit.

Table 7.46 Nonlinear Interaction Indices for Key Modes – PSS at GEN93

Without PSS				With PSS			
Mode j	II(j)	k	l	Mode j	II(j)	k	l
75	0.010	75	101	75	21.95	105	99
85	0.009	75	76	85	0.378	85	99
97	0.050	75	76	97	**50.36**	99	107
	0.017	97	98		**38.31**	99	101
	0.008	97	97		**37.09**	105	99
	0.006	85	86		**34.87**	99	99
99	0.334	75	76	99	32.12	99	107
101	0.572	75	76	101	47.20	99	108
105	0.242	75	76	105	44.98	99	99
107	0.248	75	76	107	101.3	99	108

Table 7.47 Nonlinear Interaction Indices for Key Modes – PSS at GEN104

Without PSS				With PSS			
Mode j	II(j)	k	l	Mode j	II(j)	k	L
55	0.020	55	100	55	17.81	77	103
77	0.016	77	100	77	218.8	77	104
79	0.021	77	78	79	13.50	77	103
97	0.072	77	78	97	**92.68**	97	103
	0.030	55	56		**92.58**	97	104
	0.027	78	79		**86.49**	99	103
	0.024	77	80		**82.24**	101	103
99	0.259	77	78	99	1211	97	104
101	0.312	55	56	101	29.98	103	104
103	0.233	55	56	103	113.9	103	104

Table 7.48 Nonlinear Interaction Indices for Key Modes – PSS at GEN105

Without PSS				With PSS			
Mode j	II(j)	k	l	Mode j	II(j)	k	l
73	0.021	73	107	73	0.223	77	109
77	0.012	77	97	77	0.031	77	99
79	0.013	77	97	79	4.583	79	110
97	0.097	79	80	97	**6.272**	79	80
	0.049	73	74		**3.864**	79	110
	0.025	78	79		**3.383**	79	109
	0.023	77	80		**2.980**	101	109
99	1.785	79	80	99	6.686	79	80
101	0.285	79	80	101	7.302	109	109
105	0.242	79	80	105	1.847	107	109
107	0.243	79	80	107	26.54	101	110
109	0.711	73	80	109	3.949	109	109

Table 7.49 Nonlinear Interaction Indices for Key Modes – PSS at GEN106

Without PSS				With PSS			
Mode j	II(j)	k	l	Mode j	II(j)	k	l
73	0.014	73	107	73	1.530	73	102
77	0.010	73	110	77	0.116	99	100
79	0.014	73	110	79	0.118	109	107
81	0.018	73	74	81	0.045	99	100
97	0.095	73	74	97	**0.516**	99	101
	0.043	79	80		**0.438**	99	102
	0.011	78	79		**0.396**	97	102
	0.011	79	82		**0.299**	100	102
99	1.722	73	74	99	2.210	101	101
101	0.496	73	74	101	0.647	99	102

Table 7.50 Nonlinear Interaction Indices for Key Modes – PSS at GEN110

Without PSS				With PSS			
Mode j	II(j)	k	l	Mode j	II(j)	k	L
75	0.009	75	101	75	2.920	77	100
85	0.006	95	97	85	23.09	101	99
93	0.035	85	98	93	1.249	101	99
97	0.029	75	76	97	**18.37**	99	99
	0.018	93	98		**16.75**	101	99
	0.017	97	98		**14.52**	99	100
	0.015	85	86		**14.07**	99	105
99	0.179	75	76	99	21.18	99	100
101	0.390	75	76	101	43.13	99	99
105	0.370	75	86	105	126.2	99	100

Table 7.51 Nonlinear Interaction Indices for Key Modes – PSS at GEN111

Without PSS				With PSS			
Mode j	II(j)	k	l	Mode j	II(j)	k	L
75	0.019	55	56	75	1.079	101	105
85	0.022	55	56	85	3.051	101	107
93	0.179	77	98	93	6.117	97	101
97	0.029	75	76	97	**193.3**	101	99
	0.018	93	98		**193.3**	97	102
	0.017	97	98		**183.0**	101	107
	0.015	85	86		**182.9**	103	107
99	0.627	55	56	99	136.9	101	107
101	0.820	55	56	101	27.50	101	107
103	0.365	55	56	103	519.5	97	108
107	0.500	79	80	107	31.30	101	108

From the analysis of nonlinear interaction indices in Tables 7.46 to 7.51, it is clear that the interaction indices for the inter-area mode and other key modes are much larger using the designed PSSs than without PSSs for these six units. Compared to the use of PSSs at other generators, the interaction indices for inter-area mode with a PSS at GEN111 are much larger. This confirms that GEN111 is the best PSS location for effectively damping the inter-area mode.

These results reveal that a well-designed PSS increases the modal interaction among the critical modes. This, in turn, aids in enhancing the damping of critical modes more effectively thus revealing the importance of nonlinear analysis.

7.2.8 Conclusion

From the above case study, observe that the nonlinear analysis conforms with linear analysis to predict that the best PSS location to improve the damping ratio of mode

97 for operating scenario I is a generator at bus 110. For operating scenario II, PSS sensitivity indices show that generators at bus 111 and 104 are better PSS locations than generators at bus 93 and 110 for damping the inter-area mode. Generator at bus 111 is the best location for placing a PSS. By designing a PSS for every unit and comparing the results, it has been shown that the PSS sensitivity index gives a correct prediction for PSS performance. For this high-stress operating condition, linear analysis failed to provide correct information for prediction of the best PSS location.

Nonlinear participation factors and interaction indices with properly designed PSS were also calculated. The results of this analysis demonstrate that, with a properly located and designed PSS, participation of critical generators in the inter-area mode and modal interaction among the critical modes will increase. Additionally, this will improve the effectiveness of the PSS in damping critical modes. This result confirms that the effective use of PSSs at these generator locations can improve the damping of the inter-area mode and, additionally, that GEN111 is the best PSS location for operating scenario II.

8 CONCLUSIONS

8.1 Conclusions

In this work, a systematic approach for deriving second-order normal form representations in the neighborhood of equilibrium points is presented. On the basis of this model, nonlinear modal interaction measures have been obtained to assess the extent and distribution of nonlinearity in the system. Furthermore, an understanding of the character of such nonlinearity leads to an improved strategy for effective placement of Power System Stabilizers. For low-stress conditions linear analysis usually leads to a good identification of critical machines, but, in contrast, local linearization of the system model for high-stress conditions may preclude an in-depth analysis of nonlinearity and result in an inadequate controller design. A more accurate representation of the system based on normal form theory taking into account nonlinear modal interaction has therefore been used to fully characterize these phenomena. The theory, analysis, results, and observations presented in this dissertation can be summarized as follows:

1. Based on normal form theory, second-order information can be included to generalize nonlinear modal interaction measures. This allows assessment of the extent and distribution of nonlinearity in the system. Analytical criteria have been developed to predict the existence of nonlinear modal interactions that significantly affect system dynamic performance.
2. Analysis results show that linear resonance and second-order quasi-resonance conditions could possibly happen in real power systems. When two eigenvalues pass a strong near-resonance condition, one of them reduces its damping and becomes unstable. To fully understand the cause of the oscillation, both the movement of signal mode and nearness of two critical modes must be considered.
3. Linear resonances among fundamental modes may trigger modal interactions that generate significant nonlinear behavior and lead to second-order quasi-

resonance conditions. By taking into account the effect of nonlinear modal interactions, normal form analysis provides a more accurate representation of the system and more fully characterizes these phenomena.

4. Numerical estimates of nonlinear participation factors have been proposed to provide a more precise measure of nonlinear mode-state participations than that yielded by analytical estimates of nonlinear participation factors. For low-stress conditions these two types of estimates may provide similar results, but for high-stress conditions the numerical estimate is much more accurate than the analytical approximation.
5. Many power systems face the problem of troublesome dynamic oscillations. Power system damping controllers are used to damp such oscillations by increasing the damping of certain troublesome modes. The first step in designing such a controller for a multi-machine power system is to determine its optimum location. For commonly used PSSs, conventional techniques for assessing such a location usually include only linear information about the system, and may fail to provide complete characterization of system performance, especially under heavy stress conditions.
6. Nonlinear participation factors obtained from normal form analysis were applied to predict the efficacy of PSSs at various locations. Nonlinear participation factors present more accurate information than linear indices to improve the design of PSSs.
7. A nonlinear PSS sensitivity index is proposed that includes both PSS input and its control effort. This is a useful alternative approach for assessing the effect of control action on the system response based on a close-loop framework. Assessment of the PSS effect can be improved more generally with this kind of measurement.
8. The PSS model is included as a part of the existing normal form program. Nonlinear mode-state participations are obtained to result in a more complete characterization of nonlinear phenomena with properly designed PSSs. These

studies demonstrate that with a properly located and designed PSS, the participation of critical generators in the inter-area mode will increase. Furthermore, this will improve the effectiveness of the PSS in damping critical modes. In contrast, with an improperly-located PSS, the participation of certain generators in the inter-area mode will drop, influencing the behavior of the PSS.

9. The characterization of nonlinear modal interaction of the system with properly designed PSS has been investigated. Results of the analysis suggest that a well-designed PSS increases the modal interaction among critical modes. This in turn aids in enhancing the damping of critical modes more effectively.
10. This analysis will help identify situations under which conventional linear analysis will not provide complete information and effective control support due to the absence of nonlinear information in the analysis.

8.2 Future Work

Based on the observations and experience gained in performing this research, several potentially fruitful possibilities for future work may be summarized as follows:

1. To extend the normal form method for application to large systems, the computational burden is almost always the most challenging problem, with calculation of initial values in normal form space from initial values in physical space the most time-consuming part. A more effective algorithm for solving nonlinear equations may help to alleviate this problem.
2. The analysis herein suggests that nonlinear sensitivity indices could be used to infer the effect of a given initial-state excitation for a given mode. By simultaneously perturbing the speed deviation of two or more machines, the effects of multiple PSS control actions could be effectively estimated.
3. Placement of other kinds of controllers, such as FACTS, may be assessed by

normal form analysis including second order information.

4. APPENDIX-A SYSTEM DATA FOR 4-MACHINE TEST SYSTEM

Table A.1 Power flow 4-machine bus data: operation scenario I

Bus #	|V| p.u.	ang (V) degree	P_{load} MW	Q_{load} MVAR	P_{gen} MW	Q_{gen} MVAR
1	1.0200	59.47	0.00	0.00	664.40	-12.85
2	1.0200	50.26	0.00	0.00	664.40	459.57
3	1.0200	0.00	0.00	0.00	557.65	-17.99
4	1.0200	-7.73	0.00	0.00	500.00	445.54
5	0.9818	42.90	1120.00	250.00	0.00	0.00
6	0.9802	-13.55	1180.00	250.00	0.00	0.00

Table A.2 Power flow 4-machine bus data: operation scenario II

Bus #	|V| p.u.	ang (V) degree	P_{load} MW	Q_{load} MVAR	P_{gen} MW	Q_{gen} MVAR
1	1.0200	64.31	0.00	0.00	664.40	-12.85
2	1.0200	55.11	0.00	0.00	664.40	492.61
3	1.0200	0.00	0.00	0.00	564.59	-17.74
4	1.0200	-7.82	0.00	0.00	500.00	485.16
5	0.9785	47.73	920.00	250.00	0.00	0.00
6	0.9764	-13.69	1380.00	250.00	0.00	0.00

Table A.3 Power flow 4-machine bus data: operation scenario III

Bus #	|V| p.u.	ang (V) degree	P_{load} MW	Q_{load} MVAR	P_{gen} MW	Q_{gen} MVAR
1	1.0200	68.63	0.00	0.00	664.40	13.06
2	1.0136	59.41	0.00	0.00	664.40	500.00
3	1.0200	0.00	0.00	0.00	570.69	4.54
4	1.0146	-7.92	0.00	0.00	500.00	500.00
5	0.9687	51.93	890.00	250.00	0.00	0.00
6	0.9673	-13.89	1410.00	250.00	0.00	0.00

Table A.4 Line Data (On System Base 100 MVA)

Bus#	Bus#	R	X
1	2	0.002500	0.025000
2	5	0.001000	0.010000
5	6	0.022000	0.220000
3	4	0.002500	0.025000
4	6	0.001000	0.010000

Table A.5 Generator Data (On machine base)

Machine #	Bus #	D	H	R_a	x_d	x_q	x'_d	x'_q	τ'_{d0}	τ'_{q0}	BMVA
1	1	4.0	6.5	0.0025	1.80	1.70	0.30	0.30	8.0	0.40	900
2	2	2.0	6.5	0.0025	1.80	1.70	0.30	0.30	8.0	0.40	900
3	3	11.0	6.5	0.0025	1.80	1.70	0.30	0.30	8.0	0.40	900
4	4	10.0	6.5	0.0025	1.80	1.70	0.30	0.30	8.0	0.40	900

Table A.6 Exciter Data

Bus#	K_A	T_A	T_C	T_B	T_R	V_{RMIN}	V_{RMAX}
1	180	0.01	1.0	10.0	0.01	-5.0	5.0
2	100	0.01	1.0	10.0	0.01	-5.0	5.0
3	130	0.01	1.0	10.0	0.01	-5.0	5.0
4	220	0.01	1.0	10.0	0.01	-5.0	5.0

APPENDIX-B SYSTEM DATA FOR 50-MACHINE TEST SYSTEM

Table B.1 Power flow 50-machine bus data: operation scenario I

Bus #	|V| p.u.	ang (V) degree	P_{load} MW	Q_{load} MVAR	P_{gen} MW	Q_{gen} MVAR
93	1.0000	-7.79	100.40	73.20	1080.00	408.87
104	1.0000	-2.26	30.20	7.60	1400.00	317.62
105	1.0070	-22.62	96.00	167.40	620.00	298.54
106	1.0050	-14.26	64.00	16.00	1080.00	217.91
110	1.0000	-6.81	100.40	73.20	980.00	545.10
111	1.0000	-4.03	60.40	1166.00	1800.00	489.00
34	1.1375	-10.81	45.05	46.56	0.00	0.00
35	1.1378	-10.88	49.19	27.53	0.00	0.00
51	1.1122	-18.70	58.45	28.44	0.00	0.00
58	1.1047	-19.74	76.30	-10.80	0.00	0.00
60	1.1370	-12.01	0.00	0.00	51.00	38.20
66	1.1165	-9.98	102.20	26.70	0.00	0.00
67	1.0900	-11.88	0.00	0.00	1486.00	247.77
68	1.2082	-41.12	0.00	-7.41	0.00	0.00
70	0.9987	-25.50	0.00	56.63	0.00	0.00
71	1.0264	-25.59	0.00	-21.20	0.00	0.00
74	1.0959	-22.98	81.90	43.70	0.00	0.00
78	1.0736	-15.42	89.00	26.80	0.00	0.00
79	1.0520	-18.04	9.10	3.00	250.20	-11.43
80	1.0690	-16.58	17.10	5.00	47.00	-15.26
81	1.1308	-39.10	82.20	-93.10	0.00	0.00
82	0.9750	-26.72	2.10	1.10	70.00	15.80
88	1.1077	-15.37	69.00	20.90	0.00	0.00
89	1.0660	-6.55	0.60	0.20	673.00	137.17
90	0.9500	-13.87	4.60	1.50	22.00	-3.51
91	1.0000	-19.01	0.00	0.00	64.00	-5.84
92	0.9549	-21.49	0.00	31.02	0.00	0.00
94	1.0200	-6.42	15.40	7.60	300.00	23.17
95	0.9200	15.98	6.70	2.20	131.00	14.18
96	1.0000	-22.00	0.00	0.00	60.00	20.23
97	0.9670	-11.04	0.00	0.00	140.00	46.44
98	0.9700	-5.19	0.00	0.00	426.00	-30.52
99	1.0000	-5.70	10.46	5.23	200.00	-6.15
100	1.0140	-9.56	0.00	0.00	170.00	59.19
101	1.0390	-17.41	17.80	4.50	310.90	151.76
102	1.0190	-7.76	37.60	9.20	2040.00	469.70

Table B.1 (Continued)

Bus #	|V| p.u.	ang (V) degree	P_{load} MW	Q_{load} MVAR	P_{gen} MW	Q_{gen} MVAR
103	1.0000	-8.72	0.00	0.00	135.00	5.14
107	1.0205	-23.02	-17.50	-12.80	0.00	0.00
108	1.0140	-18.82	0.00	0.00	800.00	70.83
109	0.9150	-26.59	0.00	0.00	52.00	-16.25
112	1.0370	-17.59	18.60	4.60	300.00	143.19
115	1.0490	-15.05	683.50	184.70	2493.00	156.38
116	1.0430	-17.37	792.60	315.50	2713.00	630.01
117	1.0300	-16.90	485.30	71.40	2627.00	239.25
118	1.0100	-18.51	651.90	328.40	4220.00	633.11
119	0.9547	-50.54	2094.00	5774.00	8954.00	5373.00
120	1.0280	-46.27	-408.00	175.10	0.00	0.00
121	1.0460	-20.72	237.70	-17.30	2997.00	-395.78
122	1.0000	-5.39	29.20	7.00	1009.00	128.28
123	1.0292	-31.38	-84.00	-19.00	0.00	0.00
124	1.0000	-7.11	94.10	780.30	3005.00	460.15
125	1.0193	-32.50	-712.00	-319.00	0.00	0.00
126	0.9968	-64.74	-333.00	-160.00	0.00	0.00
127	1.0065	-30.40	-546.00	-72.00	0.00	0.00
128	1.0250	-32.19	4075.00	703.50	12963.00	2732.41
129	0.9692	-65.19	-482.00	-122.00	0.00	0.00
130	1.0570	-45.07	4328.00	944.30	5937.00	2049.58
131	1.0420	-20.07	21840.00	4320.00	28300.00	7150.74
132	1.0420	-5.62	491.90	110.20	3095.00	582.38
133	1.0964	-12.67	-83.00	-36.30	0.00	0.00
134	1.0440	-9.71	22309.00	7402.00	20626.00	7364.61
135	1.1070	30.03	4298.00	1264.00	5982.00	1564.75
136	1.0830	5.50	52951.00	13552.00	51950.00	14427.20
137	1.0640	-23.58	11946.00	2608.00	12068.00	2872.49
138	1.1085	12.00	-363.00	-188.00	0.00	0.00
139	1.0400	-8.47	57718.00	13936.00	56834.00	15077.90
140	1.0500	-24.08	24775.00	6676.00	23123.00	6701.28
141	1.0530	-7.93	32799.00	11361.00	37911.00	11649.57
142	1.1550	-8.81	17737.00	3934.00	24449.00	5470.39
143	1.0310	-12.85	4672.00	1709.00	5254.00	2151.34
144	0.9970	-5.76	9602.00	2203.00	11397.00	2656.37
145	1.0520	5.02	10173.00	1555.00	14355.02	2531.11

Table B.2 Power flow 50-machine bus data: operation scenario II

Bus #	|V| p.u.	ang (V) degree	P_{load} MW	Q_{load} MVAR	P_{gen} MW	Q_{gen} MVAR
93	1.0000	73.76	100.40	73.20	1080.00	593.62
104	0.9382	91.61	30.20	7.60	2400.00	500.00
105	1.0070	67.73	96.00	167.40	1620.00	554.77
106	1.0050	67.72	64.00	16.00	1080.00	330.36
110	1.0000	74.90	100.40	73.20	1080.00	703.87
111	0.9627	83.34	60.40	1166.00	2600.00	1000.00
34	1.1237	70.39	45.05	46.56	0.00	0.00
35	1.1237	70.31	49.19	27.53	0.00	0.00
51	1.0639	59.63	58.45	28.44	0.00	0.00
58	1.0716	60.77	76.30	-10.80	0.00	0.00
60	1.1370	42.03	0.00	0.00	51.00	32.13
66	1.0512	73.75	102.20	26.70	0.00	0.00
67	1.0900	57.22	0.00	0.00	1486.00	663.97
68	1.1702	38.48	0.00	-7.41	0.00	0.00
70	0.9733	56.25	0.00	56.63	0.00	0.00
71	1.0023	56.14	0.00	-21.20	0.00	0.00
74	1.0774	58.90	81.90	43.70	0.00	0.00
78	1.0583	64.71	89.00	26.80	0.00	0.00
79	1.0520	52.17	9.10	3.00	250.20	-6.49
80	1.0690	52.75	17.10	5.00	47.00	-8.45
81	1.1150	44.29	82.20	-93.10	0.00	0.00
82	0.9750	47.82	2.10	1.10	70.00	24.34
88	1.0908	65.62	69.00	20.90	0.00	0.00
89	1.0660	73.61	0.60	0.20	673.00	169.31
90	0.9500	45.05	4.60	1.50	22.00	-3.78
91	1.0000	58.44	0.00	0.00	64.00	11.06
92	0.9482	50.00	0.00	31.02	0.00	0.00
94	1.0200	47.78	15.40	7.60	300.00	19.28
95	0.9200	55.39	6.70	2.20	131.00	9.23
96	1.0000	60.77	0.00	0.00	60.00	26.16
97	0.9670	59.34	0.00	0.00	140.00	51.52
98	0.9700	75.73	0.00	0.00	426.00	2.14
99	1.0000	75.54	10.46	5.23	200.00	19.93
100	1.0140	70.75	0.00	0.00	170.00	75.56
101	1.0279	64.52	17.80	4.50	310.90	186.50
102	0.9944	38.98	37.60	9.20	2040.00	640.00
103	1.0000	71.44	0.00	0.00	135.00	13.21
107	1.0080	52.58	-17.50	-12.80	0.00	0.00
108	1.0140	49.70	0.00	0.00	800.00	146.62
109	0.9150	48.10	0.00	0.00	52.00	-11.11
112	1.0204	64.37	18.60	4.60	300.00	160.00

Table B.2 (Continued)

Bus #	|V| p.u.	ang (V) degree	P_{load} MW	Q_{load} MVAR	P_{gen} MW	Q_{gen} MVAR
115	1.0490	10.31	683.50	184.70	2493.00	124.08
116	1.0430	15.42	792.60	315.50	2713.00	687.83
117	1.0300	22.26	485.30	71.40	2627.00	812.66
118	1.0100	17.03	651.90	328.40	4220.00	923.69
119	0.9390	-7.55	2094.00	5774.00	8954.00	5373.00
120	0.9828	3.67	-408.00	175.10	0.00	0.00
121	1.0460	39.60	237.70	-17.30	2997.00	275.33
122	1.0000	53.44	29.20	7.00	1009.00	280.39
123	0.9994	20.17	-84.00	-19.00	0.00	0.00
124	1.0000	59.38	94.10	780.30	3005.00	854.90
125	0.9901	26.19	-712.00	-319.00	0.00	0.00
126	0.9819	-21.66	-333.00	-160.00	0.00	0.00
127	0.9817	20.71	-546.00	-72.00	0.00	0.00
128	1.0250	16.29	4075.00	703.50	12963.00	3019.24
129	0.9606	-17.62	-482.00	-122.00	0.00	0.00
130	1.0570	-7.04	4328.00	944.30	5937.00	1923.66
131	1.0420	13.36	21840.00	4320.00	28300.00	6498.95
132	1.0420	32.89	491.90	110.20	3095.00	780.22
133	1.0563	37.11	-83.00	-36.30	0.00	0.00
134	1.0440	1.99	22309.00	7402.00	20626.00	7265.64
135	1.1070	46.33	4298.00	1264.00	5982.00	1589.72
136	1.0830	20.73	52951.00	13552.00	51950.00	14535.14
137	1.0640	-19.05	11946.00	2608.00	12068.00	2868.73
138	1.1202	34.90	-363.00	-188.00	0.00	0.00
139	1.0400	-2.93	57718.00	13936.00	56834.00	15042.29
140	1.0500	-18.77	24775.00	6676.00	23123.00	6698.08
141	1.0530	12.65	32799.00	11361.00	37911.00	11520.90
142	1.1550	18.46	17737.00	3934.00	24449.00	5583.03
143	1.0310	18.98	4672.00	1709.00	5254.00	2328.86
144	0.9970	21.97	9602.00	2203.00	11397.00	2776.91
145	1.0520	5.02	10173.00	1555.00	10282.21	1633.67

Table B.3 Generator Data (Two-axis model)

Bus #	D	H	x_d	x_q	x_d'	x_q'	τ_{d0}'	τ_{q0}'	BMVA
93	5	115.0366	0.09842	0.09673	0.024	0.024	8.5	1.24	100
104	5	73.8528	0.1016	0.0982	0.0122	0.0122	10	1.5	100
105	5	84.3915	0.1144	0.1092	0.0208	0.0208	6.61	1.5	100
106	5	56.261	0.17165	0.16377	0.03118	0.03118	6.61	1.5	100
110	5	115.05	0.09842	0.09673	0.024	0.024	8.5	1.24	100
111	5	73.8528	0.1016	0.0982	0.0122	0.0122	10	1.5	100

Table B.4 Generator Data (Classical model)

Bus #	H	D
60	1.41	0.30
67	52.18	10.40
79	6.65	1.30
80	1.29	0.30
82	2.12	0.40
89	20.56	4.00
90	0.76	0.15
91	1.68	0.30
94	17.34	3.40
95	5.47	1.10
96	2.12	0.40
97	5.49	1.00
98	13.96	2.80
99	17.11	3.40
100	7.56	1.50
101	12.28	2.40
102	78.44	15.60
103	8.16	1.60
108	30.43	6.00
109	2.66	0.50
112	12.28	2.40
115	97.33	19.40
116	105.50	21.00
117	102.16	20.40
118	162.74	32.40
119	69.64	13.80
121	116.54	23.20
122	39.24	7.80
124	116.86	23.20
128	50.39	10.00
130	230.90	46.00
131	110.17	22.00
132	120.35	24.00
134	200.53	40.00
135	116.32	23.20
136	201.82	40.20
137	156.44	156.20
140	224.80	224.90
142	237.70	47.40
143	204.30	40.80
144	147.67	29.40
145	518.08	103.60
141	147.43	29.40
139	221.02	44.20

Table B.5 Exciter Data

Bus#	K_A	T_A	T_C	T_B	T_R	V_{RMIN}	V_{RMAX}
93	120	0.02	1	10	0.01	-2	8.89
104	200	0.015	1	10	0.01	-7	8.86
105	50	0.02	1	10	0.01	0	7.38
106	50	0.02	1	10	0.01	0	7.38
110	120	0.02	1	10	0.01	-2	8.89
111	200	0.015	1	10	0.01	-7	8.86

BIBLIOGRAPHY

[1] Kundur, P., *Power System Stability and Control.* New York: McGraw-Hill Inc., 1994.

[2] Inter-Area Oscillations In Power Systems, IEEE Publication Catalog Number 95 TP 101, 1995.

[3] Task Force on Terms & Definitions, System Dynamic Performance Subcommittee, Power System Engineering Committee, "Proposed terms and definitions for power system stability", *IEEE Trans. PAS*, Vol. 7, pp. 1894-1898, July 1982.

[4] Yorino N, Sasaki H, Tamura Y, Yokoyama R., "A generalized analysis method of auto-parametric resonances in power systems", *IEEE Trans. Power Systems*, Vol. 4, pp. 1057-1064, August 1989.

[5] V. Vittal, N. Bhatia, and A. A. Fouad, "Analysis of the interarea mode phenomena in power systems following large disturbances", *IEEE Trans. Power Systems*, Vol. PS-6, pp. 1515-1521, Apr. 1991.

[6] Chih-Ming Lin, V. Vittal, W Kliemann, and A. A. Fouad, "Investigation of modal interaction and its effects on control performance in stressed power systems using normal forms of vector fields", *IEEE Trans. Power Systems*, Vol. 11, pp. 781-787, May 1996.

[7] Songzhe Zhu, Vijay Vittal, and Wolfgang Kliemann, "Analyzing dynamic performance of power systems over parameter space using normal forms of vector fields – Parts I and II", *IEEE Trans. Power Systems*, Vol. 16, No. 3, pp. 451-455, August 2001.

[8] Starrett, S. K. "Application of Normal Forms of Vector Fields to Stressed Power Systems", Ph.D. Thesis, Iowa State University, Ames, Iowa, 1994.

[9] Messina, A.R., and V. Vittal, "Assessment of nonlinear interaction between nonlinearly coupled modes using higher-order spectra", *IEEE Trans. on Power Systems*, Vol. 20, No. 1, pp. 375-383, Feb. 2005.

[10] Ian Dobson, Jianfeng Zhang, Scott Greene, Henrik Engdahl, and Peter W. Sauer, "Is strong modal resonance a precursor to power system oscillations?", *IEEE Trans. On Circuits and Systems*, Vol. 48, No. 3, pp. 340-349, March 2001.

[11] Gilsoo Jang, V. Vittal, and Wolfgang Kliemann, "Effect of nonlinear modal interaction on control performance: use of normal form techniques in control design", *IEEE Trans. Power Systems*, Vol. 13, No.2, pp. 401-407, May 1998.

[12] Starrett, S. K., W. Kliemann, V. Vittal and A. A. Fouad, "Power system modal behavior: significance of second and third order nonlinear terms", *Proceedings of the North American Power Symposium*, pp. 241-255, Washington, DC, October 1993.

[13] Dobson, I., and E. Barocio, "Scaling of normal form analysis coefficients under coordinate change", *IEEE Trans. on Power Systems*, Vol. 19, No. 3, pp. 1438 – 1444, August 2004.

[14] Guckenheimer, J., and P. Holmes, *Nonlinear Oscillations, Dynamical Systems, and Bifurcations of Vector Fields*. Springer-Verlag, New York, 1983.

[15] Wiggins, S., *Introduction to Applied Nonlinear Dynamical Systems and Chaos*, Springer-Verlag, New York, 1990.

[16] Nayfeh, A.H., *Method of Normal Forms*, John Wiley and Sons, Inc., New York, 1993.

[17] Arnold, V.I., *Geometrical Methods in the Theory of Ordinary Differential Equations*. Springer-Verlag, New York, 1983.

[18] Abramowitz, M. and Stegun, I. A. (Eds.). Handbook of Mathematical Functions with Formulas, Graphs, and Mathematical Tables, 9th printing. New York: Dover, 1972.

[19] S. K. Starret, A. A. Fouad, "Nonlinear measures of mode-machine participation", *IEEE Trans. Power Systems*, Vol. 13, pp. 389-394, May 1994.

[20] I. Dobson,"Strong resonance effects in normal form analysis and Subsynchronous resonance", in *Proc. Bulk Power Systems Dynamics and Control V*, Onomichi, Japan, pp. 563-574, August 26-31, 2001.

[21] Ni, Y., V. Vittal, and W. Kliemann, "A Study of System Separation Mechanisms in the Neighborhood of a Relevant Type-n UEP Via Normal Form of Vector Fields", *IEE Proceedings on Generation, Transmission and Distribution*, Vol. 145, No. 2, pp. 139-144, March 1998.

[22] Vittal, V., W. Kliemann, Y-X. Ni, D. G. Chapman, A. D. Silk, D. J. Sobajic, "Determination of Generator Groupings for an Islanding Scheme in the Manitoba Hydro System Using the Method of Normal Forms", *IEEE Trans. on Power Systems*, Vol. 13, pp. 1345-1351, No. 4, November 1998.

[23] Starrett, S. K., V. Vittal, A. A. Fouad, and W. Kliemann, "A methodology for the analysis of nonlinear, interarea interactions between power system natural modes of oscillation utilizing normal forms", *Proceedings of the 1993 International Symposium on Nonlinear Theory and Its Application*, Vol. 2, pp. 523-538, Sheraton Waikiki Hotel, Hawaii, December 5-10, 1993.

[24] J. J. Sanchez Gasca, V. Vittal, M. J. Gibbard, D. J. Vowles, S. Liu, U. D. Annakage, "Analysis of higher order terms for small signal stability analysis", *IEEE PES General Meeting 2005*, pp. 1072-1080, San Francisco, Cal, 12-16 June 2005.

[25] M. Klein, G. J. Rogers, and P. Kundur, "A fundamental study of inter-area oscillations in power systems", *IEEE Trans. Power Systems*, Vol. 6, pp. 914-921, August 1991.

[26] Vittal, V., "Transient Stability test systems for direct stability method", *IEEE Trans. on Power Systems*, Vol. 7, pp. 37-42, Feb. 1992.

[27] Anderson, P.M., and A. A. Fouad, *Power System Control and Stability*. New York: IEEE Press, 1994.

[28] A. R. Messina, E. Barocio., and E. Sanchez C., "Application of Perturbation Methods to the Analysis of Inter-area Oscillations", *Circuits and Systems, 1999. ISCAS '99. Proceedings of the 1999 IEEE International symposium on*, Vol. 5, pp. 90-93, Orlando, Florida, 30 May-2 June.

[29] Y.Ni, V. Vittal, and W. Kliemann, "Investigation of nonlinear modal behavior of HVDC/AC power systems through a scanning tool via normal form technique",

Proceeding of IEEE International Symposium on Circuits and Systems 97, Paper No. 2P1-16, pp. 945-948, Hong Kong, June 9-12, 1997.

[30] J. Thapar, V. Vittal, and W. Kliemann, "Application of the normal form of vector fields to predict inter-area separation in power systems", *IEEE Trans. Power Systems*, Vol. 12, No. 2, pp. 844-850, May 1997.

[31] S. Saha, A. A. Fouad, V. Vittal and W. Kliemann, "Stability boundary approximation of a power system using the normal form of vector fields", *IEEE Trans. Power Systems*, Vol. 12, No. 2, pp. 797-802, May 1997.

[32] Huan Xie, Baohui Zhang, Yinghui Li, Guangliang Yu, Decai Zhou, Feng Yao, and Liyong Wang, "A variable structure trajectory predictive algorithm based on transform for complex exponential time series", *IEEE/PES Transmission and Distribution Conference & Exhibition*: Asia and Pacific, 2005, Dalian, China.

[33] Gilsoo Jang, Jin-Boo Choo, and Sae-Hyuk Kwon, "Analysis of nonlinear oscillations in KEPCO systems: application of normal forms of vector fields", *IEEE PES Winter Meeting 2000*, Vol. 2, pp. 1509-1512, Singapore, 23-27 Jan. 2000.

[34] I. Dobson and E. Barocio, "Perturbation of weakly resonant power system electromechanical modes", *IEEE Trans. Power Systems*, Vol. 20, No. 1, pp. 330-337, Feb. 2005.

[35] R. J. Betancourt, E. Barocio, J. Arroyo, and A. R. Messina, "A real normal form approach to the study of resonant power systems", *IEEE Trans. on Power Systems*, Vol. 21, No. 1, pp. 431-432, Feb. 2006.

[36] Hasan Modir Shanechi, Naser Pariz, and Ebrahim Vaahedi, "General nonlinear modal representation of large scale power systems", *IEEE Trans. on Power Systems*, Vol. 18, No. 3, pp. 1103-1109, August 2003.

[37] N. E. Huang, Z. Shen, S. R. Long, M. C. Wu, H. H. Shih, Q. Zheng, N. C. Yen, C. C. Tung, and H. H. Liu, "The empirical mode decomposition and the Hilbert spectrum for nonlinear and non-stationary time series analysis", *Proc. Of the Royal Soc. Lond. A*, Vol. 454, pp. 903-995, 1998.

[38] Norden E. Huang, Man-Li C Wu, Steven R. Long, Samuel S. P. Shen, Wendong Qu, Per Gloersen and Kuang L. Fan, "A confidence limit for the empirical mode decomposition and Hilbert spectral analysis", *Proc. Of the Royal Soc. Lond. A*, Vol. 459, pp. 2317-2345, 2003.

[39] P. Kundur, M. Klein, G.J. Rogers, and M.S. Zywno, "Application of power system stabilizers for enhancement of overall system stability", *IEEE Trans. Power Systems*, Vol. 4, pp. 614-626, May 1989.

[40] E. Barocio, A. R. Messina, "Normal form analysis of stressed power systems: incorporation of SVC models", *Journal Electrical Power and Energy Systems* 25 (2003) 79-90.

[41] E. Barocio, A. R. Messina, "Analysis of nonlinear modal interaction in stressed power system with SVCs", *IEEE PES Winter Meeting 2002*, Vol. 2, pp. 1164-1169, New York City, USA, 27-31 Jan. 2002.

[42] A. R. Messina, E. Barocio, J. Arroyo, "Analysis of modal interaction in power systems with FACTS controllers using normal forms", *IEEE PSE General Meeting 2003*, Vol. 4, pp. 2117-2120, 13-17 July 2003, Toronto, Canada.

[43] Z. Y. Zou, Q. Y. Jiang, Y. J. Cao and H. F. Wang, "Normal form analysis of interactions among multiple SVC controllers in power systems", IEE Proceedings Generation, Transmission and Distribution, Vol. 152, No. 4, pp. 469-474, 8 July 2005.

[44] Z. Y. Zou, Q. Y. Jiang, Y. J. Cao, and H. F. Wang, "Investigation of Interactions among the Multi-control Channels of UPFC using Normal Forms of Vector Fields", *The 39th International Universities Power Engineering Conference*, Vol. 1, pp. 343-347, Bristol, UK, 6-8 Sept. 2004.

[45] Meng Yue, and Robert Schlueter, "Nonlinear effects of a robust control design", *IEEE Trans. on Power Systems*, Vol. 20, No. 1, pp. 508-510, February 2005.

[46] H. F. Wang, "On the connections among the electric torque, residue, functional sensitivity, participation and partial multi-modal decomposition", *UKACC International Conference on Control '98*, pp.1005-1010, 1-4 September 1998.

[47] E. Z. Zhou, O. P. Malik, and G. S. Hope, "Theory and method for Selection of Power System Stabilizer Location", *IEEE Trans. Power Systems*, Vol. 6, pp. 170-176, March 1991.

[48] E.Z. Zhou, O.P. Malik, and G.S. Hope, "Design of stabilizer for a multimachine power system based on the sensitivity of PSS effect", *IEEE Trans. on Energy Conversion*, Vol. 7, No. 3, pp. 606-613, September 1992.

[49] K. Hongesombu, Y. Mitani, S. Dechanupaprittha, I. Ngamroo, K. Pasupa, and J. Tippayachai, "Power system stabilizer tuning based on multiobjective design using hierarchical and parallel micro genetic algorithm", *2004 International Conference on Power System Technology*, Vol. 1, pp. 402-407, Singapore, 21-24 November 2004.

[50] C.Y. Chung, K.W. Wang, C.T. Tse, X.Y. Bian, and A.K. David, "Probabilistic eigenvalue sensitivity analysis and PSS design in multimachine systems", *IEEE Trans. on Power Systems*, Vol. 18, No. 4, pp. 1439-1445, November 2003.

[51] Arrowsmith, D. K., and C. M. Place. *An Introduction to Dynamical Systems*. Cambridge University Press, Cambridge, 1990.

[52] J. Carr, *Centre manifold theory*, New York: Springer-Verlag, 1981

[53] Alain Goriely, "Painlevi analysis and normal forms theory", *Physica D, 152-153*, pp. 124-144, 2001.

[54] S. Louies, and L. Brenig, "Structure and convergence of Poincaré-like normal forms", *Physics Letters A 233*, pp. 184-192, 1997.

[55] N. Kshatriya, U.D Annakage, A.M Gole, I.T Fernando, "Improving the accuracy of normal form analysis", *IEEE Trans. on Power Systems*, Vol. 20, pp. 286-293, February 2005.

[56] Shu Liu, A. R. Messina, V. Vittal, "Assessing placement of controllers and nonlinear behavior using normal form analysis ", *IEEE Trans. Power Systems*, Vol. 20, No. 3, pp. 1486-1495, August 2005.

[57] L. E. Jones, "On zero dynamics and robust conrol of large AC and DC power systems", Ph.D. dissertation, KTH Royal Institute of Technology, Stockholm, Sweden, 1999

[58] H. G. Kwatny and X.-M. Yu, "Energy analysis of load-induced flutter instability in classical models of electric power networks", *IEEE Trans. Circuits Syst.*, Vol. 38, pp. 1544-1557, Dec. 1989.

[59] H. G. Kwatny and G. E. Piper, "Frequency domain analysis of Hopf bifurcations in electric power networks", *IEEE Trans. Circuits Syst.*, Vol. 37, pp. 1317-1321, Oct. 1990.

[60] D.J. Trudnowski, J.M. Johnson, and J.F. Hauer, "SIMO system identification from measured ringdowns", in *Proc. American Control Conf.*, pp. 2968-2972, Philadelphia, PA, USA, June 1998.

[61] Michael J. Gibbard, David J. Vowles, and Pouyan Pourbeik, " Interactions between, and effectiveness of, power system stabilizers and FACTS device stabilizers in multimachine systems", *IEEE Trans. on Power Systems*, Vol. 15, pp. 748-755, May 2000.

[62] Ni, Y. X., V. Vittal, W. Kliemann, and A. A. Fouad, "Nonlinear modal interaction in HVDC/AC power systems with D. C. modulation", *IEEE Trans. on Power Systems*, Vol. 11, No. 4, pp. 2011-2017, November 1996.

[63] I. J. Perez-Arriaga, G. C. Verghese, and F. C. Schweppe, "Selective modal analysis with applications to electric power systems. Part I: Heuristic introduction", *IEEE Trans. on PAS*, Vol. 101, pp. 3117-3125, September 1982.

[64] A. P. Seyranian, A. A. Mailybaev, "Interaction of eigenvalues in multi-parameter problem", *Journal of Sound and Vibration*, 267, pp. 1047-1064, 2003.

[65] SSAT: Small Signal Analysis Tool, Powertech Labs Inc., Canada, July 17, 2005, www.powertechlabs.com.

[66] M. Klein, G. J. Rogers, S. Moorty, and P. Kundur, "Analytical investigation of factors influencing power system stabilizers performance", *IEEE Trans. Energy Conversion*, Vol. 7, pp. 382-390, September 1992.

[67] Larsen, E. V., and D. A. Swann, "Applying power system stabilizers parts I, II, and III", *IEEE Trans. on Power Apparatus and Systems*, Vol. PAS-100, No. 6, pp. 3017-3046, June 1981.